EUROPEAN ORGANIZATION FOR NUCLEAR RESEARCH (CERN)

CERN-EP-2024-016
2024/02/21

CMS-B2G-20-014

A search for bottom-type vector-like quark pair production in dileptonic and fully hadronic final states in proton-proton collisions at $\sqrt{s} = 13\,\text{TeV}$

The CMS Collaboration*

Abstract

A search is described for the production of a pair of bottom-type vector-like quarks (B VLQs) with mass greater than 1000 GeV. Each B VLQ decays into a b quark and a Higgs boson, a b quark and a Z boson, or a t quark and a W boson. This analysis considers both fully hadronic final states and those containing a charged lepton pair from a Z boson decay. The products of the H $\rightarrow$ bb boson decay and of the hadronic Z or W boson decays can be resolved as two distinct jets or merged into a single jet, so the final states are classified by the number of reconstructed jets. The analysis uses data corresponding to an integrated luminosity of 138 fb^{-1} collected in proton-proton collisions at $\sqrt{s} = 13\,\text{TeV}$ with the CMS detector at the LHC from 2016 to 2018. No excess over the expected background is observed. Lower limits are set on the B VLQ mass at 95% confidence level. These depend on the B VLQ branching fractions and are 1570 and 1540 GeV for 100% B $\rightarrow$ bH and 100% B $\rightarrow$ bZ, respectively. In most cases, the mass limits obtained exceed previous limits by at least 100 GeV.

Submitted to Physical Review D

*See Appendix A for the list of collaboration members

1 Introduction

A puzzle in elementary particle physics is the fact that the electroweak scale is so much lower than the Planck scale, which is connected to the stability of the Higgs boson (H) mass, m_{H} [1]. In the standard model (SM), the Higgs boson is a fundamental particle, first observed by the ATLAS and CMS Collaborations in 2012 [2–4] at the CERN LHC. In contrast to the leptons, quarks, and vector gauge bosons of the SM, the SM Higgs boson is a fundamental scalar particle with higher-order contributions to its mass due to vacuum fluctuations that diverge quadratically with length scale. This results in m_{H} being driven to the cutoff value of these fluctuations. If there is no new physics below the Planck scale, this cutoff value would be about 10^{19} GeV, which predicts m_{H} to be many orders of magnitude greater than the observed value of 125 GeV [5, 6].

Several theories have been proposed to solve this problem, including supersymmetry [7, 8], composite-Higgs models [9, 10] (where the Higgs boson is made up of smaller constituents bound by a new type of gauge interaction), and little-Higgs models [11, 12] (where the Higgs boson is a pseudo-Nambu–Goldstone boson arising from spontaneous breaking of a global symmetry at the TeV energy scale). In the composite-Higgs case, the mass divergence does not arise, since the UV cutoff is the scale set by the composite size, while, in the case of little-Higgs models, the Higgs boson is "naturally" light because of the collective breaking of the global symmetry via two couplings [13].

In both the composite- and little-Higgs models, a new type of particle arises [14]: a vector-like fermion that couples to the weak gauge bosons through purely vector current couplings. The strongly interacting vector-like fermions are referred to as vector-like quarks (VLQs). Unlike heavy fourth-generation sequential chiral quarks, these are not excluded by the measured H production cross section [15, 16] because the nonchirality of the VLQs allows for gauge-invariant mass terms in the Lagrangian and thus does not require Yukawa couplings.

There are four types of VLQs with renormalizable couplings to SM quarks. These are defined by their electrical charge: $-1/3$ (B), $+2/3$ (T), $+5/3$ (X), or $-4/3$ (Y) [17]. The B VLQ mixes with the chiral down-type quarks, and similarly, the T VLQ mixes with the chiral up-type quarks. Precision measurements that constrain additional couplings of the first- and second-generation SM quarks [18–20] indicate that the primary couplings of the T and B VLQs are to third-generation SM quarks. The values of the T and B VLQ branching fractions are determined by unknown parameters in the theory: the VLQ multiplet configuration, the VLQ mass, and the coupling of the VLQ to chiral quarks [21]. The possible decays of the B VLQ are $\mathrm{B} \to \mathrm{bH}$, $\mathrm{B} \to \mathrm{bZ}$, and $\mathrm{B} \to \mathrm{tW}$, so the branching fractions of these three modes sum to 100%. In TB doublet models, the branching fractions $\mathcal{B}(\mathrm{B} \to \mathrm{bH})$ and $\mathcal{B}(\mathrm{B} \to \mathrm{bZ})$ are approximately equal with values determined by the the relative mixing of the T and B VLQs with SM quarks [17]. They range from 50% each for the case of no Tt mixing to 0% each for the case of no Bb mixing. In XTB triplet models, $\mathcal{B}(\mathrm{B} \to \mathrm{bZ})$ and $\mathcal{B}(\mathrm{B} \to \mathrm{bH})$ are each approximately 50% for B VLQ masses above 1 TeV, while in TBY triplet models, $\mathcal{B}(\mathrm{B} \to \mathrm{bZ})$ and $\mathcal{B}(\mathrm{B} \to \mathrm{bH})$ are each approximately 25% for B VLQ masses above 1 TeV. In this analysis, lower limits on the B VLQ mass are presented over the full range of branching fractions.

Previous to this analysis, the best B mass limits from the CMS Collaboration for pair-produced B VLQs [22] were obtained by analyzing events with fully hadronic final states using data from proton-proton (pp) collisions at $\sqrt{s} = 13$ TeV, corresponding to an integrated luminosity of $137\,\mathrm{fb}^{-1}$. In that analysis, B masses were excluded at 95% confidence level (CL) up to 1570, 1390, and 1450 GeV in the 100% $\mathrm{B} \to \mathrm{bH}$, 100% $\mathrm{B} \to \mathrm{bZ}$, and TB doublet with no Tt mixing (50% $\mathrm{B} \to \mathrm{bH}$ and 50% $\mathrm{B} \to \mathrm{bZ}$) models, respectively. The best B mass limits from the ATLAS

Collaboration in pair-produced B events using pp collisions at $\sqrt{s} = 13\,\text{TeV}$ at 95% CL are 1030 GeV (based on $36.1\,\text{fb}^{-1}$) for the 100% $\text{B} \to \text{bH}$ case [23] and 1420 and 1320 GeV (based on $136\,\text{fb}^{-1}$) [24] for the 100% $\text{B} \to \text{bZ}$ and TB doublet with no Tt mixing models, respectively.

The analysis presented here is the first analysis to combine fully hadronic and leptonic categories and improves upon the previous CMS analysis in two ways. Firstly, the fully hadronic category is extended by including two additional modes in which one of the VLQs in an event decays to t and W so that, in addition to the bHbH, bHbZ, and bZbZ decay modes considered in [22], the bHtW and bZtW decay modes are also included. Secondly, for the first time, dileptonic events in which a Z boson in either the bHbZ or bZbZ mode decays to a pair of opposite-sign electrons or muons are included. Because the dileptonic branching fraction of the Z boson is an order of magnitude smaller than its hadronic branching fraction, the number of events in these channels is significantly less than in the fully hadronic ones. However, this is offset by the substantially lower background in these channels and results in significantly improved sensitivity to events in which a VLQ decays to bZ, leading to improved sensitivity for large $\mathcal{B}(\text{B} \to \text{bZ})$.

2 Analysis overview

In this analysis, we search for for events featuring the production of a pair of bottom-type VLQs, B, with mass greater than 1000 GeV, in data collected with the CMS detector from pp collisions at $\sqrt{s} = 13\,\text{TeV}$ at the LHC in 2016–2018, corresponding to an integrated luminosity of $138\,\text{fb}^{-1}$ [25–27]. We consider three possible decays of the B: a b quark and a Higgs boson ($\text{B} \to \text{bH}$), a b quark and a Z boson ($\text{B} \to \text{bZ}$), and a t quark and a W boson ($\text{B} \to \text{tW}$). Events are classified into different channels depending on three properties. The first is whether the event falls into the "fully hadronic" category, in which all of the bosons in an event decay into hadronic jets, or the "leptonic" category, where an event contains a $\text{B} \to \text{bZ}$ decay in which the Z boson decays into a pair of leptons, either electrons (ee) or muons ($\mu\mu$). Events with leptonic W boson decays are not considered because the missing energy from the neutrino makes reconstruction difficult. Figures 1 and 2 show the representative Feynman diagrams for the different decay modes in the fully hadronic and leptonic categories, respectively.

The second property determining the event classification is the reconstructed decay mode, which is determined by the decays of the two B VLQs. The leptonic category includes only bHbZ and bZbZ decay modes (i.e., events with one $\text{B} \to \text{bH}$ and one $\text{B} \to \text{bZ}$ decay, and events with two $\text{B} \to \text{bZ}$ decays, respectively), while the fully hadronic category includes in addition bHbH, bHtW, and bZtW decay modes. The tWtW mode is not considered since its high jet multiplicity results in a large number of possible jet combinations.

The third property determining the event classification is the number of reconstructed jets. Because the bosons produced in the B VLQ decay often have a significant Lorentz boost, the two jets produced in the hadronic decay of a W, Z, or Higgs boson can merge and be reconstructed as a single merged jet. In the tW case, the t quark decay into bW can produce three jets (one from the b quark and two from the W boson), two jets (one from the b quark and a merged jet from the W boson), or one fully merged jet. As a result, the final state can have a different jet multiplicity, depending on the number of merged jets. In the leptonic category, we also include events where an additional jet is produced from initial- or final-state radiation (ISR or FSR). Events containing ISR and FSR are not included in the hadronic category due to the large number of possible jet combinations resulting from the higher jet multiplicities.

The reconstruction of events and assignment of jets to parent particles is performed using a

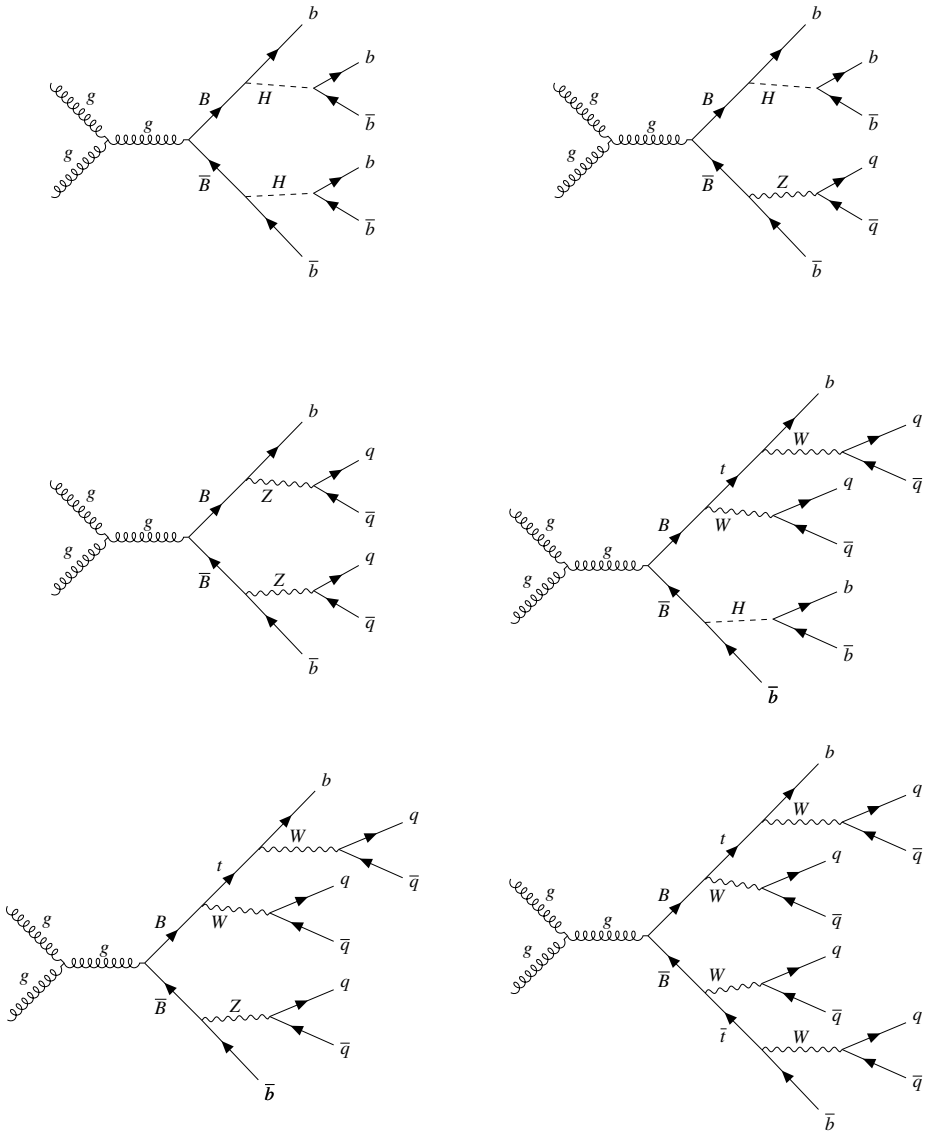

Figure 1: Feynman diagrams for the pair production of bottom-type VLQs that decay into a b or t quark or antiquark and either a Higgs, Z, or W boson with fully hadronic final states. Upper row: bHbH and bHbZ; middle row: bZbZ and bHtW; lower row: bZtW and tWtW. The B and $\overline{\text{B}}$ can be exchanged in the decays.

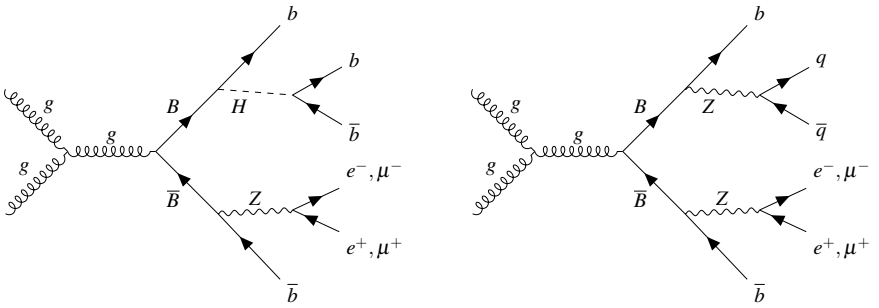

Figure 2: Feynman diagrams of the pair production of bottom-type VLQ quarks that decay into a b quark or antiquark and either a Higgs or Z boson with a dilepton final state: bHbZ mode (left) and bZbZ mode (right). The B and $\overline{\mathrm{B}}$ can be exchanged in the decays.

modified χ^2 metric, χ^2_{mod}, which uses as input the mass differences between the two reconstructed bosons and the Higgs, Z, or W boson, normalized by their resolutions, and the fractional mass difference of the two reconstructed VLQs. The value of $\chi^2_{\mathrm{mod}}/\mathrm{ndf}$, where ndf is the number of degrees of freedom, is calculated for each possible reconstructed decay mode and jet assignment, and the mode with the lowest value is selected as the reconstructed mode. Thus, each event is assigned to exactly one reconstructed mode. In the leptonic case, the $\chi^2_{\mathrm{mod}}/\mathrm{ndf}$ value is also used to identify extra jets that are likely to be from ISR and FSR.

The signature in the leptonic category consists of three or four final-state jets and a pair of oppositely charged, same-flavor electrons or muons with an invariant mass consistent with the Z boson mass. In the fully hadronic category, the signature consists of four, five, or six final-state jets. Table 1 summarizes the final event classification, showing the set of "channels" defined by the event category, decay mode, and jet multiplicity.

Table 1: Summary of channels considered for each category and jet multiplicity. Although events with a jet from ISR or FSR are included in the leptonic category, for these events the extra jet is not included in the categorization of the jet multiplicity of the event.

Jet multiplicity	Leptonic category	Fully hadronic category
3	bHbZ, bZbZ	—
4	bHbZ, bZbZ	bHbH, bHbZ, bZbZ
5	—	bHbH, bHbZ, bZbZ, bHtW, bZtW
6	—	bHbH, bHbZ, bZbZ, bHtW, bZtW

The main background in the leptonic category consists of Drell–Yan (DY) dilepton production in association with jets, while in the fully hadronic category the background is predominantly from SM events composed uniquely of jets produced through the strong interaction, referred to as quantum chromodynamics (QCD) multijet events.

The χ^2_{mod} requirement also aids in separating potential signal events from background by ensuring that the jets are kinematically consistent with production from a Higgs, Z, or W boson and that the reconstructed VLQs have masses consistent with each other. Further signal separation is achieved by requiring that some of the jets are tagged as originating from b quarks, either using tagging of individual jets or tagging of $\mathrm{b\bar{b}}$ pairs in merged jets from $\mathrm{H} \to \mathrm{b\bar{b}}$ decays. In addition, in the dileptonic case, the two leptons are also required to be kinematically consistent with the decay of a Z boson.

Tabulated results are provided in the HEPData record for this analysis [28].

3 The CMS detector

The central feature of the CMS apparatus is a superconducting solenoid of 6 m internal diameter, providing a magnetic field of 3.8 T. Within the solenoid volume are a silicon pixel and strip tracker, a lead tungstate crystal electromagnetic calorimeter (ECAL), and a brass and scintillator hadron calorimeter (HCAL), each composed of a barrel and two endcap sections. Forward calorimeters extend the pseudorapidity (η) coverage provided by the barrel and endcap detectors. Muons are measured in gaseous detectors embedded in the steel flux-return yoke outside the solenoid.

The ECAL consists of 75 848 lead tungstate crystals, which provide coverage in $|\eta| < 1.48$ in a barrel region and $1.48 < |\eta| < 3.0$ in two endcap regions. In the region $|\eta| < 1.74$, the HCAL cells have widths of 0.087 in η and 0.087 in azimuth (ϕ). For $|\eta| < 1.48$, the HCAL cells map in the η-ϕ plane on to 5×5 arrays of ECAL crystals to form calorimeter towers projecting radially outwards from close to the nominal interaction point. For $|\eta| > 1.74$, the coverage of the towers increases progressively to a maximum of 0.174 in $\Delta\eta$ and $\Delta\phi$. Within each tower, the energy deposits in ECAL and HCAL cells are summed to define the calorimeter tower energies, which are subsequently used to provide the energies and directions of hadronic jets. When combining information from the entire detector, the jet energy resolution amounts typically to 15–20% at 30 GeV, 10% at 100 GeV, and 5% at 1 TeV. The electron momentum is estimated by combining the energy measurement in the ECAL with the momentum measurement in the tracker. The momentum resolution for electrons with $p_{\mathrm{T}} \approx 45$ GeV from $\mathrm{Z} \to \mathrm{ee}$ decays ranges from 1.6 to 5%. It is generally better in the barrel region than in the endcaps, and also depends on the bremsstrahlung energy emitted by the electron as it traverses the material in front of the ECAL [29, 30].

Muons are measured in the pseudorapidity range $|\eta| < 2.4$, with detection planes made using three technologies: drift tubes, cathode strip chambers, and resistive-plate chambers. The single muon trigger efficiency exceeds 90% over the full η range, and the efficiency to reconstruct and identify muons is greater than 96%. Matching muons to tracks measured in the silicon tracker results in a relative transverse momentum (p_{T}) resolution, for muons with p_{T} up to 100 GeV, of 1% in the barrel and 3% in the endcaps. The p_{T} resolution in the barrel is better than 7% for muons with p_{T} up to 1 TeV [31].

Events of interest are selected using a two-tiered trigger system. The first level, composed of custom hardware processors, uses information from the calorimeters and muon detectors to select events at a rate of around 100 kHz within a fixed latency of about 4 μs [32]. The second level, known as the high-level trigger, consists of a farm of processors running a version of the full event reconstruction software optimized for fast processing, and reduces the event rate to around 1 kHz before data storage [33].

A more detailed description of the CMS detector, together with a definition of the coordinate system used and the relevant kinematic variables, can be found in Ref. [34].

4 Data and simulated events

Signal events with pair production of VLQs were simulated using the Monte Carlo generator MADGRAPH5_aMC@NLO [35]. For samples corresponding to 2016 data, version v2.3.3 was used with NNPDF3.0 next-to-leading order (NLO) parton distribution functions (PDFs) [36]; for samples corresponding to 2017–2018 data, v2.4.2 was used with NNPDF3.1 next-to-NLO PDFs [37]. The generated VLQ masses m_{B} cover the range 1000–1800 GeV in steps of 100 GeV.

Hadronization of the underlying partons was simulated using PYTHIA v8.212 [38] with the CUETP8M1 tune [39] for samples corresponding to 2016 data, and with the CP5 tune [40] for samples corresponding to 2017 and 2018 data. Corrections to the cross sections to next-to-NLO and next-to-next-to-leading logarithmic soft-gluon resummation were obtained using TOP++ 2.0 [41–43] with the MSTW2008NNLO68CL PDF set from the LHAPDF 5.9.0 library [44–46].

Although the background estimate is derived purely from data, simulated background samples are used for cross-checks of the data distributions. The background processes considered include DY + jets, QCD multijet, W + jets, Z + jets, and $t\bar{t}$ + jets. The DY + jets process is simulated with MADGRAPH5_aMC@NLO v2.6.0 at NLO, using the FxFx prescription [47] for jet merging, while the other four backgrounds are simulated using MADGRAPH5_aMC@NLO v2.4.2 at leading order with the MLM prescription [48] for jet merging. The hadronization is simulated in the same way as for the signal samples.

In order to simulate the effect of additional pp interactions within the same or nearby bunch crossings ("pileup"), PYTHIA v8.226 with a total inelastic pp cross section of 69.2 mb [49] was used to simulate minimum bias events to overlay on the hard scattering process. Following event generation, the GEANT4 package [50, 51] was used to simulate the CMS detector response. Scale factors corresponding to jet energy corrections, jet energy resolutions [52], QCD renormalization and factorization scales, pileup, and jet tagging [53, 54] are applied to the simulated signal events so that the corresponding distributions agree with those in data.

5 Lepton and jet reconstruction and jet tagging

The particle-flow algorithm [55] aims to reconstruct and identify each individual particle in an event, with an optimized combination of information from the various elements of the CMS detector. The primary vertex is taken to be the vertex corresponding to the hardest scattering in the event, evaluated using tracking information alone, as described in Section 9.4.1 of Ref. [56]. The energy of photons is obtained from the ECAL measurement. The energy of electrons is determined from a combination of the electron momentum from the track, the energy of the corresponding ECAL cluster, and the energy sum of all bremsstrahlung photons spatially compatible with originating from the electron track. The energy of muons is obtained from the curvature of the corresponding track. The energy of charged hadrons is determined from a combination of their momentum measured in the tracker and the matching ECAL and HCAL energy deposits, corrected for the response function of the calorimeters to hadronic showers. Finally, the energy of neutral hadrons is obtained from the corresponding corrected ECAL and HCAL energies.

For each event, hadronic jets are clustered from these reconstructed particles using the infrared and collinear safe anti-k_T algorithm via FASTJET [57, 58]. To account for the difference between merged and resolved jets, two separate clusterings are performed on the input particles, one using a distance parameter of 0.4 ("AK4 jets"), and the other using a distance parameter of 0.8 ("AK8 jets"). Jet momentum is determined as the vectorial sum of all particle momenta in the jet, and is found from simulation to be, on average, within 5 to 10% of the true momentum over the entire p_T spectrum and detector acceptance. Pileup can contribute additional tracks and calorimetric energy depositions to the jet momentum. The pileup-per-particle identification algorithm (PUPPI) [59, 60] is used to mitigate the effect of pileup at the reconstructed-particle level, making use of local shape information, event pileup properties, and tracking information. A local shape variable is defined, which distinguishes between collinear and soft diffuse distributions of other particles surrounding the particle under consideration. The former is attributed to particles originating from the hard scatter and the latter to particles originating

from pileup interactions. Charged particles identified to be originating from pileup vertices are discarded. For each neutral particle, a local shape variable is computed using the surrounding charged particles compatible with the primary vertex within the tracker acceptance ($|\eta| < 2.5$), and using both charged and neutral particles in the region outside of the tracker coverage. The momenta of the neutral particles are then rescaled according to their probability to originate from the primary interaction vertex deduced from the local shape variable, superseding the need for jet-based pileup corrections [59].

Jet energy corrections are derived from simulation studies so that the average measured energy of jets becomes identical to that of particle-level jets. In situ measurements of the momentum balance in dijet, photon + jet, Z + jet, and multijet events are used to account for any residual differences in the jet energy scale between data and simulation [52]. Additional selection criteria are applied to each jet to remove jets potentially dominated by anomalous contributions from various subdetector components or reconstruction failures.

We require AK4 jets to have $p_T > 50\,\text{GeV}$ and AK8 jets to have $p_T > 200\,\text{GeV}$, with $|\eta| < 2.4$ in both cases. The event jet multiplicity is determined by the number of AK4 jets in the event passing these requirements. For the AK8 jets, a grooming algorithm is applied. In this algorithm, the constituents of the AK8 jets are reclustered using the Cambridge–Aachen algorithm [61, 62]. The "modified mass drop tagger" algorithm [63, 64], also known as the "soft-drop" (SD) algorithm, with angular exponent $\beta = 0$, soft cutoff threshold $z_{\text{cut}} < 0.1$, and characteristic radius $R_0 = 0.8$ [65], is applied to remove soft, wide-angle radiation from the jet. The resulting "soft-drop mass" provides a more accurate estimate of the mass of the parent Higgs, Z, or W boson in the case of merged jets, and so is used in these cases.

The final state is expected to contain two b jets from the decays of the VLQs, and may contain additional $\mathrm{b\bar{b}}$ pairs from $\mathrm{H} \to \mathrm{b\bar{b}}$ or $\mathrm{Z} \to \mathrm{b\bar{b}}$ decays. Consequently, identification of these b jets provides an effective way to discriminate signal events from SM background. For individual jets, the DEEPJET b discriminant [53, 54, 66] is applied to AK4 jets to obtain single b tags, while for merged jets containing $\mathrm{b\bar{b}}$ pairs, an algorithm developed for $\mathrm{H} \to \mathrm{b\bar{b}}$ tagging [54] is applied to AK8 jets to obtain double-b tags.

In the leptonic category, electrons or muons are selected with $p_T > 50\,\text{GeV}$ and $|\eta| < 2.4$. Electrons and muons are required to pass a loose set of identification requirements, and muons are additionally required to pass a loose isolation requirement to reject muons within jets from, e.g., semileptonic decays of b quarks [29, 31]. Studies of the dileptonic mass distributions in simulation showed that this additional loose isolation requirement on muons improved the Z boson purity, while a similar loose isolation requirement on electrons was not needed.

6 Event selection, reconstruction, and categorization

In this section, the selection and categorization of events is described. This consists of the online selection of events by selected triggers, the offline requirements on jets, leptons and b-tagged jets, and the reconstruction of the VLQ candidates and selection of the event category.

6.1 Online event selection

Events are selected online by the following high-level trigger requirements:

- For the fully hadronic category, the trigger requires the scalar sum of the measured jet p_T values to be greater than 900 (1050) GeV in the 2016 (2017–2018) data set.
- For leptonic events containing muons, the trigger requires a muon with $p_T > 50\,\text{GeV}$.

For 2017–2018, muons identified from their signature in the tracker with $p_T > 100\,\text{GeV}$ are also accepted.

- For leptonic events containing electrons, a set of triggers is used to increase the efficiency, selecting any of the following: an electron passing a tight set of identification criteria with $p_T > 27$, 35, or 32 GeV in 2016, 2017, or 2018, respectively; an electron with $p_T > 115\,\text{GeV}$; a photon with $p_T > 200\,\text{GeV}$ (175 GeV in 2016); a pair of isolated electrons with $p_T > 23\,(12)$ GeV for the leading (subleading) electron; a pair of electrons with $p_T > 33\,\text{GeV}$; or a pair of photons with $p_T > 70\,\text{GeV}$ (60 GeV in 2016).

The trigger efficiencies are measured using data sets collected by triggers independent of those used in the analysis. For the fully hadronic category, the trigger efficiencies are parameterized byH_T, defined as the scalar sum of the p_T of all offline AK4 jets satisfying the above p_T and η requirements. The efficiency exceeds 99% for values of H_T greater than 1350 GeV. For the leptonic category, the trigger efficiencies are parameterized by the highest p_T lepton. Both the electron and muon trigger efficiencies exceed 98% for values of the highest lepton p_T greater than 50 GeV.

6.2 Offline requirements on jets, leptons, and b-tagged jets

Offline selection requirements are then applied. For the leptonic category, the event is required to have at least three and no more than five AK4 jets with $p_T > 50\,\text{GeV}$ and $|\eta| < 2.4$, and to have at least one pair of opposite-sign, same-flavor leptons with an invariant mass in the range $80 < m_{\ell\ell} < 102\,\text{GeV}$, consistent with the Z boson mass. If there are two such pairs each with invariant mass within the Z boson mass window, the pair with the mass closest to that of the Z boson is used. For the fully hadronic category, there must be at least four and no more than six AK4 jets with $p_T > 50\,\text{GeV}$ and $|\eta| < 2.4$, and the event must have $H_T > 1350\,\text{GeV}$. In addition, to ensure orthogonality with both the leptonic analysis and with other B VLQ searches using a single lepton, any event with an isolated electron or muon with $p_T > 50\,\text{GeV}$, or at least one lepton pair meeting the criteria for the leptonic category, is rejected.

A requirement is also placed on the minimum number of jets tagged as originating from a b quark. For the fully hadronic category, the number of tagged b jets and the working points (WPs) for the taggers are optimized for discovery of a 1400 GeV VLQ signal. The WPs used for the single-b tagger, "loose", "medium", and "tight", correspond to an identification efficiency of approximately 93, 82, and 65%, respectively, for b jets with $p_T > 30\,\text{GeV}$ in simulated $\mathrm{t\bar{t}}$ events, with a misidentification probability for light (u, d, s) quark and gluon jets of 10%, 1%, and 0.1%, respectively [53]. For the $\mathrm{b\bar{b}}$ tagger, two WPs, "loose" and "medium 2", are used, corresponding to an identification efficiency of approximately 75 and 45%, respectively, with a misidentification probability of 11 and 3%, respectively [54]. For the leptonic category, the medium WP is used for the single b tagger in all channels. Table 2 summarizes the final requirements.

6.3 Event reconstruction and categorization

We define a "preselection" sample, which consists of events that pass all of the selection requirements except for the b tagging. Before the b tagging requirements are applied, the event sample is dominated by SM backgrounds, primarily QCD multijet and $\mathrm{t\bar{t}}$ processes, and any potential contribution from signal is negligible. Using the "preselection" events, candidate bosons (Higgs, Z, or W) and VLQs are reconstructed. A candidate boson is formed from either two AK4 jets or a single AK8 jet, with the mass taken as the invariant mass of the two jets in the former case and the soft-drop mass of the jet in the latter case. Only those AK8

Table 2: Required minimum number of single (N_{b}) and double ($N_{\mathrm{b\bar{b}}}$) b tags, and working points (WPs) used for each category, decay mode, and jet multiplicity. The working points are described in the text. For a given event mode, there can be several jet multiplicities depending on the number of merged jets.

Decay mode	Jet multiplicity	Min N_{b}	b tagger WP	Min $N_{\mathrm{b\bar{b}}}$	$\mathrm{b\bar{b}}$ tagger WP
Fully hadronic bHbH	4	2	Medium	1	Loose
Fully hadronic bHbH	5	3	Medium	1	Loose
Fully hadronic bHbH	6	4	Medium	—	—
Fully hadronic bHbZ	4	2	Loose	1	Medium 2
Fully hadronic bHbZ	5	3	Medium	0	Loose
Fully hadronic bHbZ	6	4	Medium	—	—
Fully hadronic bZbZ	4	2	Medium	0	Loose
Fully hadronic bZbZ	5	2	Medium	0	Loose
Fully hadronic bZbZ	6	2	Tight	—	—
Fully hadronic bHtW	5	2	Medium	0	Loose
Fully hadronic bHtW	6	3	Medium	0	Loose
Fully hadronic bZtW	5	2	Medium	0	Loose
Fully hadronic bZtW	6	2	Tight	0	Loose
Leptonic bHbZ	3	1	Medium	—	—
Leptonic bHbZ	4	1	Medium	—	—
Leptonic bZbZ	3	1	Medium	—	—
Leptonic bZbZ	4	1	Medium	—	—

jets are used that have a soft-drop mass greater than 50 GeV and match to an AK4 jet within $\Delta R = \sqrt{(\Delta\eta)^2 + (\Delta\phi)^2} < 0.3$. In order to avoid overlap with another AK4 jet which could affect the AK8 jet mass, the AK8 jet is discarded if there is another AK4 jet that matches to it within $\Delta R < 0.6$.

A VLQ candidate decaying to bH or bZ is then formed by combining an additional jet with a boson candidate, with its reconstructed mass m_{VLQ} taken to be the invariant mass of this combination. In the tW case, a t quark candidate can be reconstructed either from a single AK8 jet, with the mass taken to be the soft-drop mass of the jet, or from two or three AK4 jets, with the mass taken to be the invariant mass of these jets.

The decay mode, as well as the assignment of reconstructed jets to their parent particles, is determined using the modified χ^2 parameter, χ^2_{mod}, evaluated for all possible decay modes and jet assignments. Because the inputs to χ^2_{mod} are not necessarily distributed as Gaussian variables, the resulting expression does not follow a true χ^2 distribution, and thus χ^2_{mod} is used to denote it. However, since χ^2_{mod} is used for the event selection to choose the channel and jet configuration as well as provide a discriminant, this difference does not affect the outcome of the analysis.

The general form of χ^2_{mod} is as follows in the fully hadronic category:

$$\chi^2_{\mathrm{mod}} = \frac{(\Delta m_{\mathrm{VLQ}} - \overline{\Delta m}_{\mathrm{VLQ}})^2}{\sigma^2_{\Delta m_{\mathrm{VLQ}}}} + \frac{(m_1 - \overline{m_1})^2}{\sigma^2_{m_1}} + \frac{(m_2 - \overline{m_2})^2}{\sigma^2_{m_2}}, \tag{1}$$

where Δm_{VLQ} is the fractional mass difference of the two reconstructed VLQ candidates in the event, given by $\Delta m_{\mathrm{VLQ}} = 2(m_{\mathrm{VLQ}_1} - m_{\mathrm{VLQ}_2})/(m_{\mathrm{VLQ}_1} + m_{\mathrm{VLQ}_2})$, $m_{1,2}$ are the masses of the two reconstructed bosons, $\overline{m}_{1,2}$ and $\overline{\Delta m}_{\mathrm{VLQ}}$ are the average masses of the bosons and Δm_{VLQ}, respectively, and the σ are the standard deviations. The values of $\overline{m}_i$, σ_{m_i}, $\overline{\Delta m}_{\mathrm{VLQ}}$, and $\sigma_{\Delta m_{\mathrm{VLQ}}}$ are computed by using simulated signal samples with $m_{\mathrm{B}} = 1400$ GeV and selecting events where the jets are closely matched to the generated partons in simulation.

In the case where the decay mode contains a $\mathrm{B} \to \mathrm{tW}$ decay, another term is added to the χ^2_{mod} expression for each reconstructed t quark: $(m_{\mathrm{t}} - \overline{m}_{\mathrm{t}})/\sigma^2_{m_{\mathrm{t}}}$, where m_{t} is the reconstructed t quark mass, and $\overline{m}_{\mathrm{t}}$ and $\sigma_{m_{\mathrm{t}}}$ are the average and standard deviation of the t quark mass in simulation. This term is added to aid in distinguishing such events from events where one of the B VLQs decays to bZ.

In the leptonic category, only the mass of the hadronically decaying boson is included in χ^2_{mod}, so the expression is simply:

$$\chi^2_{\mathrm{mod}} = \frac{(\Delta m_{\mathrm{VLQ}} - \overline{\Delta m}_{\mathrm{VLQ}})^2}{\sigma^2_{\Delta m_{\mathrm{VLQ}}}} + \frac{(m_1 - \overline{m_1})^2}{\sigma^2_{m_1}}, \tag{2}$$

where m_1 is the mass of the hadronically decaying Higgs or Z boson.

Mass distributions for the parent Z, W, H, or t are obtained, and then fitted with a bifurcated Gaussian (i.e., a Gaussian that has a different σ parameter above and below the mean). Consequently, when the χ^2_{mod} value is computed, the appropriate σ value is used depending on whether the reconstructed mass is above or below $\overline{m}$. These distributions are computed separately depending on whether the final state is reconstructed as two resolved jets or one merged jet, and also separately for each jet multiplicity. The values for $\sigma_{\Delta m_{\mathrm{VLQ}}}$ are typically around 0.1, while the values for σ_{m_i} are roughly 10–20 GeV.

Once the χ^2_{mod} value has been computed for all channels within an event category, the channel with the smallest χ^2_{mod}/ndf is selected. The value of ndf is 2 for the leptonic channels; 3 for the fully hadronic modes bHbH, bHbZ, and bZbZ; and 4 for the fully hadronic modes bHtW and bZtW. This method was found to have good accuracy, as determined by tests with the signal simulations.

The performance of the χ^2_{mod}-based reconstruction is indicated by the average of the two reconstructed VLQ masses, referred to as m_{VLQ}, which is shown for simulated signal samples with $m_{\text{B}} = 1400\,\text{GeV}$ in Fig. 3 (channels in the fully hadronic category) and Fig. 4 (channels in the dileptonic category). The mass is well reconstructed for events near the peak; the low-mass tail corresponds to events in which the selected jet permutation is incorrect. Tests on simulated signal samples with different B VLQ masses showed similar performance.

In the leptonic category, in order to account for a possible jet due to ISR or FSR, an extra jet reconstructed by the method described in Section 5 but not originating from VLQ pair production is allowed. Specifically, for events that contain five reconstructed jets, the χ^2_{mod}/ndf is evaluated for all possible assignments of four jets with one jet discarded, and the event is then treated as a four-jet event using the four jets that resulted in the best χ^2_{mod}/ndf. For events that contain four reconstructed jets, the χ^2_{mod}/ndf is calculated for these four jets, and then also for each possible jet assignment for a three-jet event. If the four-jet χ^2_{mod}/ndf is less than each of the three-jet χ^2_{mod}/ndf values, then it is treated as a four-jet event. Otherwise, it is treated as a three-jet event using those three jets.

Figures 5 and 6 show the resulting distributions in the fully hadronic and leptonic categories, respectively, of the value of the least χ^2_{mod}/ndf for simulated signal events compared to the distributions for data events before any b tagging requirements are applied. In these plots, the two distributions are normalized to the same area.

Since the χ^2_{mod}/ndf values tend to be lower for signal events than for background events, an upper limit is set on the least χ^2_{mod}/ndf in order to provide background rejection. This limit is optimized for signal sensitivity separately for each category and channel, using a B mass of 1400 GeV. For the fully hadronic category, equal branching fractions for $\text{B} \to \text{bH}$, $\text{B} \to \text{bZ}$, and $\text{B} \to \text{tW}$ are assumed, and for the leptonic category, branching fractions of $\mathcal{B}(\text{B} \to \text{bH}) = 30\%$ and $\mathcal{B}(\text{B} \to \text{bZ}) = 70\%$ are used. Table 3 shows the optimized χ^2_{mod}/ndf limits obtained for each category. These values do not depend significantly on the B mass assumed in the optimization since the χ^2_{mod}/ndf measure in Eqs. (1) and (2) depends on the mass difference between the two reconstructed VLQ candidates, and not the VLQ mass itself. As a cross check, the optimization was performed with other B masses, resulting in only small changes in the optimal χ^2_{mod}/ndf limit values. These optimized χ^2_{mod}/ndf limits are then used in conjunction with b tagging, to provide signal discrimination in the reconstructed m_{VLQ} spectrum, used to obtain a background estimate described in the next section.

7 Background estimation

As the QCD multijet background is difficult to precisely model in simulation, the background estimation is based exclusively on control samples in data. Since the composition and behavior of the background is different between the fully hadronic and dileptonic categories, separate methods are used for each category.

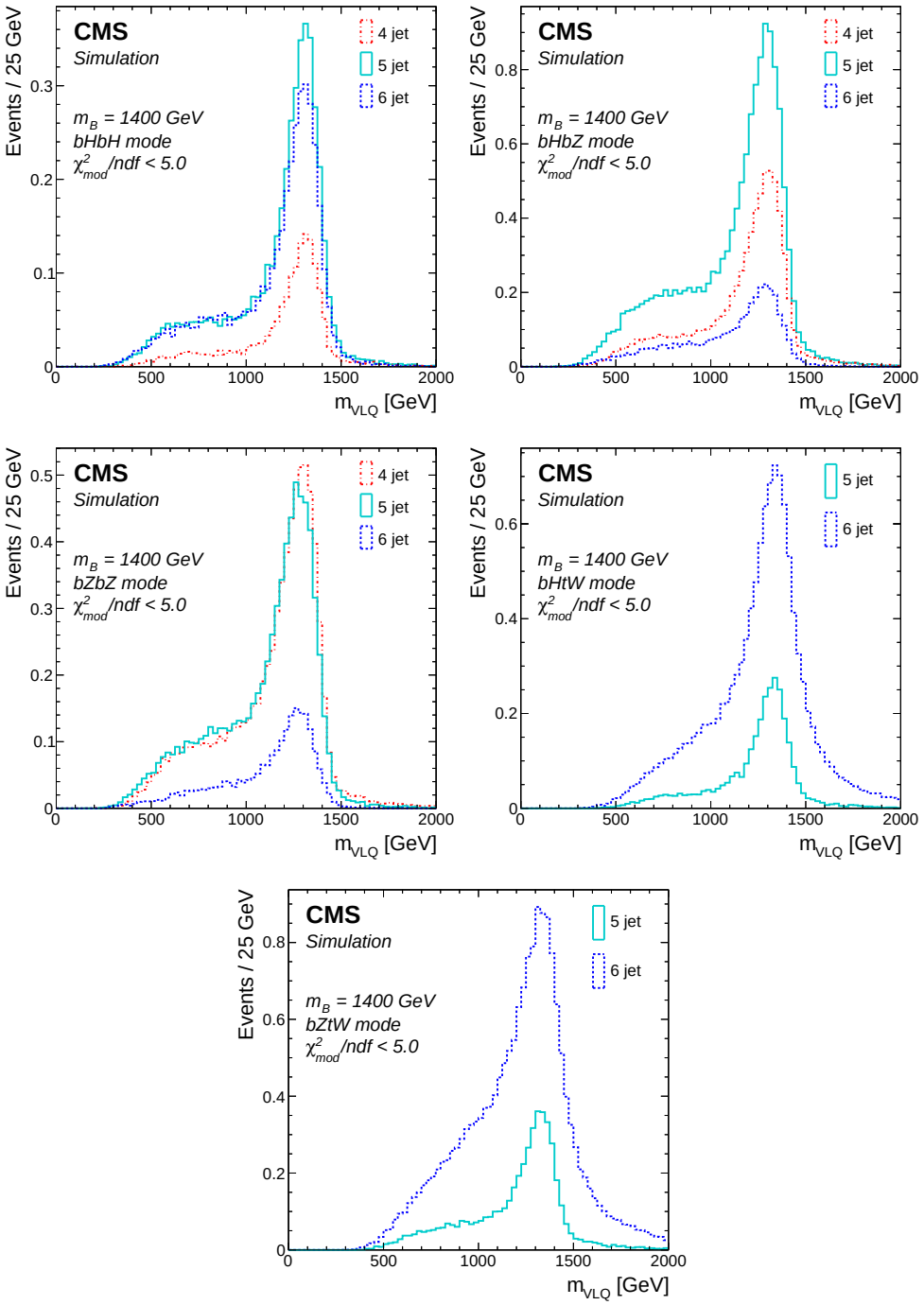

Figure 3: Reconstructed VLQ mass distributions for simulated events for the channels in the fully hadronic category with $m_{\mathrm{B}} = 1400\,\mathrm{GeV}$. Upper row: Channels in the bHbH (left) and bHbZ (right) decay mode. Middle row: Channels in the bZbZ (left) and bHtW (right) decay mode. Lower row: Channels in the bZtW decay mode. The different colors indicate the different jet multiplicities. A selection of $\chi^2_{\mathrm{mod}}/\mathrm{ndf} < 5$ has been applied. The values represent the expected number of events over the background in the 2016–2018 data sample.

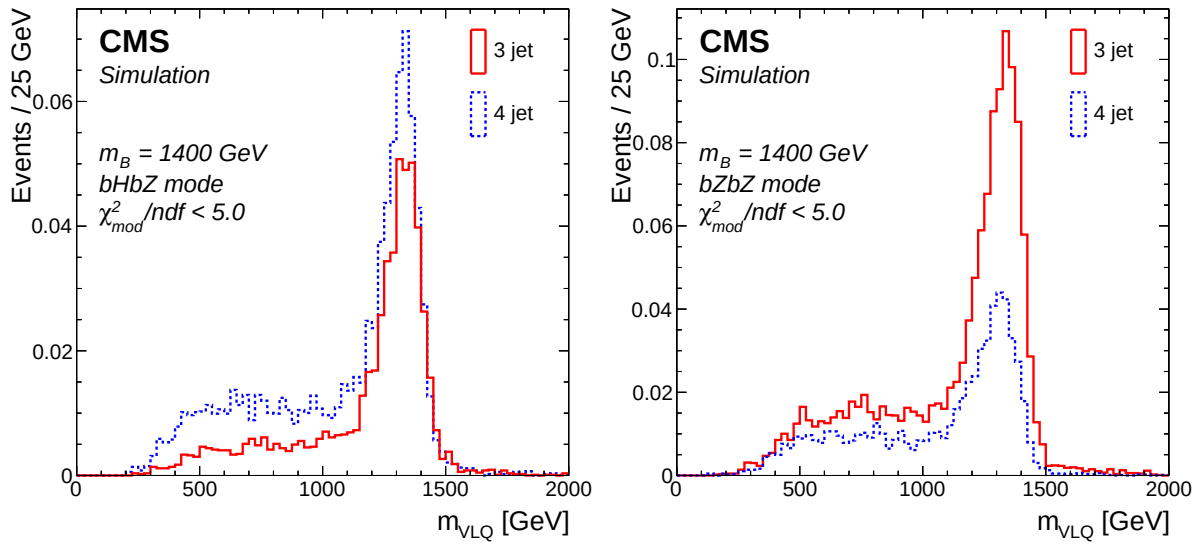

Figure 4: Reconstructed VLQ mass distributions for simulated events passing the b tag requirement for the channels in the dileptonic category with $m_B = 1400$ GeV in the bHbZ (left) and bZbZ (right) event modes. A selection of $\chi^2_{mod}/ndf < 5$ has been applied. The values represent the expected number of events over the background in the 2016–2018 data sample.

Table 3: Optimized upper limit values of the χ^2_{mod}/ndf selection as a function of jet multiplicity and decay mode.

Decay mode	Jet multiplicity			
	3	4	5	6
Fully hadronic bHbH	—	1.5	2.75	1.0
Fully hadronic bHbZ	—	2.0	1.25	1.25
Fully hadronic bZbZ	—	0.75	1.25	1.75
Fully hadronic bHtW	—	—	2.5	5.0
Fully hadronic bZtW	—	—	1.5	6.0
Leptonic bHbZ	2.9	2.5	—	—
Leptonic bZbZ	2.0	2.6	—	—

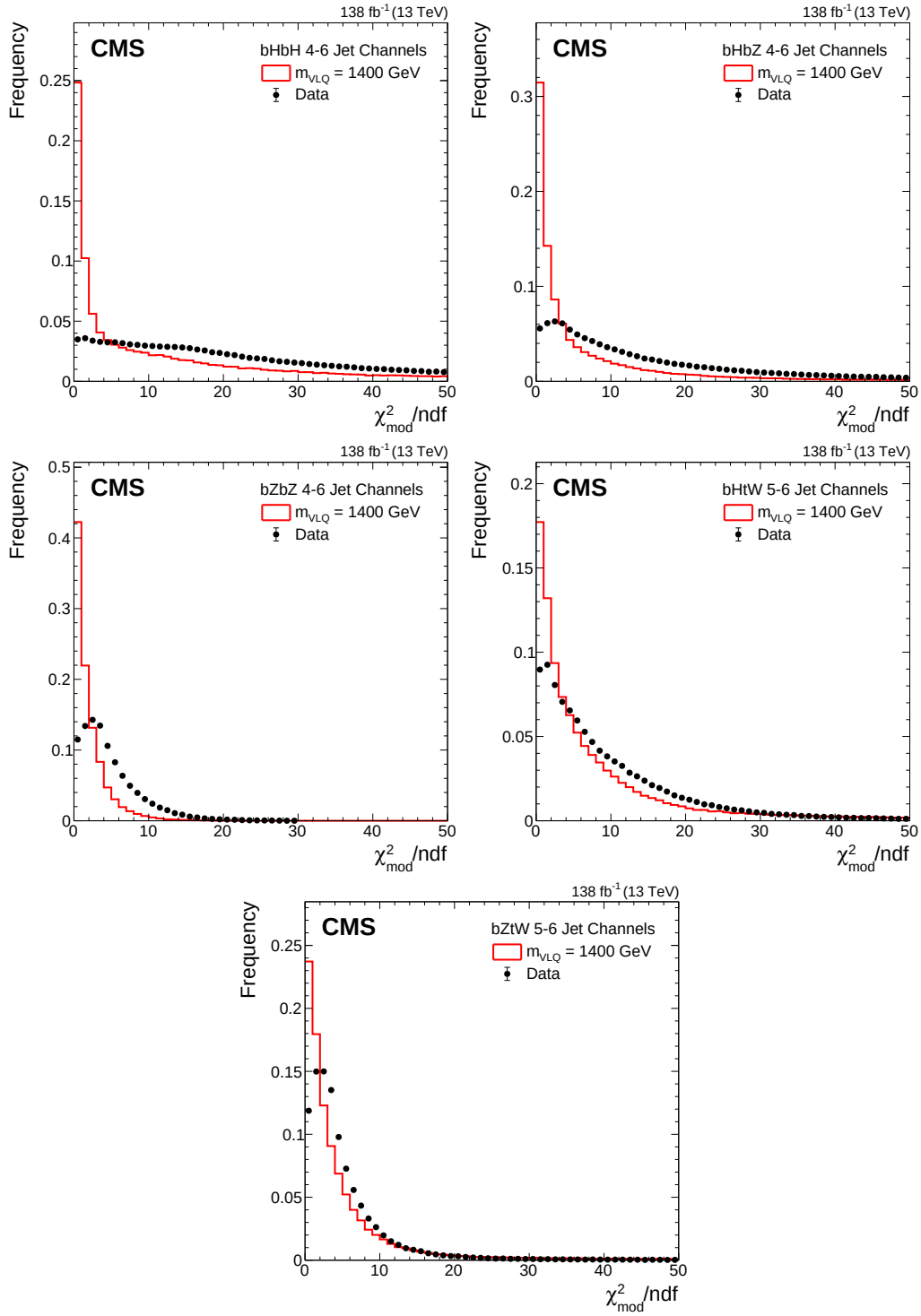

Figure 5: Normalized distributions of the value of the least $\chi^2_{\text{mod}}/\text{ndf}$ for simulated signal events and data events in the fully hadronic category before any b tagging requirements are applied in the fully hadronic category. Upper row: bHbH (left), bHbZ (center), and bZbZ (right) decay modes. Lower row: bHtW (left), and bZtW (right) decay modes. A signal mass of $m_{\text{B}} = 1400\,\text{GeV}$ is used and compared against all three years of data. All jet multiplicities have been combined together.

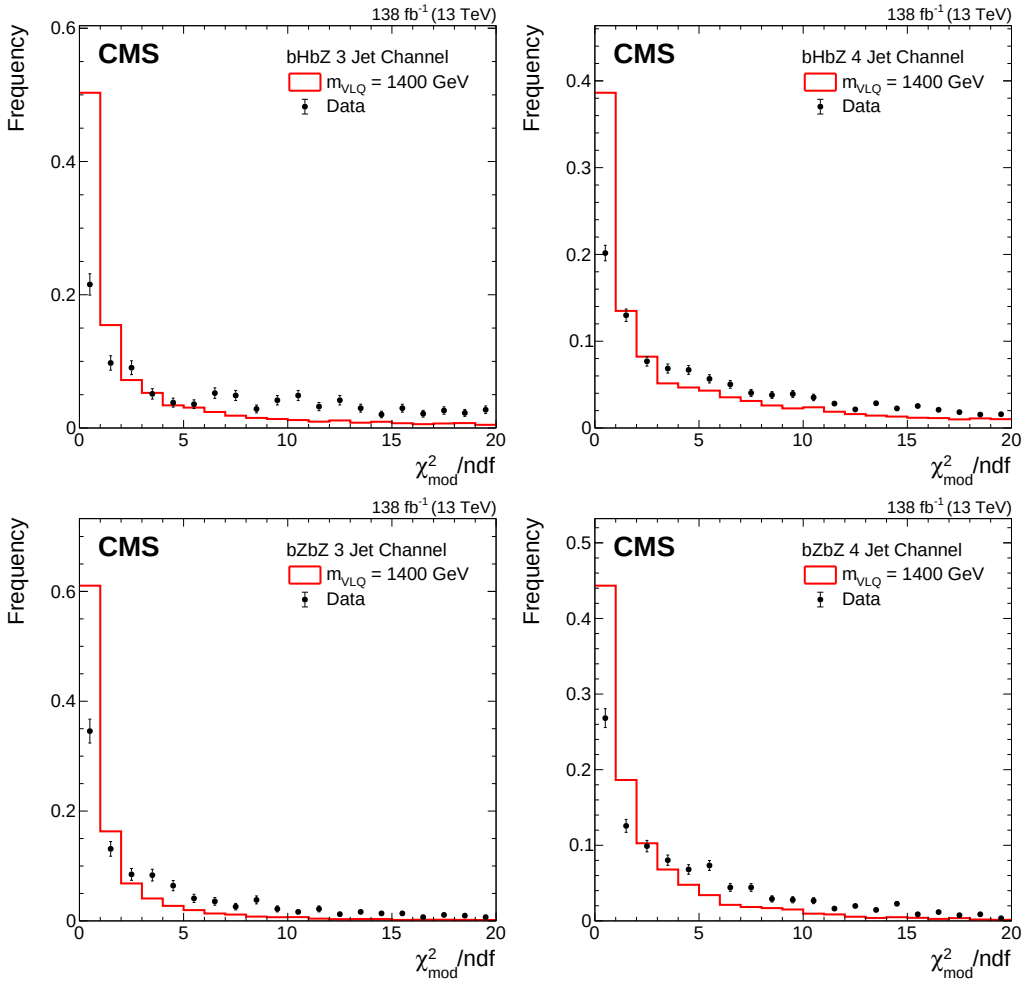

Figure 6: Normalized distributions of the value of the least $\chi^2_{\text{mod}}/\text{ndf}$ for simulated signal events and data events in the leptonic category before any b tagging requirements are applied. Upper row: bHbZ decay mode, 3-jet (left) and 4-jet (right) events. Lower row: bZbZ decay mode, 3-jet (left) and 4-jet (right) events. A signal mass of $m_{\text{B}} = 1400\,\text{GeV}$ is used and compared against all three years of data.

7.1 Background estimation in the fully hadronic category

The background estimation for the fully hadronic category generally follows the procedure described in Ref. [22]. Using the preselection sample defined in Section 6.3, the expected distribution of the number of events as a function of the VLQ candidate mass is obtained, and then fit with the function

$$n(x) = p_0 \exp\left[-(p_1 x + \theta(-x) p_2 x^2)\right] \tag{3}$$

in the range $m_{\mathrm{VLQ}} > 800\,\mathrm{GeV}$, where $x \equiv m/\mathrm{GeV} - 1200$ and $\theta(x)$ is the Heaviside step function. The second-order term is applied only for mass values less than 1200 GeV to account for the shape change of the distribution in the low-mass region compared to a traditional exponential function caused by the trigger turn on. This is also the reason the fit only includes $m_{\mathrm{VLQ}} > 800\,\mathrm{GeV}$. Figure 7 shows the resulting fit results for six representative fully hadronic channels.

The second step is to estimate the reduction in background that results from applying the jet b tagging requirements. This factor is called the background jet-tagged fraction (BJTF). It is obtained by using events in a sideband region defined by the mass range $500 < m_{\mathrm{VLQ}} < 800\,\mathrm{GeV}$. This mass range is chosen to ensure that the sideband region is free of any potential signal, as this range is below the current lower exclusion limits on the VLQ mass [22, 67, 68]. Table 4 summarizes the values of the BJTF derived from this sideband region, denoted ε_0 in Eq. (4), for the different channels considered.

Table 4: Values of the BJTF for data events in the control region with $500 < m_{\mathrm{VLQ}} < 800\,\mathrm{GeV}$ for each of the fully hadronic channels considered. The uncertainties shown are statistical.

	bHbH	bHbZ	bZbZ	bHtW	bZtW
4 jets	0.0010 ± 0.0007	0.0032 ± 0.0005	0.0075 ± 0.0016	—	—
5 jets	0.0009 ± 0.0002	0.0040 ± 0.0004	0.0492 ± 0.0020	0.0243 ± 0.0019	0.0223 ± 0.0019
6 jets	0.0020 ± 0.0003	0.0018 ± 0.0003	0.0368 ± 0.0018	0.0089 ± 0.0003	0.0311 ± 0.0005

We allow for a dependence of the BJTF factor on m_{VLQ} that could occur, for example, because the jet tagging efficiency depends on the p_{T} of the jet, and VLQs with higher mass will generally produce jets with higher p_{T}. For this, we define a control region as events with $\chi^2_{\mathrm{mod}}/\mathrm{ndf}$ in the range $12 < \chi^2_{\mathrm{mod}}/\mathrm{ndf} < 48$. The dependence of the BJTF on m_{VLQ} in this control region is then fit with a first-order polynomial, denoted $\varepsilon(m) = p_0 + p_1 m$. Checks with F-tests indicate that the first-order polynomial fit is preferred over higher-order fits. Figure 8 shows the BJTF distribution in the control regions along with the first-order polynomial fits for a few representative fully hadronic channels.

The estimate of the number of background events in the signal region, n_{bkg}, as a function of m_{VLQ} is then given by the following expression:

$$n_{\mathrm{bkg}}(m_{\mathrm{VLQ}}) = n(m_{\mathrm{VLQ}}) \varepsilon_0 \frac{\varepsilon(m_{\mathrm{VLQ}})}{\left(\int_{500\,\mathrm{GeV}}^{800\,\mathrm{GeV}} \varepsilon(m')\,\mathrm{d}m'\right)/(300\,\mathrm{GeV})}, \tag{4}$$

where $n(m_{\mathrm{VLQ}})$ is the number of candidates as a function of m_{VLQ} in the preselected sample, as shown in Fig. 7, ε_0 is the BJTF determined from the sideband with low VLQ mass, as shown in Table 4, and the last factor is the correction for the dependence of the BJTF on m_{VLQ}, as shown in Fig. 8.

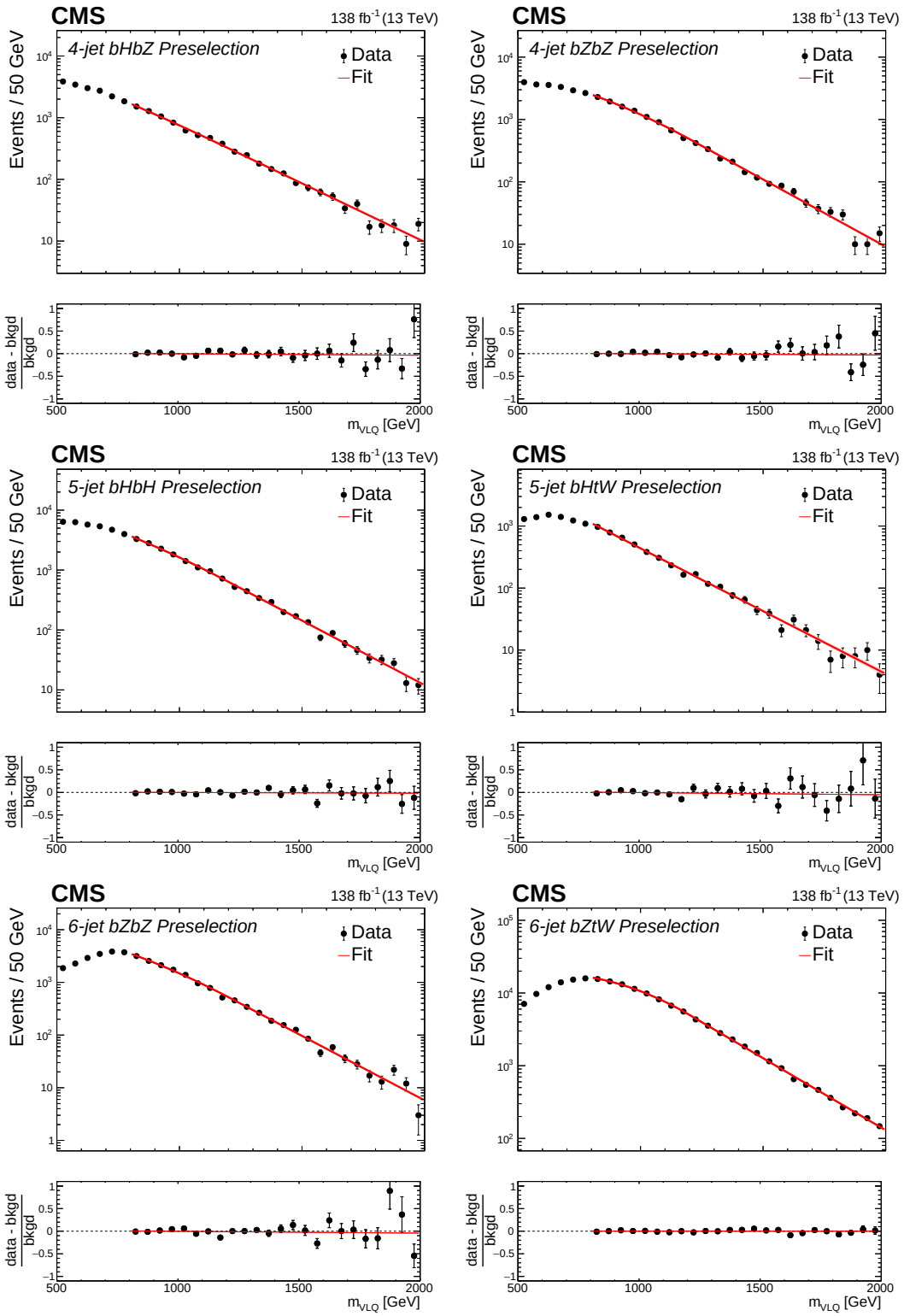

Figure 7: Distributions of m_{VLQ} for the preselected data sample in the fully hadronic category for some selected channels. Upper row: 4-jet bHbZ (left) and 4-jet bZbZ (right) modes. Middle row: 5-jet bHbH (left) and 5-jet bHtW (right) modes. Lower row: 6-jet bZbZ (left) and 6-jet bZtW (right) modes. The fit to the data (shown by the black points) is given by the red line, and the bottom panel displays the fractional difference between the data and fit, (data-fit)/fit.

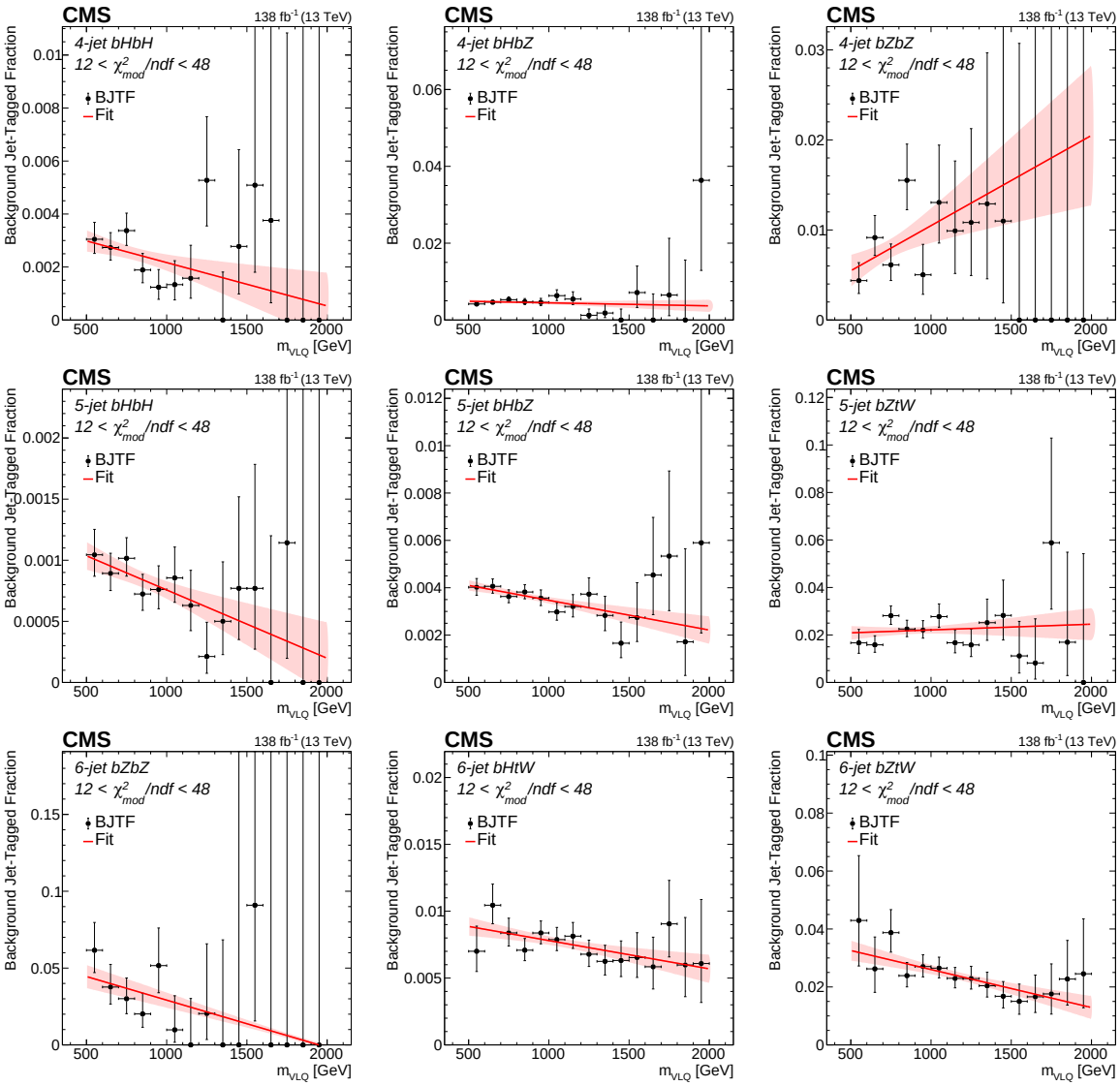

Figure 8: Value of BJTF as a function of m_{VLQ} in the control region with $12 < \chi^2_{\mathrm{mod}}/\mathrm{ndf} < 48$ for some selected fully hadronic channels. Upper row: 4-jet events in the bHbH (left), bHbZ (center), and bZbZ (right) modes. Middle row: 5-jet events in the bHbH (left), bHbZ (center), and bZtW (right) modes. Lower row: 6-jet events in the bZbZ (left), bHtW (center), and bZtW (right) modes. The linear fit is shown by the red line, and the associated uncertainty in the fit is shown by the shaded band.

7.2 Background estimation in the leptonic category

The background estimation for the leptonic category is based on a similar procedure to that for the fully hadronic category, but with different definitions of the signal and control regions. In particular, the use of b tagging is different for the two categories. For the leptonic category, the BJTF factor described above is not used. Instead, for the leptonic category, the signal region is defined to be events with $\chi^2_{\text{mod}}/\text{ndf} < 5$ for which at least one of the jets directly originating from the B VLQ candidate (i.e., not associated with an H or Z boson decay) is b tagged (called b-tag events). The control region is defined to be events with the same $\chi^2_{\text{mod}}/\text{ndf} < 5$ requirement, but where neither of the jets directly originating from a B VLQ candidate is b tagged (called b-veto events). Notably, these requirements are both independent of the hadronically decaying H or Z boson.

First, the VLQ mass distribution in the control region is fit with an exponential function over the mass range $800 < m_{\text{VLQ}} < 2000\,\text{GeV}$. Figure 9 shows the resulting distributions and the exponential fits for each of the four leptonic channels. Then, this distribution is normalized to the expected distribution in the signal region by multiplying by a normalization factor, the ratio of b-tag events to b-veto events in the low-mass range of $450 < m_{\text{VLQ}} < 900\,\text{GeV}$. Table 5 shows the resulting normalization factors for the four channels.

Table 5: Values of the b-tag to b-veto ratio for events in the mass range $450 < m_{\text{VLQ}} < 900\,\text{GeV}$ with $\chi^2_{\text{mod}}/\text{ndf} < 5$, for each of the dileptonic channels. The uncertainties shown are statistical only.

	bHbZ	bZbZ
3 jets	0.101 ± 0.010	0.130 ± 0.006
4 jets	0.127 ± 0.009	0.125 ± 0.074

Next, events with $\chi^2_{\text{mod}}/\text{ndf}$ in the range $5 < \chi^2_{\text{mod}}/\text{ndf} < 20$ are used to check for possible dependence of the normalization factors on the VLQ candidate mass. Figure 10 shows the b-tag to b-veto ratio as a function of m_{VLQ} for events in the range $5 < \chi^2_{\text{mod}}/\text{ndf} < 20$ for all four leptonic channels. As a cross-check, the dependence of the b-tag to b-veto ratio as a function of m_{VLQ} for simulated Drell–Yan events, which constitute the dominant background, is shown in Fig. 11 over the full mass range, which verifies that the normalization factors do not have a significant dependence on the VLQ mass.

We next check that the b-tag to b-veto ratio in the range $5 < \chi^2_{\text{mod}}/\text{ndf} < 20$ correctly represents the ratio in the range $\chi^2_{\text{mod}}/\text{ndf} < 5$ by plotting the ratio as a function of $\chi^2_{\text{mod}}/\text{ndf}$, shown in Fig. 12. No significant dependence over the $\chi^2_{\text{mod}}/\text{ndf}$ region is observed.

The fit to a constant value is therefore sufficient for all channels, as there is no statistically significant evidence for a mass dependence of the b-tag to b-veto ratio. The normalization factor is thereby set to be the ratio of b-tag events to b-veto events in the 450 to 900 GeV mass range using events with $\chi^2_{\text{mod}}/\text{ndf} < 5$, that is, the ratio of low-mass signal region events to low-mass control region events. Although there is no statistically significant evidence of a normalization factor mass dependence, steps are taken to estimate the uncertainty that such a dependence may create in this factor. For this, we compare the ratio of b-tag events to b-veto events in the low-mass range to the ratio of b-tag to b-veto events in the high-mass range, using events in the $\chi^2_{\text{mod}}/\text{ndf}$ range of $5 < \chi^2_{\text{mod}}/\text{ndf} < 20$. Figure 13 (left) shows that the low-mass and high-mass ratios are consistent for all four channels. As a check on this procedure, the same comparison is performed for simulated Drell–Yan events using the optimally tuned $\chi^2_{\text{mod}}/\text{ndf}$. The results, displayed in Fig. 13 (right), show that the low-mass and high-mass ratios are consistent, even after an upper limit is applied on the value of $\chi^2_{\text{mod}}/\text{ndf}$.

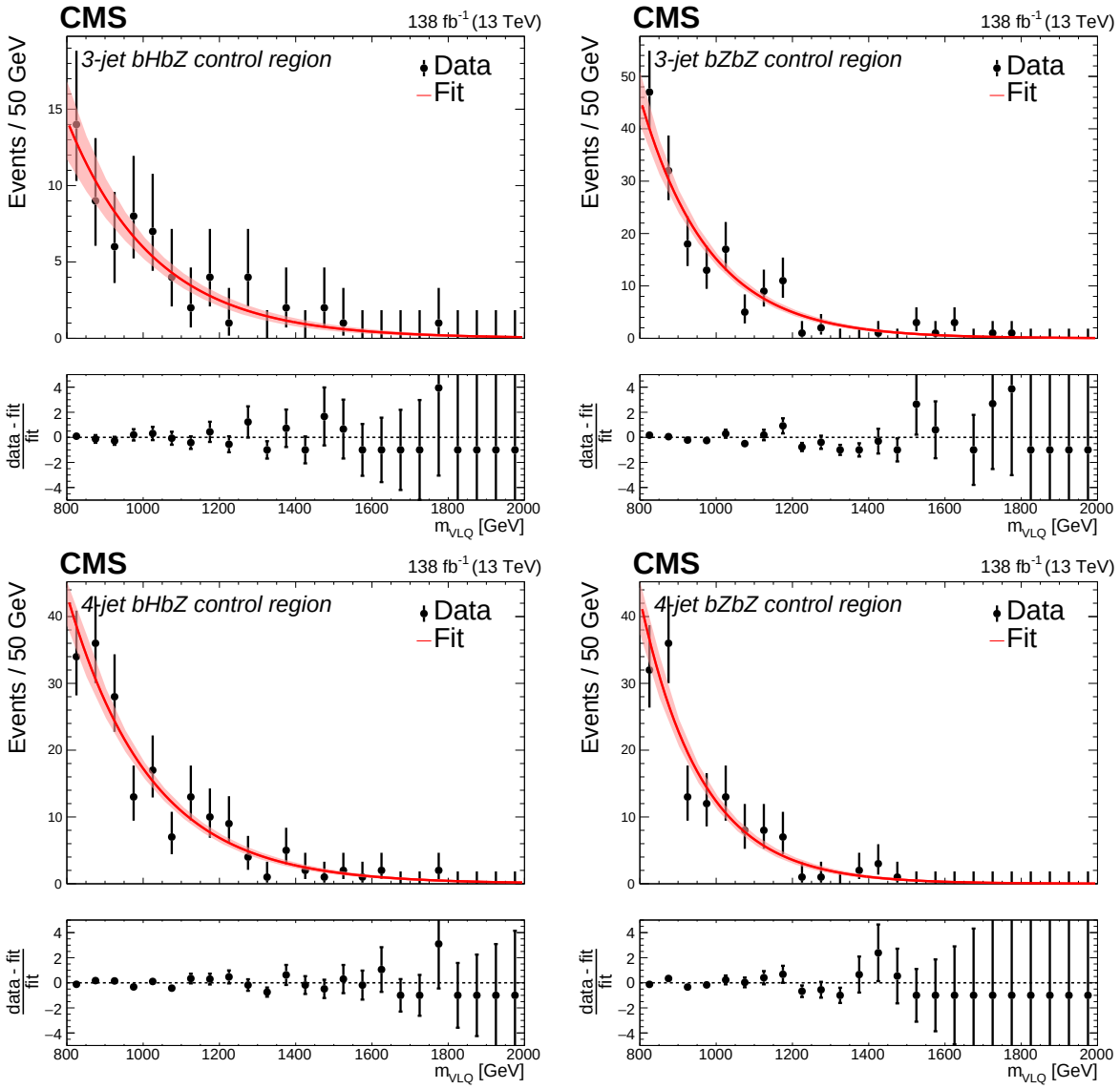

Figure 9: Distributions of m_{VLQ} for events in the control region for the channels in the leptonic category. Upper row: 3-jet events in the bHbZ (left) and bZbZ (right) modes. Lower row: 4-jet events in the bHbZ (left) and bZbZ (right) modes. The exponential fit and its uncertainty are shown by the red line and the light red shaded band, respectively. The bottom panel shows the fractional difference between the data and fit, (data-fit)/fit.

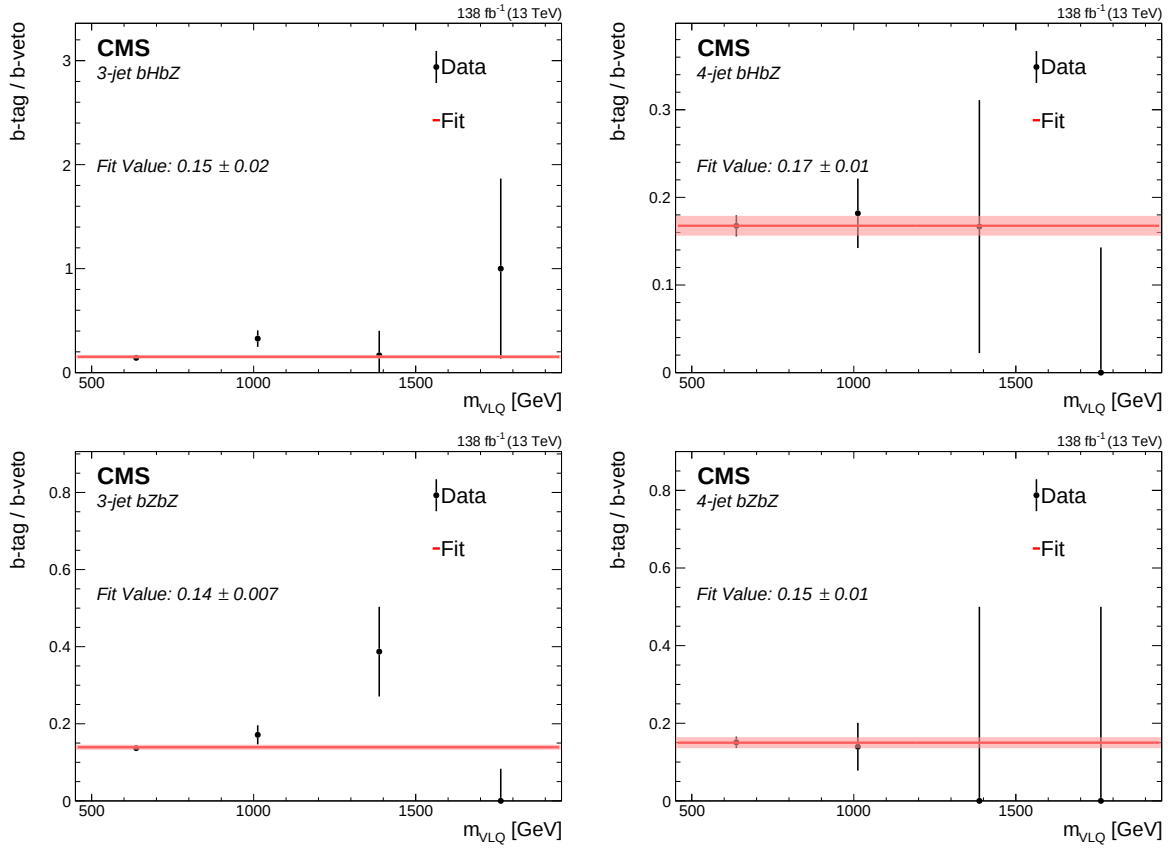

Figure 10: Normalization factor as a function of m_{VLQ} for leptonic events in the $5 < \chi^2_{\mathrm{mod}}/\mathrm{ndf} < 20$ region. Upper row: bHbZ events in the 3-jet (left) and 4-jet (right) channels. Lower row: bZbZ events in the 3-jet (left) and 4-jet (right) channels. The fit to a constant value and its uncertainty are shown by the red line and the light red shaded band, respectively.

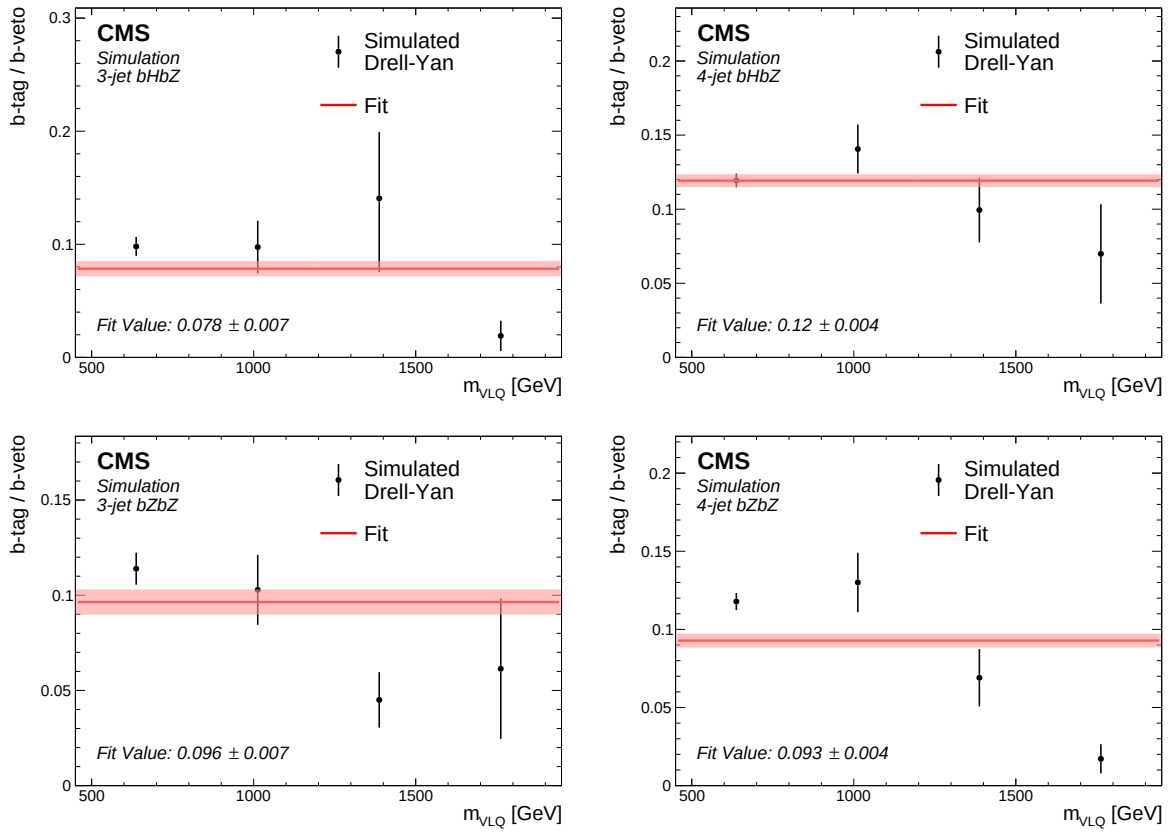

Figure 11: Normalization factor in the leptonic category as a function of m_{VLQ} for simulated Drell–Yan events with $\chi^2_{\mathrm{mod}}/\mathrm{ndf} < 5$. Upper row: bHbZ events in the 3-jet (left) and 4-jet (right) channels. Lower row: bZbZ events in the 3-jet (left) and 4-jet (right) channels. The fit to a constant value and its uncertainty are shown by the red line and the light red shaded band, respectively.

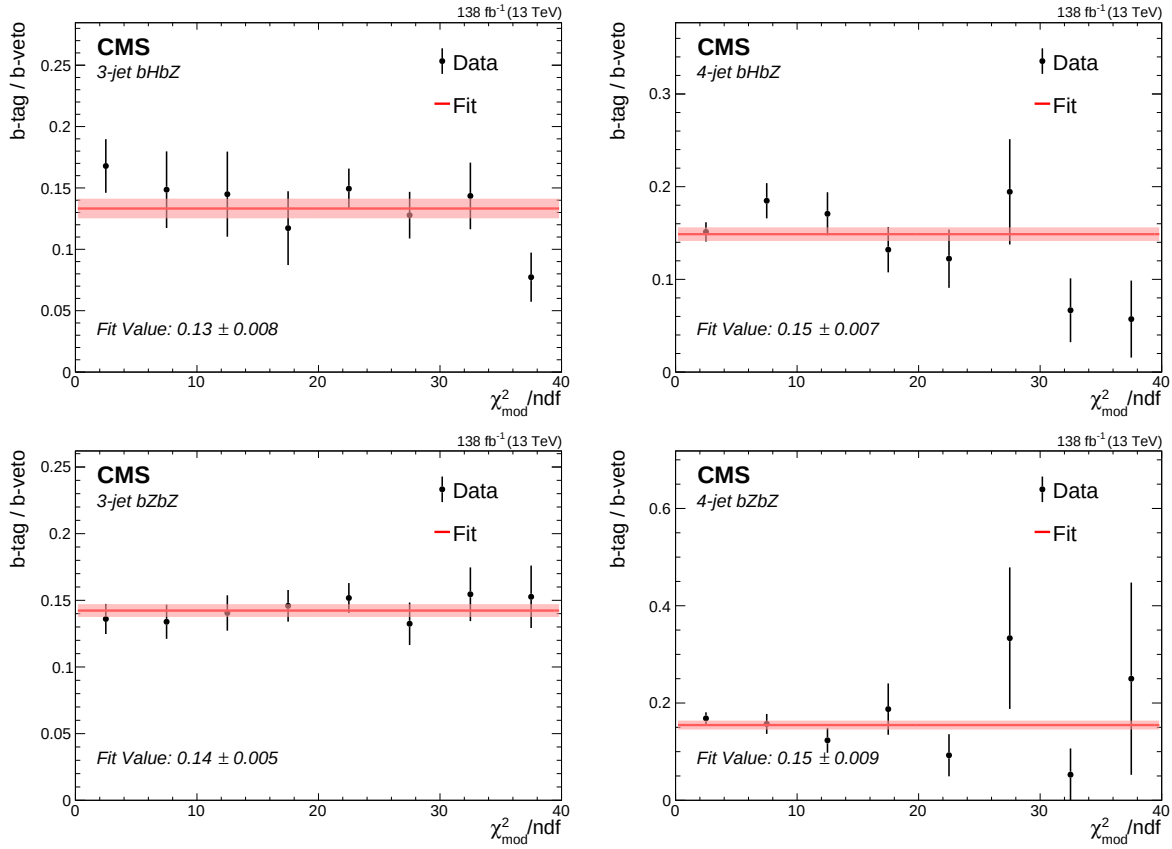

Figure 12: Normalization factor in the leptonic category as a function of $\chi^2_{\text{mod}}/\text{ndf}$. Upper row: 3-jet events in the bHbZ (left) and bZbZ (right) decay modes. Lower row: 4-jet events in the bHbZ (left) and bZbZ (right) decay modes. The fit to a constant value and its uncertainty are shown by the red line and the light red shaded band, respectively.

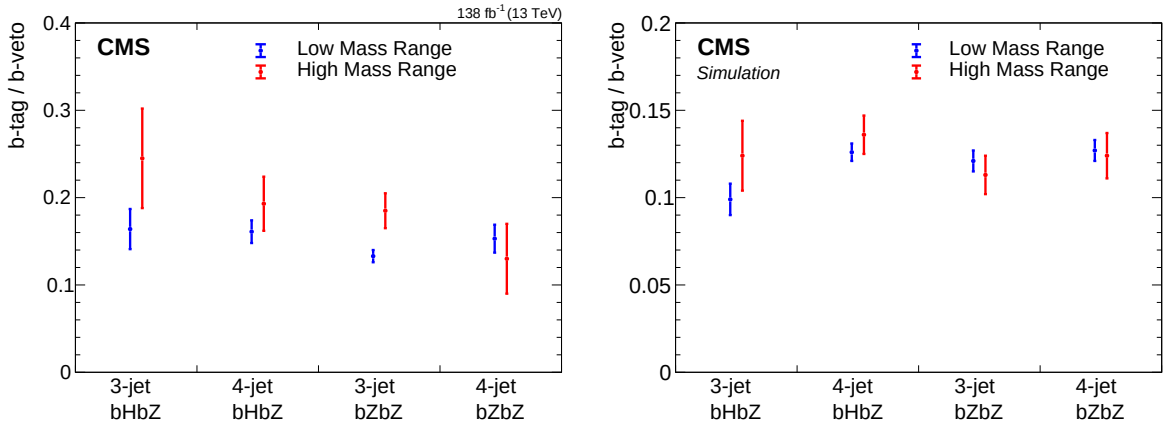

Figure 13: Normalization factor in the low-mass region (450 to 900 GeV) and the high-mass region (800 to 2000 GeV) for events with $5 < \chi^2_{\text{mod}}/\text{ndf} < 20$ in data (left) and simulated Drell–Yan events with $\chi^2_{\text{mod}}/\text{ndf} < 5$ (right).

The estimate of the number of background events in the signal region, n_{bkg}, as a function of m_{VLQ} is given by the following expression:

$$n_{\mathrm{bkg}}(m_{\mathrm{VLQ}}) = f(m_{\mathrm{VLQ}}) \frac{\int_{450\,\mathrm{GeV}}^{900\,\mathrm{GeV}} n_{\mathrm{signal}}(m')\,\mathrm{d}m'}{\int_{450\,\mathrm{GeV}}^{900\,\mathrm{GeV}} n_{\mathrm{control}}(m')\,\mathrm{d}m'}, \tag{5}$$

where $f(m_{\mathrm{VLQ}})$ is the fitted function for the number of candidates as a function of m_{VLQ} in the control region, as shown in Fig. 9, and the second term is the normalization factor, as determined by the ratio of the number of events in the signal region to the control region with $450 < m_{\mathrm{VLQ}} < 900\,\mathrm{GeV}$. For the final evaluation of the number of events in the sideband region, the $\chi^2_{\mathrm{mod}}/\mathrm{ndf}$ requirement for each particular channel is applied.

8 Systematic uncertainties

The systematic uncertainties are listed in Tables 6 and 7. They include the following:

- Integrated luminosity: The integrated luminosities for the 2016, 2017, and 2018 data-taking years have 1.2–2.5% individual uncertainties [25–27], while the overall uncertainty for the 2016–2018 period is 1.6%.
- Trigger: The uncertainties in the trigger efficiencies are determined from the uncertainties in the fitting parameters from fits of the trigger efficiencies with respect to H_{T}, using constant functions for channels in the hadronic category and logistic functions for channels in the leptonic category. For 2016, 2017, and 2018 they are 2.0, 0.05, and 0.01%, respectively, for the jet triggers used; 0.3, 0.2, and 0.2% for the muon triggers, and 0.2, 0.3, and 0.2% for the electron triggers.
- Dilepton Z boson efficiency: The total dimuon and dielectron efficiencies are determined using simulated signal events. The net efficiency is calculated by multiplying the efficiencies for each step in the dilepton Z boson selection process: exactly two leptons, both leptons pass the identification and isolation requirements, and the dilepton Z boson invariant mass is between 80 and 102 GeV. The uncertainty in the total efficiency is found to be 0.3% for both the dimuon and dielectron cases.
- Scale factors: Scale factors for jet energy, jet energy resolution, b tagging efficiency, and lepton efficiency (including isolation, identification, and reconstruction for individual leptons) are needed to correct the distributions in simulation to match those in data. The resulting uncertainty in the simulated signal efficiency is determined by varying each scale factor up and down by one standard deviation. The uncertainties over each year are treated as uncorrelated. The uncertainties depend upon the event channel. Typical values are: 0.5–4.0% for jet energy, 0.5–2.5% for jet resolution, 5.0–12% for b tagging, and 10–12% for the overall lepton efficiency (where the larger value is due to the combination of isolation, identification, and reconstruction scale factors for the individual leptons).
- Background estimation in the fully hadronic category: There are two sources of uncertainty in the background estimate as a function of the average mass of the two VLQ candidates, $n_{\mathrm{bkg}}(m_{\mathrm{VLQ}})$ in Eq. (4). The first is from the fit for $n(m_{\mathrm{VLQ}})$, and is determined from the uncertainties in the fit parameters p_0, p_1, and p_2. The second is the uncertainty in the mass dependence of the BJTF factor, which is similarly determined from the uncertainties in the first-order polynomial fit parameters, p_0 and p_1, shown in the definition of $\varepsilon(m)$. For each of the fits, the nuisance parameters are

determined by decorrelating the fit parameters using the covariance matrix of the fit.

- Background estimation in the dileptonic category: Similarly, there are two sources of uncertainty in the background estimate as a function of the average mass of the two VLQ candidates, $n_{\mathrm{bkg}}(m_{\mathrm{VLQ}})$ in Eq. (5). The first arises from the fit for $f(m_{\mathrm{VLQ}})$, and is determined from the uncertainties in the exponential fit parameters. The second is the uncertainty in the mass dependence of the normalization factor, the b-tag to b-veto ratio, which is assigned to be one-half of the absolute value of the difference between this ratio in the low- and high-mass ranges, as shown in Fig. 13 (left).
- PDFs: The uncertainty associated with the choice of PDF set is calculated by following the PDF4LHC procedure to generate a set of weights for each uncertainty in the NNPDF3.0 distribution [69]. The uncertainty in the signal acceptance is then determined from the standard deviation of the distribution of the signal acceptance for each weight.
- QCD scale: The systematic uncertainty on the QCD scale is estimated by independently multiplying the default values of the renormalization and factorization scales, μ_{R} and μ_{F}, by factors of 2.0 and 0.5, and assigning the systematic error to be half of the resulting range of cross sections. In this procedure, following the results from [70], the cases of varying one scale by 2.0 and the other by 0.5 are excluded, since these correspond to unjustified values of $\log(\mu_{\mathrm{R}}/\mu_{\mathrm{F}})$. The range over the remaining seven combinations is then used.
- Pileup: The uncertainty due to the number of pileup events in the simulated events is evaluated by varying the pp inelastic cross section [49] by ± 1 standard deviation and determining the resulting change in the event selection efficiency.
- Trigger prefiring: Because of detector effects, ECAL and muon triggers can appear in the bunch crossing preceding the actual collision. This effect is not accounted for in simulation, and so corrections are applied to obtain the correct trigger efficiency. The uncertainties in these corrections are propagated to the event efficiency to obtain the resulting uncertainty.

Tables 6 and 7 summarize these uncertainties for the case of 40% $\mathcal{B}(\mathrm{B} \to \mathrm{bH})$, 40% $\mathcal{B}(\mathrm{B} \to \mathrm{bZ})$, and 20% $\mathcal{B}(\mathrm{B} \to \mathrm{tW})$ branching fractions and a VLQ mass of 1400 GeV. For each uncertainty, it is noted whether it affects the signal efficiency or the background estimate and whether it affects the shape of the mass distribution or only the overall rate.

In addition, an uncertainty of 6% is assigned to account for uncertainties in the VLQ pair production cross section [46]. This uncertainty is separate from the others described above, and is used only for the error band on the theory curve shown in the exclusion limit plots in Fig. 18.

Table 6: Table of systematic uncertainties for the fully hadronic channels for a simulated signal mass of 1400 GeV and branching fractions of $\mathcal{B}(\mathrm{B} \to \mathrm{bH}) = 40\%$, $\mathcal{B}(\mathrm{B} \to \mathrm{bZ}) = 40\%$, and $\mathcal{B}(\mathrm{B} \to \mathrm{tW}) = 20\%$. The only parameters in the fits that have significant uncertainties (>0.01%) are the scaling parameters (denoted by p_0).

Systematic	Signal/Background	Rate/Shape	4 jets	5 jets	6 jets
Jet trigger efficiency	Signal	Rate	0.6%	0.6%	0.6%
Luminosity	Signal	Rate	1.6%	1.6%	1.6%
PDFs	Signal	Rate	1.5%	1.5%	1.5%
QCD μ_R and μ_F scales	Signal	Rate	14.0%	14.0%	14.0%
Fully hadronic bHbH event mode					
Low-mass BJTF	Background	Rate	70.7%	18.9%	13.5%
Background fit p_0	Background	Shape	9.7%	9.6%	9.6%
BJTF fit form	Background	Rate	5.6%	21.4%	0.1%
BJTF fit p_0	Background	Shape	9.7%	9.6%	9.6%
Jet tag scale factors	Signal	Shape	4.6%	5.8%	7.1%
Jet energy resolution	Signal	Shape	0.3%	1.4%	2.0%
Jet energy scale	Signal	Shape	1.3%	2.1%	3.4%
Pileup	Signal	Shape	0.3%	0.3%	1.5%
Fully hadronic bHbZ event mode					
Low-mass BJTF	Background	Rate	17.2%	8.2%	14.6%
Background fit p_0	Background	Shape	9.7%	9.6%	9.4%
BJTF fit form	Background	Rate	0.7%	1.5%	1.3%
BJTF fit p_0	Background	Shape	9.7%	9.6%	9.4%
Jet tag scale factors	Signal	Shape	4.8%	5.7%	7.2%
Jet energy resolution	Signal	Shape	0.2%	1.0%	1.6%
Jet energy scale	Signal	Shape	1.2%	0.3%	1.4%
Pileup	Signal	Shape	0.1%	0.0%	1.1%
Fully hadronic bZbZ event mode					
Low-mass BJTF	Background	Rate	20.9%	3.8%	4.5%
Background fit p_0	Background	Shape	9.8%	9.8%	9.5%
BJTF fit form	Background	Rate	10.4%	0.0%	34.3%
BJTF fit p_0	Background	Shape	9.8%	9.8%	9.5%
Jet tag scale factors	Signal	Shape	5.0%	5.0%	4.9%
Jet energy resolution	Signal	Shape	0.3%	0.5%	1.0%
Jet energy scale	Signal	Shape	1.0%	2.8%	3.9%
Pileup	Signal	Shape	0.4%	0.1%	0.2%
Fully hadronic bHtW event mode					
Low-mass BJTF	Background	Rate	—	7.4%	3.2%
Background fit p_0	Background	Shape	—	9.4%	10.2%
BJTF fit form	Background	Rate	—	0.3%	0.6%
BJTF fit p_0	Background	Shape	—	9.4%	10.2%
Jet tag scale factors	Signal	Shape	—	4.1%	5.6%
Jet energy resolution	Signal	Shape	—	0.7%	0.4%
Jet energy scale	Signal	Shape	—	0.3%	1.5%
Pileup	Signal	Shape	—	0.1%	0.7%
Fully hadronic bZtW event mode					
Low-mass BJTF	Background	Rate	—	8.0%	1.6%
Background fit p_0	Background	Shape	—	9.7%	10.6%
BJTF fit form	Background	Rate	—	0.6%	1.9%
BJTF fit p_0	Background	Shape	—	9.7%	10.6%
Jet tag scale factors	Signal	Shape	—	3.6%	4.1%
Jet energy resolution	Signal	Shape	—	1.0%	0.4%
Jet energy scale	Signal	Shape	—	0.5%	1.4%
Pileup	Signal	Shape	—	0.0%	0.6%

Table 7: Table of systematic uncertainties for the dileptonic bHbZ and bZbZ channels for a simulated signal mass of 1400 GeV and branching fractions of $\mathcal{B}(\mathrm{B} \to \mathrm{bH}) = 40\%$, $\mathcal{B}(\mathrm{B} \to \mathrm{bZ}) = 40\%$, and $\mathcal{B}(\mathrm{B} \to \mathrm{tW}) = 20\%$.

Systematic	Signal/Background	Rate/Shape	3 jets	4 jets
$\mathrm{Z} \to \mathrm{ee}$ efficiency	Signal	Rate	0.8%	0.8%
$\mathrm{Z} \to \mu\mu$ efficiency	Signal	Rate	0.6%	0.6%
Electron trigger efficiency	Signal	Rate	0.4%	0.4%
Muon trigger efficiency	Signal	Rate	0.1%	0.1%
Luminosity	Signal	Rate	1.6%	1.6%
PDFs	Signal	Rate	2.0%	2.0%
QCD μ_R and μ_F scales	Signal	Rate	15.1%	15.1%
Dileptonic bHbZ event mode				
Background exponential fit	Background	Shape	24.4%	16.1%
Jet tag scale factors	Signal	Shape	6.9%	7.8%
Normalization factor mass dependence	Background	Rate	55.9%	7.1%
Normalization factor (b-tag/b-veto)	Background	Rate	14.4%	8.2%
Jet energy resolution	Signal	Shape	0.4%	1.3%
Jet energy scale	Signal	Shape	0.5%	2.5%
Lepton scale factors	Signal	Shape	12.4%	11.4%
Pileup	Signal	Shape	0.5%	1.1%
Trigger prefiring	Signal	Shape	0.3%	0.3%
Dileptonic bZbZ event mode				
Background exponential fit	Background	Shape	26.0%	20.1%
Jet tag scale factors	Signal	Shape	7.1%	8.0%
Normalization factor mass dependence	Background	Rate	4.6%	10.6%
Normalization factor (b-tag/b-veto)	Background	Rate	14.6%	9.4%
Jet energy resolution	Signal	Shape	0.4%	0.8%
Jet energy scale	Signal	Shape	0.2%	0.6%
Lepton scale factors	Signal	Shape	11.7%	11.6%
Pileup	Signal	Shape	0.5%	0.4%
Trigger prefiring	Signal	Shape	0.3%	0.3%

9 Results

The data distributions in each channel are fit with respect to the reconstructed VLQ mass, including the relevant systematic uncertainties listed in Tables 6 and 7 as nuisance parameters. Figures 14–16 show, for the hadronic category, the comparison of the distribution of the reconstructed VLQ mass, after the final optimized selection requirements have been applied, for data, expected background, and simulated signal events with VLQ masses of 1000, 1200, 1400, 1600, and 1800 GeV. Figure 17 shows the same comparison for selected channels in the leptonic category. Branching fractions of $\mathcal{B}(\mathrm{B} \to \mathrm{bH}) = 50\%$ and $\mathcal{B}(\mathrm{B} \to \mathrm{bZ}) = 50\%$ are assumed.

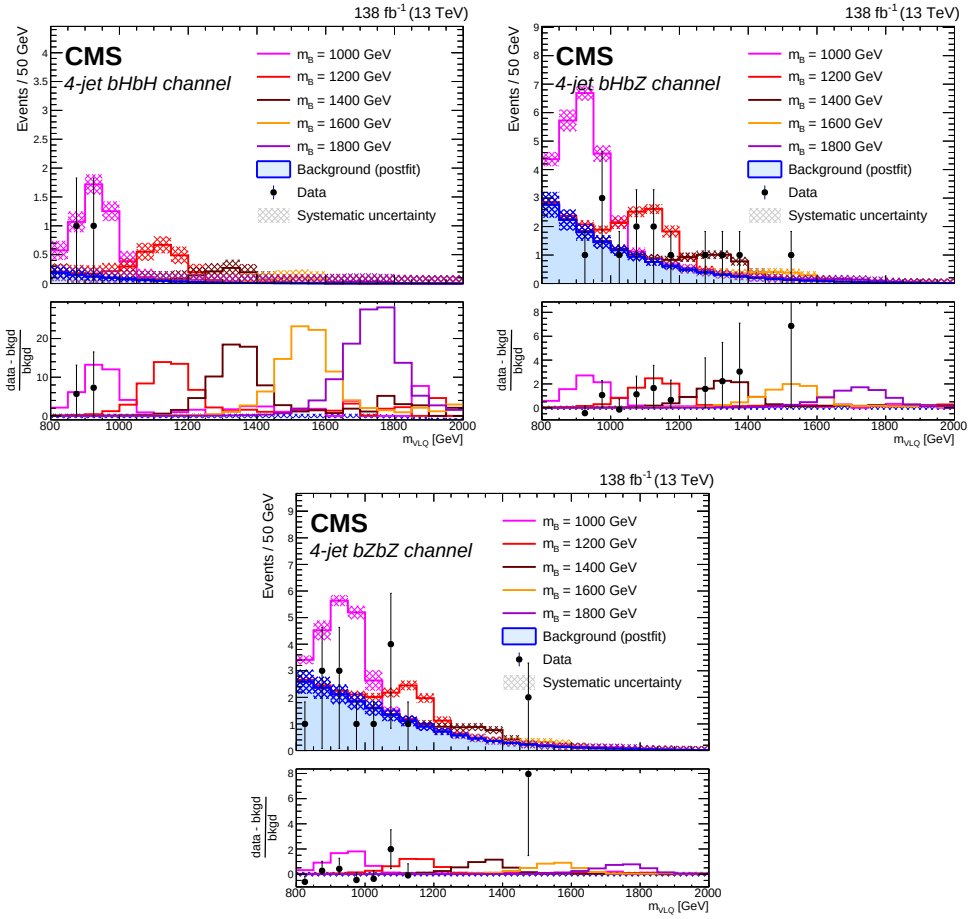

Figure 14: Distributions of reconstructed VLQ mass for expected postfit background (blue histogram), signal plus background (colored lines), and observed data (black points) for events in the hadronic category. The channels shown are 4-jet bHbH (upper left), 4-jet bHbZ (upper right), 4-jet bZbZ (lower center). Five signal masses are shown: 1000 (magenta), 1200 (red), 1400 (maroon), 1600 (orange), and 1800 GeV (purple). The signal distributions are normalized to the number of events estimated from the expected VLQ production cross section. The assumed branching fractions are $\mathcal{B}(\mathrm{B} \to \mathrm{bH}) = \mathcal{B}(\mathrm{B} \to \mathrm{bZ}) = 50\%$, $\mathcal{B}(\mathrm{B} \to \mathrm{tW}) = 0\%$. The background distribution is independent of the signal branching fractions. The hatched regions indicate the total systematic uncertainties in the background estimate.

No statistically significant excess of data over the background expectation is observed in this mass range. We set exclusion limits on the VLQ mass as a function of the branching fractions $\mathcal{B}(\mathrm{B} \to \mathrm{bH})$, $\mathcal{B}(\mathrm{B} \to \mathrm{bZ})$, and $\mathcal{B}(\mathrm{B} \to \mathrm{tW})$. The results for the fully hadronic and leptonic categories, and for all jet multiplicities and event modes, are combined to set the limits. The signal

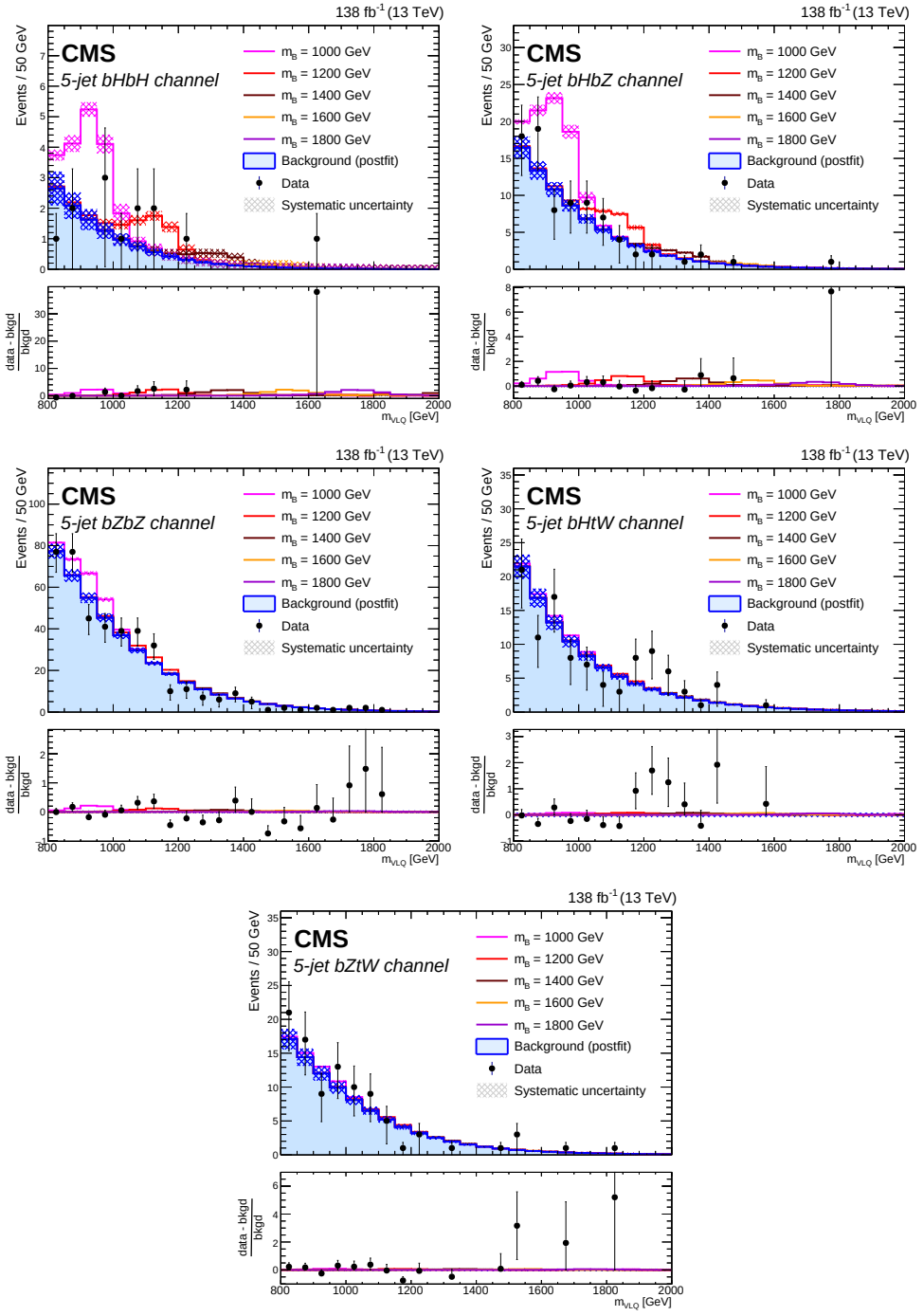

Figure 15: Distributions of reconstructed VLQ mass for expected postfit background (blue histogram), signal plus background (colored lines), and observed data (black points) for events in the hadronic category. The channels shown are 5-jet bHbH (upper left), 5-jet bHbZ (upper right), 5-jet bZbZ (middle left), 5-jet bHtW (middle right), and 5-jet bZtW (lower center). Five signal masses are shown: 1000 (magenta), 1200 (red), 1400 (maroon), 1600 (orange), and 1800 GeV (purple). The signal distributions are normalized to the number of events estimated from the expected VLQ production cross section. The assumed branching fractions are $\mathcal{B}(\mathrm{B} \to \mathrm{bH}) = \mathcal{B}(\mathrm{B} \to \mathrm{bZ}) = 50\%$, $\mathcal{B}(\mathrm{B} \to \mathrm{tW}) = 0\%$. The background distribution is independent of the signal branching fractions. The hatched regions indicate the total systematic uncertainties in the background estimate.

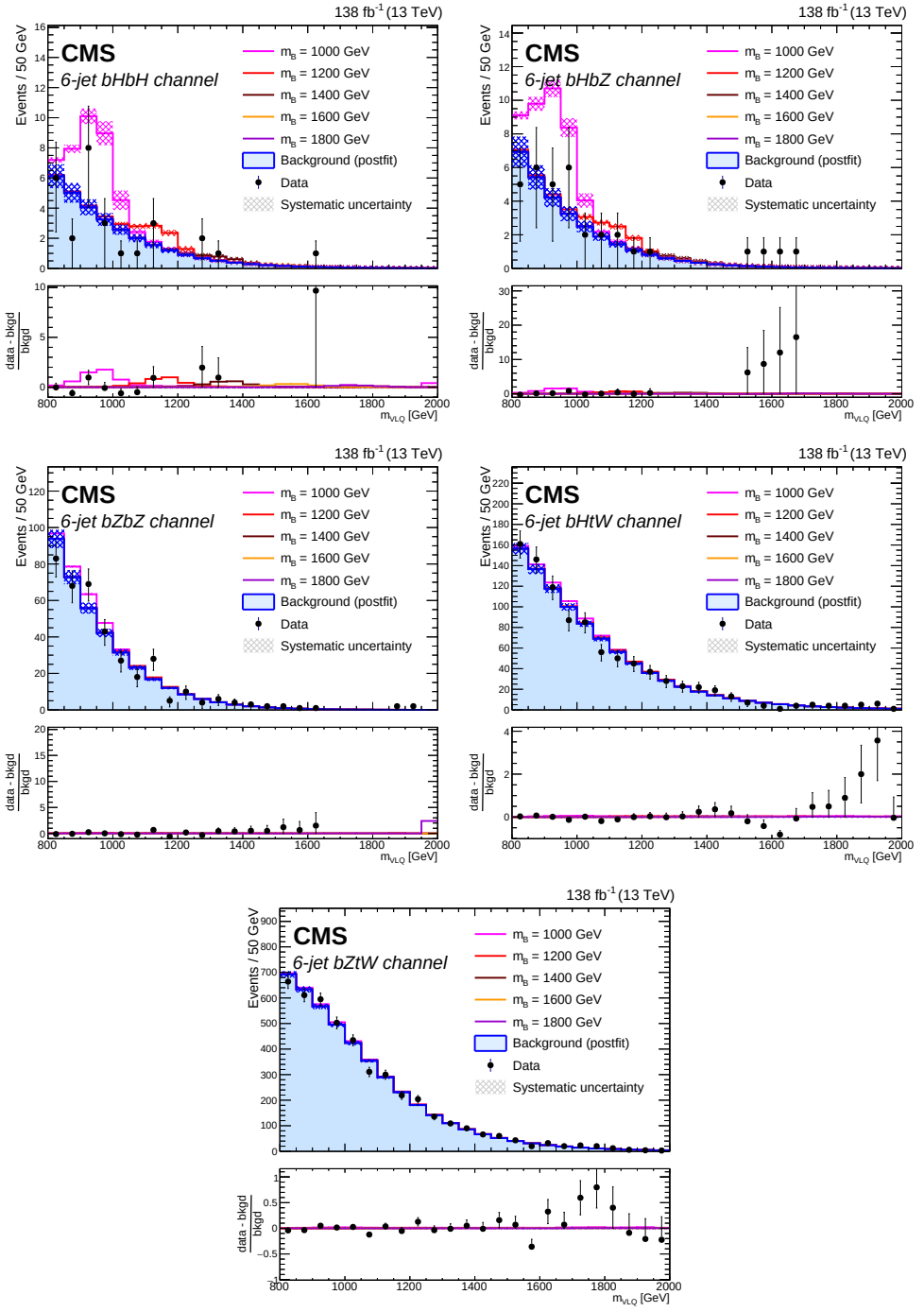

Figure 16: Distributions of reconstructed VLQ mass for expected postfit background (blue histogram), signal plus background (colored lines), and observed data (black points) for events in the hadronic category. The channels shown are 6-jet bHbH (upper left), 6-jet bHbZ (upper right), 6-jet bZbZ (middle left), 6-jet bHtW (middle right), and 6-jet bZtW (lower center). Five signal masses are shown: 1000 (magenta), 1200 (red), 1400 (maroon), 1600 (orange), and 1800 GeV (purple). The signal distributions are normalized to the number of events estimated from the expected VLQ production cross section. The assumed branching fractions are $\mathcal{B}(\mathrm{B} \to \mathrm{bH}) = \mathcal{B}(\mathrm{B} \to \mathrm{bZ}) = 50\%$, $\mathcal{B}(\mathrm{B} \to \mathrm{tW}) = 0\%$. The background distribution is independent of the signal branching fractions. The hatched regions indicate the total systematic uncertainties in the background estimate.

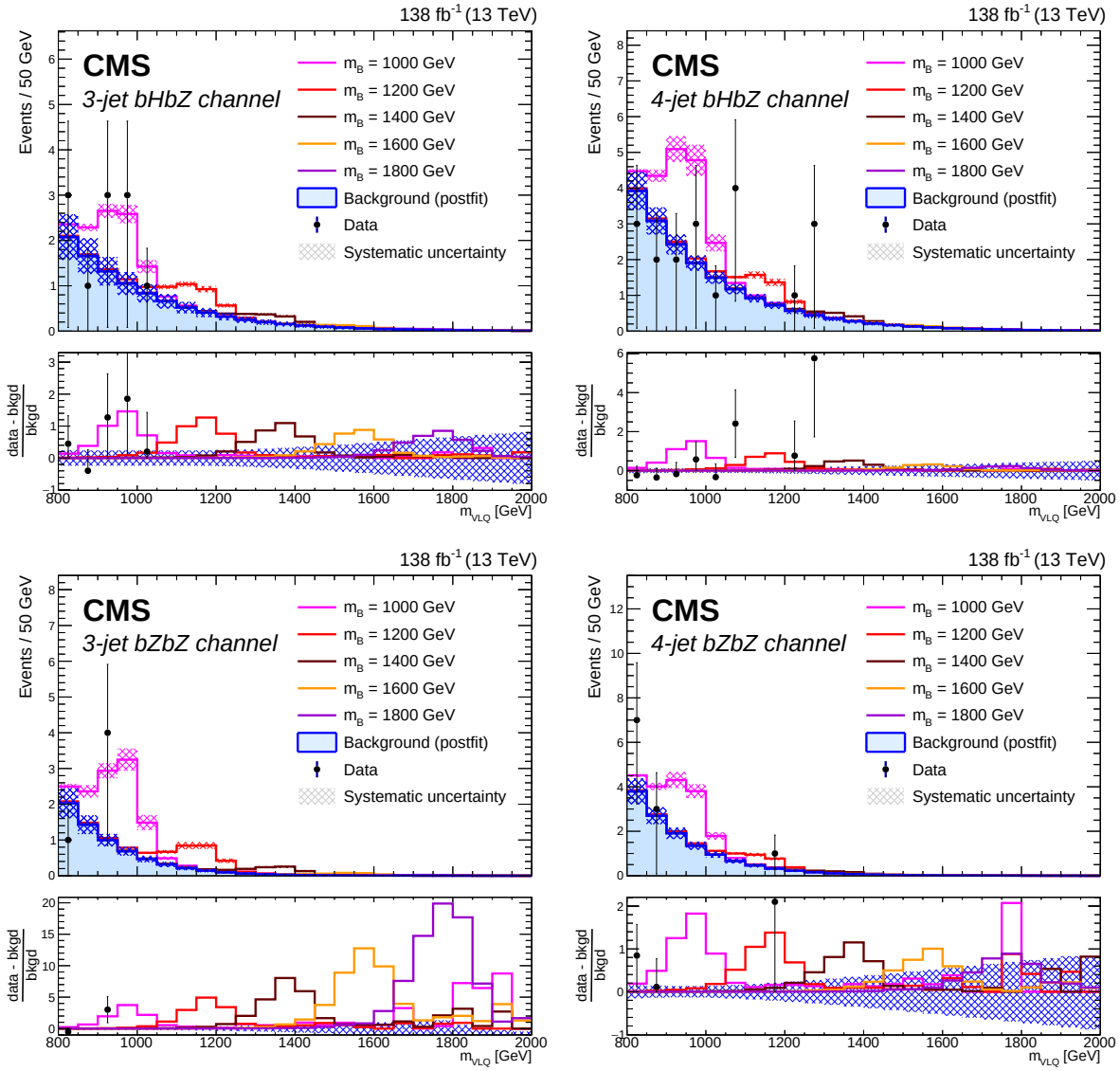

Figure 17: Distributions of reconstructed VLQ mass for expected postfit background (blue histogram), signal plus background (colored lines), and observed data (black points) for events in the leptonic category. The channels shown are 3-jet bHbZ (upper left), 4-jet bHbZ (upper right), 3-jet bZbZ (lower left), and 4-jet bZbZ (lower right). Five signal masses are shown: 1000 (magenta), 1200 (red), 1400 (maroon), 1600 (orange), and 1800 GeV (purple). The signal distributions are normalized to the number of events estimated from the expected VLQ production cross section. The assumed branching fractions are $\mathcal{B}(\mathrm{B} \to \mathrm{bH}) = \mathcal{B}(\mathrm{B} \to \mathrm{bZ}) = 50\%$, $\mathcal{B}(\mathrm{B} \to \mathrm{tW}) = 0\%$. The background distribution is independent of the signal branching fractions. The hatched regions indicate the total systematic uncertainties in the background estimate.

extraction procedure is based on a binned maximum likelihood fit, where each systematic uncertainty is incorporated as a nuisance parameter into the fit, with the effect of the systematic uncertainty included as a lognormal probability distribution per bin. The CL_s criterion [71, 72] is used to obtain a limit at 95% CL using the profile likelihood test statistic in the asymptotic approximation [73].

The exclusion limit on the VLQ mass is derived from the intersection of the limit curve with the predicted theoretical cross section as a function of the VLQ mass. Figure 18 shows the observed and expected limits at 95% CL on the cross section of VLQ pair production as functions of VLQ mass, for four representative branching fraction hypotheses: $\mathcal{B}(\mathrm{B} \to \mathrm{bH}) = 100\%$; $\mathcal{B}(\mathrm{B} \to \mathrm{bZ}) = 100\%$; $\mathcal{B}(\mathrm{B} \to \mathrm{bH}) = \mathcal{B}(\mathrm{B} \to \mathrm{bZ}) = 50\%$, corresponding to the TB doublet model with no Tt mixing and also to the large VLQ mass XTB triplet model; and $\mathcal{B}(\mathrm{B} \to \mathrm{bH}) = \mathcal{B}(\mathrm{B} \to \mathrm{bZ}) = 25\%$, $\mathcal{B}(\mathrm{B} \to \mathrm{tW}) = 50\%$, corresponding to the large VLQ mass TBY triplet model.

Figures 19 and 20 show the expected and observed exclusion limits, respectively, on VLQ mass as a function of $\mathcal{B}(\mathrm{B} \to \mathrm{bH})$ and $\mathcal{B}(\mathrm{B} \to \mathrm{tW})$, omitting points for which the exclusion limit is less than 1000 GeV. In the 100% $\mathrm{B} \to \mathrm{bZ}$ model, the limits on the B VLQ mass have been improved by 120 GeV compared to the previous best limits, set by ATLAS [24], and in the TB doublet model with no Tt mixing, the limits have been improved by 50 GeV compared to the previous best limits, set by CMS [22].

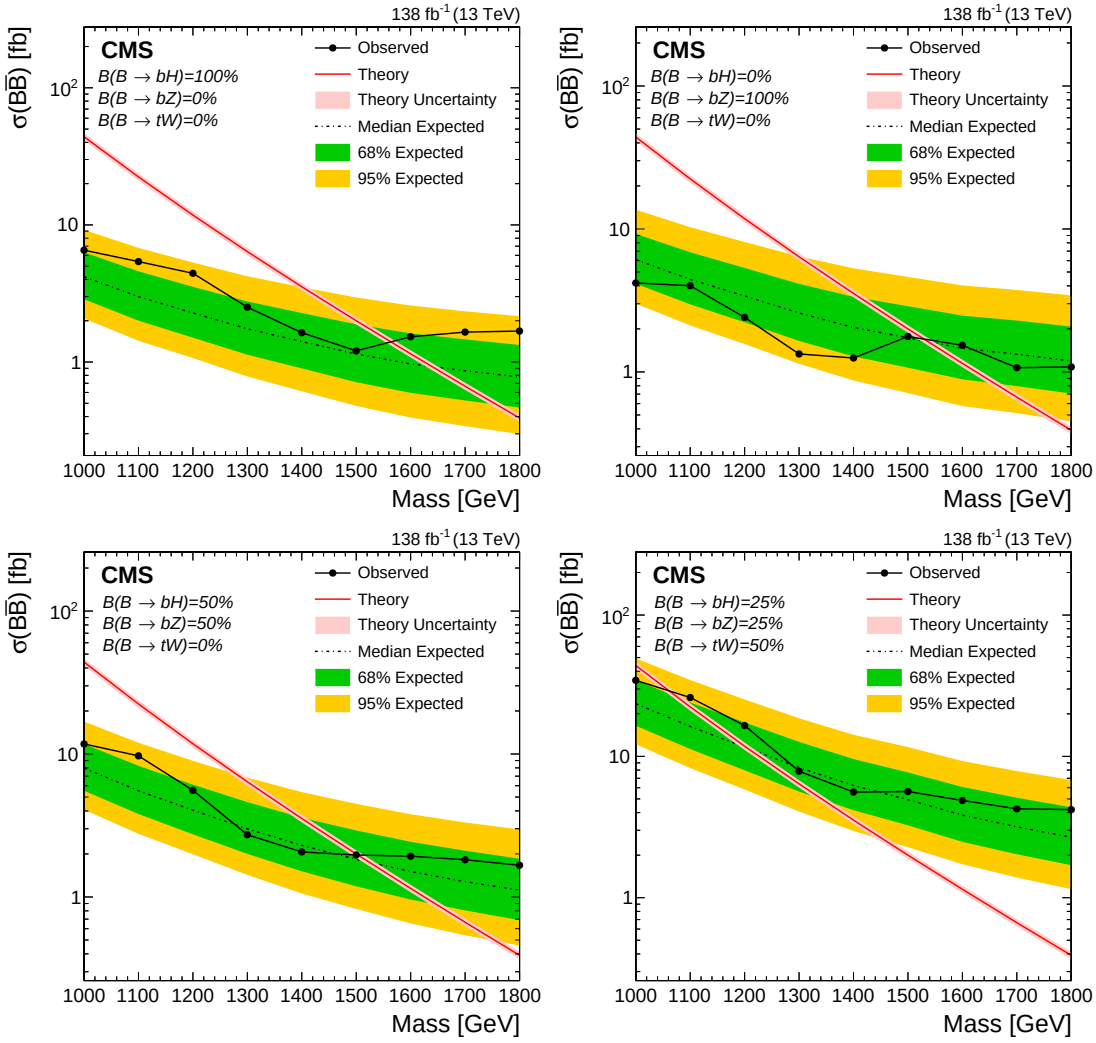

Figure 18: The limit at 95% CL on the cross section for VLQ pair production for four different branching fraction hypothesis: $\mathcal{B}(\mathrm{B} \to \mathrm{bH}) = 100\%$ (upper left), $\mathcal{B}(\mathrm{B} \to \mathrm{bZ}) = 100\%$ (upper right), $\mathcal{B}(\mathrm{B} \to \mathrm{bH}) = \mathcal{B}(\mathrm{B} \to \mathrm{bZ}) = 50\%$, corresponding to the TB doublet model with no Tt mixing and also to the large VLQ mass XTB triplet model (lower left), and $\mathcal{B}(\mathrm{B} \to \mathrm{bH}) = \mathcal{B}(\mathrm{B} \to \mathrm{bZ}) = 25\%$, $\mathcal{B}(\mathrm{B} \to \mathrm{tW}) = 50\%$, corresponding to the large VLQ mass TBY triplet model (lower right). The expected limit is shown as the dashed line, with the 68 and 95% uncertainties shown by the green (inner) and yellow (outer) bands, respectively. The theoretical cross section and its uncertainty are shown by the red line and light-red band.

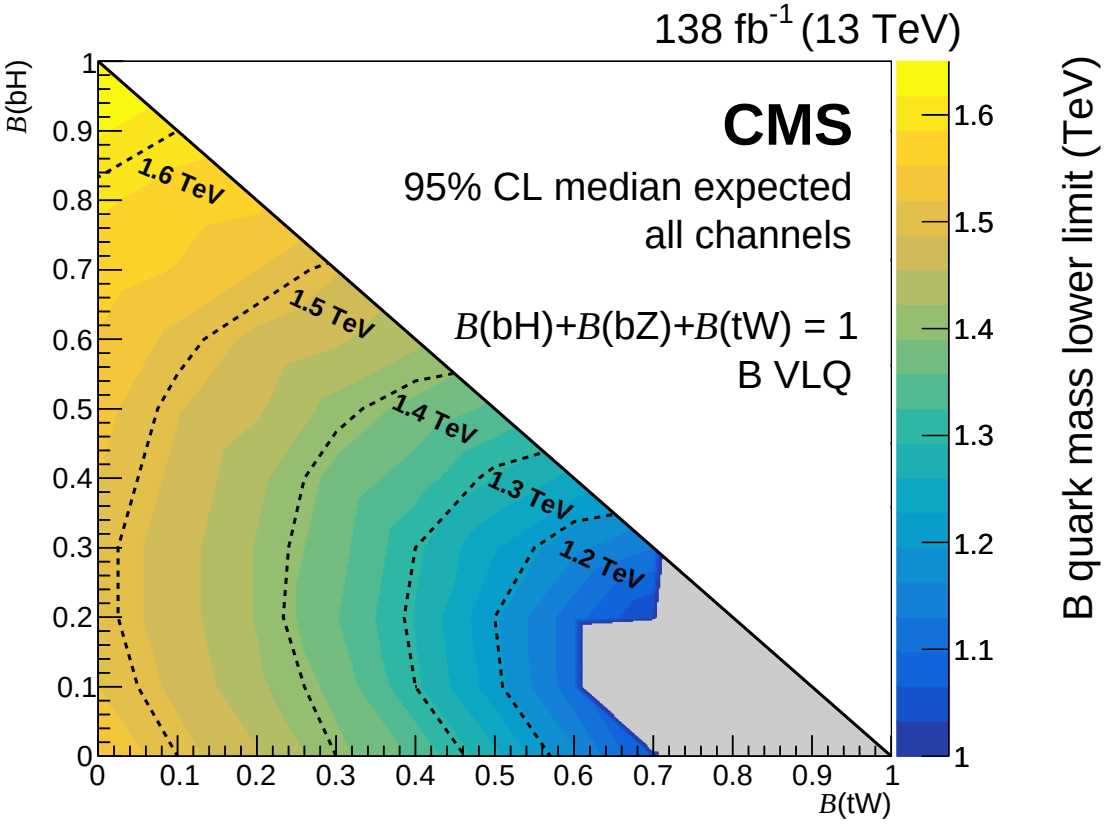

Figure 19: Median expected exclusion limits on the VLQ mass at 95% CL as a function of the branching fractions $\mathcal{B}(\mathrm{B} \to \mathrm{bH})$ and $\mathcal{B}(\mathrm{B} \to \mathrm{tW})$, with $\mathcal{B}(\mathrm{B} \to \mathrm{tW}) = 1 - \mathcal{B}(\mathrm{B} \to \mathrm{bH}) - \mathcal{B}(\mathrm{B} \to \mathrm{bZ})$. The gray area corresponds to the region where the exclusion limit is less than 1000 GeV.

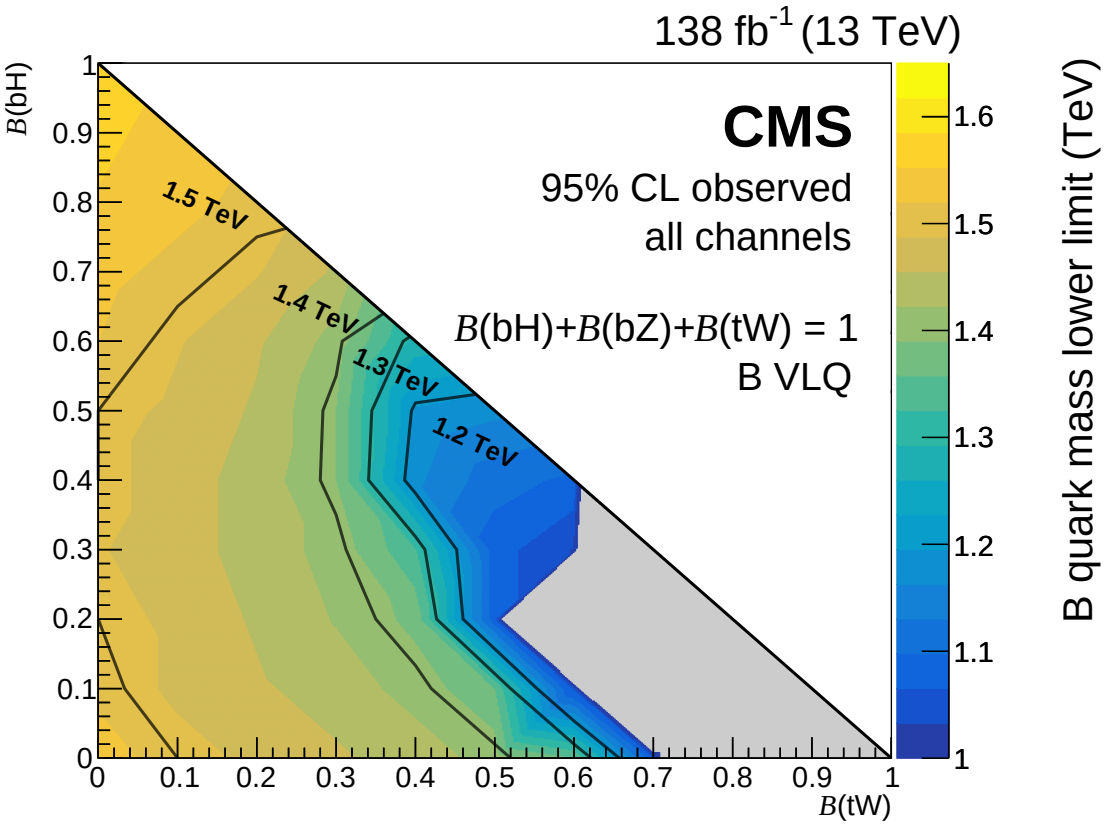

Figure 20: Observed exclusion limits on the VLQ mass at 95% CL as a function of the branching fractions $\mathcal{B}(\mathrm{B} \to \mathrm{bH})$ and $\mathcal{B}(\mathrm{B} \to \mathrm{tW})$, with $\mathcal{B}(\mathrm{B} \to \mathrm{tW}) = 1 - \mathcal{B}(\mathrm{B} \to \mathrm{bH}) - \mathcal{B}(\mathrm{B} \to \mathrm{bZ})$. The gray area corresponds to the region where the exclusion limit is less than 1000 GeV.

10 Summary

A search for bottom-type vector-like quarks (B VLQs) has been presented, using data from proton-proton collisions collected by the CMS detector in 2016–2018 at $\sqrt{s} = 13\,\text{TeV}$. Results are combined from the fully hadronic category, where each B VLQ decays into either a b quark and a Higgs boson (H), a b quark and a Z boson, or a t quark and a W boson, and the leptonic category, where each B VLQ decays into a b quark and either an H or a Z boson, and at least one decay includes a Z boson that decays into a pair of charged leptons. To account for the fact that the two jets from an H, Z, or W boson decay may be reconstructed separately, or may be merged into a single reconstructed jet due to a high Lorentz boost, events are separated into different jet multiplicity categories and reconstructed appropriately. Backgrounds are estimated from data and limits are set on the VLQ mass at 95% confidence level as a function of the branching fractions $\mathcal{B}(\text{B} \to \text{bH})$, $\mathcal{B}(\text{B} \to \text{bZ})$, and $\mathcal{B}(\text{B} \to \text{tW})$. The most significant improvement over previous results is an increased sensitivity for scenarios with large $\mathcal{B}(\text{B} \to \text{bZ})$ due to the inclusion of events with leptonic Z boson decays. The current results represent the most stringent limits on B VLQs to date.

Acknowledgments

We congratulate our colleagues in the CERN accelerator departments for the excellent performance of the LHC and thank the technical and administrative staffs at CERN and at other CMS institutes for their contributions to the success of the CMS effort. In addition, we gratefully acknowledge the computing centers and personnel of the Worldwide LHC Computing Grid and other centers for delivering so effectively the computing infrastructure essential to our analyses. Finally, we acknowledge the enduring support for the construction and operation of the LHC, the CMS detector, and the supporting computing infrastructure provided by the following funding agencies: SC (Armenia), BMBWF and FWF (Austria); FNRS and FWO (Belgium); CNPq, CAPES, FAPERJ, FAPERGS, and FAPESP (Brazil); MES and BNSF (Bulgaria); CERN; CAS, MoST, and NSFC (China); MINCIENCIAS (Colombia); MSES and CSF (Croatia); RIF (Cyprus); SENESCYT (Ecuador); ERC PRG, RVTT3 and MoER TK202 (Estonia); Academy of Finland, MEC, and HIP (Finland); CEA and CNRS/IN2P3 (France); SRNSF (Georgia); BMBF, DFG, and HGF (Germany); GSRI (Greece); NKFIH (Hungary); DAE and DST (India); IPM (Iran); SFI (Ireland); INFN (Italy); MSIP and NRF (Republic of Korea); MES (Latvia); LMTLT (Lithuania); MOE and UM (Malaysia); BUAP, CINVESTAV, CONACYT, LNS, SEP, and UASLP-FAI (Mexico); MOS (Montenegro); MBIE (New Zealand); PAEC (Pakistan); MES and NSC (Poland); FCT (Portugal); MESTD (Serbia); MCIN/AEI and PCTI (Spain); MOSTR (Sri Lanka); Swiss Funding Agencies (Switzerland); MST (Taipei); MHESI and NSTDA (Thailand); TUBITAK and TENMAK (Turkey); NASU (Ukraine); STFC (United Kingdom); DOE and NSF (USA).

Individuals have received support from the Marie-Curie programme and the European Research Council and Horizon 2020 Grant, contract Nos. 675440, 724704, 752730, 758316, 765710, 824093, 101115353, and COST Action CA16108 (European Union); the Leventis Foundation; the Alfred P. Sloan Foundation; the Alexander von Humboldt Foundation; the Science Committee, project no. 22rl-037 (Armenia); the Belgian Federal Science Policy Office; the Fonds pour la Formation à la Recherche dans l'Industrie et dans l'Agriculture (FRIA-Belgium); the Agentschap voor Innovatie door Wetenschap en Technologie (IWT-Belgium); the F.R.S.-FNRS and FWO (Belgium) under the "Excellence of Science – EOS" – be.h project n. 30820817; the Beijing Municipal Science & Technology Commission, No. Z191100007219010 and Fundamental Research Funds for the Central Universities (China); the Ministry of Education, Youth and Sports

(MEYS) of the Czech Republic; the Shota Rustaveli National Science Foundation, grant FR-22-985 (Georgia); the Deutsche Forschungsgemeinschaft (DFG), under Germany's Excellence Strategy – EXC 2121 "Quantum Universe" – 390833306, and under project number 400140256 - GRK2497; the Hellenic Foundation for Research and Innovation (HFRI), Project Number 2288 (Greece); the Hungarian Academy of Sciences, the New National Excellence Program - ÚNKP, the NKFIH research grants K 124845, K 124850, K 128713, K 128786, K 129058, K 131991, K 133046, K 138136, K 143460, K 143477, 2020-2.2.1-ED-2021-00181, and TKP2021-NKTA-64 (Hungary); the Council of Science and Industrial Research, India; ICSC – National Research Center for High Performance Computing, Big Data and Quantum Computing, funded by the EU NexGeneration program (Italy); the Latvian Council of Science; the Ministry of Education and Science, project no. 2022/WK/14, and the National Science Center, contracts Opus 2021/41/B/ST2/01369 and 2021/43/B/ST2/01552 (Poland); the Fundação para a Ciência e a Tecnologia, grant CEECIND/01334/2018 (Portugal); the National Priorities Research Program by Qatar National Research Fund; MCIN/AEI/10.13039/501100011033, ERDF "a way of making Europe", and the Programa Estatal de Fomento de la Investigación Científica y Técnica de Excelencia María de Maeztu, grant MDM-2017-0765 and Programa Severo Ochoa del Principado de Asturias (Spain); the Chulalongkorn Academic into Its 2nd Century Project Advancement Project, and the National Science, Research and Innovation Fund via the Program Management Unit for Human Resources & Institutional Development, Research and Innovation, grant B37G660013 (Thailand); the Kavli Foundation; the Nvidia Corporation; the SuperMicro Corporation; the Welch Foundation, contract C-1845; and the Weston Havens Foundation (USA).

References

[1] G. 't Hooft, "Naturalness, chiral symmetry, and spontaneous chiral symmetry breaking", *NATO Sci. Ser. B* **59** (1980) 135, doi:10.1007/978-1-4684-7571-5_9.

[2] ATLAS Collaboration, "Observation of a new particle in the search for the standard model Higgs boson with the ATLAS detector at the LHC", *Phys. Lett. B* **716** (2012) 1, doi:10.1016/j.physletb.2012.08.020, arXiv:1207.7214.

[3] CMS Collaboration, "Observation of a new boson at a mass of 125 GeV with the CMS experiment at the LHC", *Phys. Lett. B* **716** (2012) 30, doi:10.1016/j.physletb.2012.08.021, arXiv:1207.7235.

[4] CMS Collaboration, "Observation of a new boson with mass near 125 GeV in pp collisions at $\sqrt{s} = 7$ and 8 TeV", *JHEP* **06** (2013) 081, doi:10.1007/JHEP06(2013)081, arXiv:1303.4571.

[5] CMS Collaboration, "A measurement of the Higgs boson mass in the diphoton decay channel", *Phys. Lett. B* **805** (2020) 135425, doi:10.1016/j.physletb.2020.135425, arXiv:2002.06398.

[6] H. Georgi and A. Pais, "Calculability and naturalness in gauge theories", *Phys. Rev. D* **10** (1974) 539, doi:10.1103/PhysRevD.10.539.

[7] J. Wess and B. Zumino, "A Lagrangian model invariant under supergauge transformations", *Phys. Lett. B* **49** (1974) 52, doi:10.1016/0370-2693(74)90578-4.

[8] P. Fayet and S. Ferrara, "Supersymmetry", *Phys. Rept.* **32** (1977) 249, doi:10.1016/0370-1573(77)90066-7.

[9] D. B. Kaplan, H. Georgi, and S. Dimopoulos, "Composite Higgs scalars", *Phys. Lett. B* **136** (1984) 187, doi:10.1016/0370-2693(84)91178-X.

[10] K. Agashe, R. Contino, and A. Pomarol, "The minimal composite Higgs model", *Nucl. Phys. B* **719** (2005) 165, doi:10.1016/j.nuclphysb.2005.04.035, arXiv:hep-ph/0412089.

[11] N. Arkani-Hamed, A. G. Cohen, and H. Georgi, "Electroweak symmetry breaking from dimensional deconstruction", *Phys. Lett. B* **513** (2001) 232, doi:10.1016/S0370-2693(01)00741-9, arXiv:hep-ph/0105239.

[12] N. Arkani-Hamed, A. G. Cohen, E. Katz, and A. E. Nelson, "The littlest Higgs", *JHEP* **07** (2002) 034, doi:10.1088/1126-6708/2002/07/034, arXiv:hep-ph/0206021.

[13] M. Schmaltz, "Physics beyond the standard model (theory): Introducing the little Higgs", *Nucl. Phys. B Proc. Suppl.* **117** (2003) 40, doi:10.1016/S0920-5632(03)01409-9, arXiv:hep-ph/0210415.

[14] F. del Aguila and M. J. Bowick, "The possibility of new fermions with $\Delta I = 0$ mass", *Nucl. Phys. B* **224** (1983) 107, doi:10.1016/0550-3213(83)90316-4.

[15] ATLAS Collaboration, "Combined measurements of Higgs boson production and decay using up to 80 fb^{-1} of proton-proton collision data at $\sqrt{s} = 13$ TeV collected with the ATLAS experiment", *Phys. Rev. D* **101** (2020) 012002, doi:10.1103/PhysRevD.101.012002, arXiv:1909.02845.

[16] CMS Collaboration, "Measurement and interpretation of differential cross sections for Higgs boson production at $\sqrt{s} = 13$ TeV", *Phys. Lett. B* **792** (2019) 369, doi:10.1016/j.physletb.2019.03.059, arXiv:1812.06504.

[17] J. A. Aguilar-Saavedra, R. Benbrik, S. Heinemeyer, and M. Pérez-Victoria, "Handbook of vectorlike quarks: Mixing and single production", *Phys. Rev. D* **88** (2013) 094010, doi:10.1103/PhysRevD.88.094010, arXiv:1306.0572.

[18] A. Atre, M. Carena, T. Han, and J. Santiago, "Heavy quarks above the top at the Tevatron", *Phys. Rev. D* **79** (2009) 054018, doi:10.1103/PhysRevD.79.054018, arXiv:0806.3966.

[19] A. Atre et al., "Model-independent searches for new quarks at the LHC", *JHEP* **08** (2011) 080, doi:10.1007/JHEP08(2011)080, arXiv:1102.1987.

[20] F. del Aguila, M. Pérez-Victoria, and J. Santiago, "Observable contributions of new exotic quarks to quark mixing", *JHEP* **09** (2000) 011, doi:10.1088/1126-6708/2000/09/011, arXiv:hep-ph/0007316.

[21] J. A. Aguilar-Saavedra, "Mixing with vector-like quarks: constraints and expectations", *EPJ Web Conf.* **60** (2013) 16012, doi:10.1051/epjconf/20136016012, arXiv:1306.4432.

[22] CMS Collaboration, "A search for bottom-type, vector-like quark pair production in a fully hadronic final state in proton-proton collisions at $\sqrt{s} = 13$ TeV", *Phys. Rev. D* **102** (2020) 112004, doi:10.1103/PhysRevD.102.112004, arXiv:2008.09835.

[23] ATLAS Collaboration, "Combination of the searches for pair-produced vector-like partners of the third-generation quarks at $\sqrt{s} = 13$ TeV with the ATLAS detector", *Phys. Rev. Lett.* **121** (2018) 211801, doi:10.1103/PhysRevLett.121.211801, arXiv:1808.02343.

[24] ATLAS Collaboration, "Search for pair-production of vector-like quarks in pp collision events at $\sqrt{s} = 13$ TeV with at least one leptonically decaying Z boson and a third-generation quark with the ATLAS detector", *Phys. Lett. B* **843** (2023) 138019, doi:10.1016/j.physletb.2023.138019, arXiv:2210.15413.

[25] CMS Collaboration, "Precision luminosity measurement in proton-proton collisions at $\sqrt{s} = 13$ TeV in 2015 and 2016 at CMS", *Eur. Phys. J. C* **81** (2021) 800, doi:10.1140/epjc/s10052-021-09538-2, arXiv:2104.01927.

[26] CMS Collaboration, "CMS luminosity measurement for the 2017 data-taking period at $\sqrt{s}$ = 13 TeV", CMS Physics Analysis Summary CMS-PAS-LUM-17-004, 2018.

[27] CMS Collaboration, "CMS luminosity measurement for the 2018 data-taking period at $\sqrt{s} = 13$ TeV", CMS Physics Analysis Summary CMS-PAS-LUM-18-002, 2019.

[28] HEPData record for this analysis, 2023. doi:10.17182/hepdata.145997.

[29] CMS Collaboration, "Electron and photon reconstruction and identification with the CMS experiment at the CERN LHC", *JINST* **16** (2021) P05014, doi:10.1088/1748-0221/16/05/P05014, arXiv:2012.06888.

[30] CMS Collaboration, "ECAL 2016 refined calibration and Run2 summary plots", CMS Detector Performance Summary CMS-DP-2020-021, 2020.

[31] CMS Collaboration, "Performance of the CMS muon detector and muon reconstruction with proton-proton collisions at $\sqrt{s} = 13$ TeV", *JINST* **13** (2018) P06015, doi:10.1088/1748-0221/13/06/P06015, arXiv:1804.04528.

[32] CMS Collaboration, "Performance of the CMS Level-1 trigger in proton-proton collisions at $\sqrt{s} = 13$ TeV", *JINST* **15** (2020) P10017, doi:10.1088/1748-0221/15/10/P10017, arXiv:2006.10165.

[33] CMS Collaboration, "The CMS trigger system", *JINST* **12** (2017) P01020, doi:10.1088/1748-0221/12/01/P01020, arXiv:1609.02366.

[34] CMS Collaboration, "The CMS experiment at the CERN LHC", *JINST* **3** (2008) S08004, doi:10.1088/1748-0221/3/08/S08004.

[35] J. Alwall et al., "The automated computation of tree-level and next-to-leading order differential cross sections, and their matching to parton shower simulations", *JHEP* **07** (2014) 079, doi:10.1007/JHEP07(2014)079, arXiv:1405.0301.

[36] NNPDF Collaboration, "Parton distributions for the LHC Run II", *JHEP* **04** (2015) 040, doi:10.1007/JHEP04(2015)040, arXiv:1410.8849.

[37] NNPDF Collaboration, "Parton distributions from high-precision collider data", *Eur. Phys. J. C* **77** (2017) 663, doi:10.1140/epjc/s10052-017-5199-5, arXiv:1706.00428.

[38] T. Sjöstrand et al., "An introduction to PYTHIA 8.2", *Comput. Phys. Commun.* **191** (2015) 159, doi:10.1016/j.cpc.2015.01.024, arXiv:1410.3012.

[39] CMS Collaboration, "Event generator tunes obtained from underlying event and multiparton scattering measurements", *Eur. Phys. J. C* **76** (2016) 155, doi:10.1140/epjc/s10052-016-3988-x, arXiv:1512.00815.

[40] CMS Collaboration, "Extraction and validation of a new set of CMS PYTHIA8 tunes from underlying-event measurements", *Eur. Phys. J. C* **80** (2020) 4, doi:10.1140/epjc/s10052-019-7499-4, arXiv:1903.12179.

[41] M. Czakon, P. Fiedler, and A. Mitov, "Total top-quark pair-production cross section at hadron colliders through $O(\alpha_S^4)$", *Phys. Rev. Lett.* **110** (2013) 252004, doi:10.1103/PhysRevLett.110.252004, arXiv:1303.6254.

[42] M. Czakon and A. Mitov, "Top++: A program for the calculation of the top-pair cross-section at hadron colliders", *Comput. Phys. Commun.* **185** (2014) 2930, doi:10.1016/j.cpc.2014.06.021, arXiv:1112.5675.

[43] M. Cacciari et al., "Top-pair production at hadron colliders with next-to-next-to-leading logarithmic soft-gluon resummation", *Phys. Lett. B* **710** (2012) 612, doi:10.1016/j.physletb.2012.03.013, arXiv:1111.5869.

[44] M. R. Whalley, D. Bourilkov, and R. C. Group, "The Les Houches accord PDFs (LHAPDF) and LHAGLUE", in *HERA and the LHC: A workshop on the implications of HERA for LHC physics. Proceedings, Part B*, p. 575. 2005. arXiv:hep-ph/0508110.

[45] D. Bourilkov, R. C. Group, and M. R. Whalley, "LHAPDF: PDF use from the Tevatron to the LHC", in *TeV4LHC Workshop - 4th meeting Batavia, Illinois, October 20-22, 2005*. 2006. arXiv:hep-ph/0605240.

[46] CMS Collaboration, "Search for vector-like T and B quark pairs in final states with leptons at $\sqrt{s} = 13$ TeV", *JHEP* **08** (2018) 177, doi:10.1007/JHEP08(2018)177, arXiv:1805.04758.

[47] R. Frederix and S. Frixione, "Merging meets matching in MC@NLO", *JHEP* **12** (2012) 061, doi:10.1007/JHEP12(2012)061, arXiv:1209.6215.

[48] J. Alwall et al., "Comparative study of various algorithms for the merging of parton showers and matrix elements in hadronic collisions", *Eur. Phys. J. C* **53** (2008) 473, doi:10.1140/epjc/s10052-007-0490-5, arXiv:0706.2569.

[49] CMS Collaboration, "Measurement of the inelastic proton-proton cross section at $\sqrt{s} = 13$ TeV", *JHEP* **07** (2018) 161, doi:10.1007/JHEP07(2018)161, arXiv:1802.02613.

[50] GEANT4 Collaboration, "GEANT4—a simulation toolkit", *Nucl. Instrum. Meth. A* **506** (2003) 250, doi:10.1016/S0168-9002(03)01368-8.

[51] J. Allison et al., "Geant4 developments and applications", *IEEE Trans. Nucl. Sci.* **53** (2006) 270, doi:10.1109/TNS.2006.869826.

[52] CMS Collaboration, "Jet energy scale and resolution in the CMS experiment in pp collisions at 8 TeV", *JINST* **12** (2017) P02014, doi:10.1088/1748-0221/12/02/P02014, arXiv:1607.03663.

[53] CMS Collaboration, "Performance of the DeepJet b tagging algorithm using 41.9/fb of data from proton-proton collisions at 13 TeV with phase 1 CMS detector", CMS Detector Performance Summary CMS-DP-2018-058, 2018.

[54] CMS Collaboration, "Identification of heavy-flavour jets with the CMS detector in pp collisions at 13 TeV", *JINST* **13** (2018) P05011, doi:10.1088/1748-0221/13/05/P05011, arXiv:1712.07158.

[55] CMS Collaboration, "Particle-flow reconstruction and global event description with the CMS detector", *JINST* **12** (2017) P10003, doi:10.1088/1748-0221/12/10/P10003, arXiv:1706.04965.

[56] CMS Collaboration, "Technical proposal for the Phase-II upgrade of the Compact Muon Solenoid", CMS Technical Proposal CERN-LHCC-2015-010, CMS-TDR-15-02, 2015.

[57] M. Cacciari, G. P. Salam, and G. Soyez, "The anti-k_{T} jet clustering algorithm", *JHEP* **04** (2008) 063, doi:10.1088/1126-6708/2008/04/063, arXiv:0802.1189.

[58] M. Cacciari, G. P. Salam, and G. Soyez, "FastJet user manual", *Eur. Phys. J. C* **72** (2012) 1896, doi:10.1140/epjc/s10052-012-1896-2, arXiv:1111.6097.

[59] CMS Collaboration, "Pileup mitigation at CMS in 13 TeV data", *JINST* **15** (2020) P09018, doi:10.1088/1748-0221/15/09/p09018, arXiv:2003.00503.

[60] D. Bertolini, P. Harris, M. Low, and N. Tran, "Pileup per particle identification", *JHEP* **10** (2014) 059, doi:10.1007/JHEP10(2014)059, arXiv:1407.6013.

[61] Y. L. Dokshitzer, G. D. Leder, S. Moretti, and B. R. Webber, "Better jet clustering algorithms", *JHEP* **08** (1997) 001, doi:10.1088/1126-6708/1997/08/001, arXiv:hep-ph/9707323.

[62] M. Wobisch and T. Wengler, "Hadronization corrections to jet cross-sections in deep inelastic scattering", in *Proceedings of the Workshop on Monte Carlo Generators for HERA Physics, Hamburg, Germany*, p. 270. 1998. arXiv:hep-ph/9907280.

[63] M. Dasgupta, A. Fregoso, S. Marzani, and G. P. Salam, "Towards an understanding of jet substructure", *JHEP* **09** (2013) 029, doi:10.1007/JHEP09(2013)029, arXiv:1307.0007.

[64] J. M. Butterworth, A. R. Davison, M. Rubin, and G. P. Salam, "Jet substructure as a new Higgs search channel at the LHC", *Phys. Rev. Lett.* **100** (2008) 242001, doi:10.1103/PhysRevLett.100.242001, arXiv:0802.2470.

[65] A. J. Larkoski, S. Marzani, G. Soyez, and J. Thaler, "Soft drop", *JHEP* **05** (2014) 146, doi:10.1007/JHEP05(2014)146, arXiv:1402.2657.

[66] E. Bols et al., "Jet flavour classification using DeepJet", *JINST* **15** (2020) P12012, doi:10.1088/1748-0221/15/12/P12012, arXiv:2008.10519.

[67] CMS Collaboration, "Search for pair production of vectorlike quarks in the fully hadronic final state", *Phys. Rev. D* **100** (2019) 072001, doi:10.1103/PhysRevD.100.072001, arXiv:1906.11903.

[68] ATLAS Collaboration, "Search for pair production of heavy vector-like quarks decaying into hadronic final states in pp collisions at $\sqrt{s} = 13$ TeV with the ATLAS detector", *Phys. Rev. D* **98** (2018) 092005, doi:10.1103/PhysRevD.98.092005, arXiv:1808.01771.

[69] J. Butterworth et al., "PDF4LHC recommendations for LHC Run II", *J. Phys. G* **43** (2016) 023001, doi:10.1088/0954-3899/43/2/023001, arXiv:1510.03865.

[70] S. Catani, D. de Florian, M. Grazzini, and P. Nason, "Soft gluon resummation for Higgs boson production at hadron colliders", *JHEP* **07** (2003) 028, doi:10.1088/1126-6708/2003/07/028, arXiv:hep-ph/0306211.

[71] T. Junk, "Confidence level computation for combining searches with small statistics", *Nucl. Instrum. Meth. A* **434** (1999) 435, doi:10.1016/S0168-9002(99)00498-2, arXiv:hep-ex/9902006.

[72] A. L. Read, "Presentation of search results: The CL_s technique", *J. Phys. G* **28** (2002) 2693, doi:10.1088/0954-3899/28/10/313.

[73] G. Cowan, K. Cranmer, E. Gross, and O. Vitells, "Asymptotic formulae for likelihood-based tests of new physics", *Eur. Phys. J. C* **71** (2011) 1554, doi:10.1140/epjc/s10052-011-1554-0, arXiv:1007.1727. [Erratum: doi:10.1140/epjc/s10052-013-2501-z].

A The CMS Collaboration

Yerevan Physics Institute, Yerevan, Armenia
A. Hayrapetyan, A. Tumasyan[1]

Institut für Hochenergiephysik, Vienna, Austria
W. Adam, J.W. Andrejkovic, T. Bergauer, S. Chatterjee, K. Damanakis, M. Dragicevic, P.S. Hussain, M. Jeitler[2], N. Krammer, A. Li, D. Liko, I. Mikulec, J. Schieck[2], R. Schöfbeck, D. Schwarz, M. Sonawane, S. Templ, W. Waltenberger, C.-E. Wulz[2]

Universiteit Antwerpen, Antwerpen, Belgium
M.R. Darwish[3], T. Janssen, P. Van Mechelen

Vrije Universiteit Brussel, Brussel, Belgium
E.S. Bols, J. D'Hondt, S. Dansana, A. De Moor, M. Delcourt, H. El Faham, S. Lowette, I. Makarenko, D. Müller, A.R. Sahasransu, S. Tavernier, M. Tytgat[4], G.P. Van Onsem, S. Van Putte, D. Vannerom

Université Libre de Bruxelles, Bruxelles, Belgium
B. Clerbaux, A.K. Das, G. De Lentdecker, L. Favart, D. Hohov, J. Jaramillo, A. Khalilzadeh, K. Lee, M. Mahdavikhorrami, A. Malara, S. Paredes, L. Pétré, N. Postiau, L. Thomas, M. Vanden Bemden, C. Vander Velde, P. Vanlaer

Ghent University, Ghent, Belgium
M. De Coen, D. Dobur, Y. Hong, J. Knolle, L. Lambrecht, G. Mestdach, K. Mota Amarilo, C. Rendón, A. Samalan, K. Skovpen, N. Van Den Bossche, J. van der Linden, L. Wezenbeek

Université Catholique de Louvain, Louvain-la-Neuve, Belgium
A. Benecke, A. Bethani, G. Bruno, C. Caputo, C. Delaere, I.S. Donertas, A. Giammanco, K. Jaffel, Sa. Jain, V. Lemaitre, J. Lidrych, P. Mastrapasqua, K. Mondal, T.T. Tran, S. Wertz

Centro Brasileiro de Pesquisas Fisicas, Rio de Janeiro, Brazil
G.A. Alves, E. Coelho, C. Hensel, T. Menezes De Oliveira, A. Moraes, P. Rebello Teles, M. Soeiro

Universidade do Estado do Rio de Janeiro, Rio de Janeiro, Brazil
W.L. Aldá Júnior, M. Alves Gallo Pereira, M. Barroso Ferreira Filho, H. Brandao Malbouisson, W. Carvalho, J. Chinellato[5], E.M. Da Costa, G.G. Da Silveira[6], D. De Jesus Damiao, S. Fonseca De Souza, R. Gomes De Souza, J. Martins[7], C. Mora Herrera, L. Mundim, H. Nogima, A. Santoro, A. Sznajder, M. Thiel, A. Vilela Pereira

Universidade Estadual Paulista, Universidade Federal do ABC, São Paulo, Brazil
C.A. Bernardes[6], L. Calligaris, T.R. Fernandez Perez Tomei, E.M. Gregores, P.G. Mercadante, S.F. Novaes, B. Orzari, Sandra S. Padula

Institute for Nuclear Research and Nuclear Energy, Bulgarian Academy of Sciences, Sofia, Bulgaria
A. Aleksandrov, G. Antchev, R. Hadjiiska, P. Iaydjiev, M. Misheva, M. Shopova, G. Sultanov

University of Sofia, Sofia, Bulgaria

A. Dimitrov, L. Litov, B. Pavlov, P. Petkov, A. Petrov, E. Shumka

Instituto De Alta Investigación, Universidad de Tarapacá, Casilla 7 D, Arica, Chile
S. Keshri, S. Thakur

Beihang University, Beijing, China
T. Cheng, Q. Guo, T. Javaid, L. Yuan

Department of Physics, Tsinghua University, Beijing, China
Z. Hu, J. Liu, K. Yi[8,9]

Institute of High Energy Physics, Beijing, China
G.M. Chen[10], H.S. Chen[10], M. Chen[10], F. Iemmi, C.H. Jiang, A. Kapoor[11], H. Liao, Z.-A. Liu[12], R. Sharma[13], J.N. Song[12], J. Tao, C. Wang[10], J. Wang, Z. Wang[10], H. Zhang

State Key Laboratory of Nuclear Physics and Technology, Peking University, Beijing, China
A. Agapitos, Y. Ban, A. Levin, C. Li, Q. Li, Y. Mao, S.J. Qian, X. Sun, D. Wang, H. Yang, L. Zhang, C. Zhou

Sun Yat-Sen University, Guangzhou, China
Z. You

University of Science and Technology of China, Hefei, China
N. Lu

Nanjing Normal University, Nanjing, China
G. Bauer[14]

Institute of Modern Physics and Key Laboratory of Nuclear Physics and Ion-beam Application (MOE) - Fudan University, Shanghai, China
X. Gao[15], D. Leggat, H. Okawa

Zhejiang University, Hangzhou, Zhejiang, China
Z. Lin, C. Lu, M. Xiao

Universidad de Los Andes, Bogota, Colombia
C. Avila, D.A. Barbosa Trujillo, A. Cabrera, C. Florez, J. Fraga, J.A. Reyes Vega

Universidad de Antioquia, Medellin, Colombia
J. Mejia Guisao, F. Ramirez, M. Rodriguez, J.D. Ruiz Alvarez

University of Split, Faculty of Electrical Engineering, Mechanical Engineering and Naval Architecture, Split, Croatia
D. Giljanovic, N. Godinovic, D. Lelas, A. Sculac

University of Split, Faculty of Science, Split, Croatia
M. Kovac, T. Sculac[16]

Institute Rudjer Boskovic, Zagreb, Croatia
P. Bargassa, V. Brigljevic, B.K. Chitroda, D. Ferencek, S. Mishra, A. Starodumov[17], T. Susa

University of Cyprus, Nicosia, Cyprus
A. Attikis, K. Christoforou, S. Konstantinou, J. Mousa, C. Nicolaou, F. Ptochos, P.A. Razis, H. Rykaczewski, H. Saka, A. Stepennov

Charles University, Prague, Czech Republic

M. Finger, M. Finger Jr., A. Kveton

Escuela Politecnica Nacional, Quito, Ecuador
E. Ayala

Universidad San Francisco de Quito, Quito, Ecuador
E. Carrera Jarrin

Academy of Scientific Research and Technology of the Arab Republic of Egypt, Egyptian Network of High Energy Physics, Cairo, Egypt
Y. Assran[18,19], S. Elgammal[19]

Center for High Energy Physics (CHEP-FU), Fayoum University, El-Fayoum, Egypt
M.A. Mahmoud, Y. Mohammed

National Institute of Chemical Physics and Biophysics, Tallinn, Estonia
K. Ehataht, M. Kadastik, T. Lange, S. Nandan, C. Nielsen, J. Pata, M. Raidal, L. Tani, C. Veelken

Department of Physics, University of Helsinki, Helsinki, Finland
H. Kirschenmann, K. Osterberg, M. Voutilainen

Helsinki Institute of Physics, Helsinki, Finland
S. Bharthuar, E. Brücken, F. Garcia, K.T.S. Kallonen, R. Kinnunen, T. Lampén, K. Lassila-Perini, S. Lehti, T. Lindén, L. Martikainen, M. Myllymäki, M.m. Rantanen, H. Siikonen, E. Tuominen, J. Tuominiemi

Lappeenranta-Lahti University of Technology, Lappeenranta, Finland
P. Luukka, H. Petrow

IRFU, CEA, Université Paris-Saclay, Gif-sur-Yvette, France
M. Besancon, F. Couderc, M. Dejardin, D. Denegri, J.L. Faure, F. Ferri, S. Ganjour, P. Gras, G. Hamel de Monchenault, V. Lohezic, J. Malcles, J. Rander, A. Rosowsky, M.Ö. Sahin, A. Savoy-Navarro[20], P. Simkina, M. Titov, M. Tornago

Laboratoire Leprince-Ringuet, CNRS/IN2P3, Ecole Polytechnique, Institut Polytechnique de Paris, Palaiseau, France
C. Baldenegro Barrera, F. Beaudette, A. Buchot Perraguin, P. Busson, A. Cappati, C. Charlot, F. Damas, O. Davignon, A. De Wit, B.A. Fontana Santos Alves, S. Ghosh, A. Gilbert, R. Granier de Cassagnac, A. Hakimi, B. Harikrishnan, L. Kalipoliti, G. Liu, J. Motta, M. Nguyen, C. Ochando, L. Portales, R. Salerno, J.B. Sauvan, Y. Sirois, A. Tarabini, E. Vernazza, A. Zabi, A. Zghiche

Université de Strasbourg, CNRS, IPHC UMR 7178, Strasbourg, France
J.-L. Agram[21], J. Andrea, D. Apparu, D. Bloch, J.-M. Brom, E.C. Chabert, C. Collard, S. Falke, U. Goerlach, C. Grimault, R. Haeberle, A.-C. Le Bihan, M. Meena, G. Saha, M.A. Sessini, P. Van Hove

Institut de Physique des 2 Infinis de Lyon (IP2I), Villeurbanne, France
S. Beauceron, B. Blancon, G. Boudoul, N. Chanon, J. Choi, D. Contardo, P. Depasse, C. Dozen[22], H. El Mamouni, J. Fay, S. Gascon, M. Gouzevitch, C. Greenberg, G. Grenier, B. Ille, I.B. Laktineh, M. Lethuillier, L. Mirabito, S. Perries, A. Purohit, M. Vander Donckt, P. Verdier, J. Xiao

Georgian Technical University, Tbilisi, Georgia
G. Adamov, I. Lomidze, Z. Tsamalaidze[17]

RWTH Aachen University, I. Physikalisches Institut, Aachen, Germany
V. Botta, L. Feld, K. Klein, M. Lipinski, D. Meuser, A. Pauls, N. Röwert, M. Teroerde

RWTH Aachen University, III. Physikalisches Institut A, Aachen, Germany
S. Diekmann, A. Dodonova, N. Eich, D. Eliseev, F. Engelke, J. Erdmann, M. Erdmann, P. Fackeldey, B. Fischer, T. Hebbeker, K. Hoepfner, F. Ivone, A. Jung, M.y. Lee, L. Mastrolorenzo, F. Mausolf, M. Merschmeyer, A. Meyer, S. Mukherjee, D. Noll, A. Novak, F. Nowotny, A. Pozdnyakov, Y. Rath, W. Redjeb, F. Rehm, H. Reithler, U. Sarkar, V. Sarkisovi, A. Schmidt, A. Sharma, J.L. Spah, A. Stein, F. Torres Da Silva De Araujo[23], L. Vigilante, S. Wiedenbeck, S. Zaleski

RWTH Aachen University, III. Physikalisches Institut B, Aachen, Germany
C. Dziwok, G. Flügge, W. Haj Ahmad[24], T. Kress, A. Nowack, O. Pooth, A. Stahl, T. Ziemons, A. Zotz

Deutsches Elektronen-Synchrotron, Hamburg, Germany
H. Aarup Petersen, M. Aldaya Martin, J. Alimena, S. Amoroso, Y. An, S. Baxter, M. Bayatmakou, H. Becerril Gonzalez, O. Behnke, A. Belvedere, S. Bhattacharya, F. Blekman[25], K. Borras[26], A. Campbell, A. Cardini, C. Cheng, F. Colombina, S. Consuegra Rodríguez, G. Correia Silva, M. De Silva, G. Eckerlin, D. Eckstein, L.I. Estevez Banos, O. Filatov, E. Gallo[25], A. Geiser, A. Giraldi, G. Greau, V. Guglielmi, M. Guthoff, A. Hinzmann, A. Jafari[27], L. Jeppe, N.Z. Jomhari, B. Kaech, M. Kasemann, C. Kleinwort, R. Kogler, M. Komm, D. Krücker, W. Lange, D. Leyva Pernia, K. Lipka[28], W. Lohmann[29], R. Mankel, I.-A. Melzer-Pellmann, M. Mendizabal Morentin, A.B. Meyer, G. Milella, A. Mussgiller, L.P. Nair, A. Nürnberg, Y. Otarid, J. Park, D. Pérez Adán, E. Ranken, A. Raspereza, B. Ribeiro Lopes, J. Rübenach, A. Saggio, M. Scham[30,26], S. Schnake[26], P. Schütze, C. Schwanenberger[25], D. Selivanova, K. Sharko, M. Shchedrolosiev, R.E. Sosa Ricardo, D. Stafford, F. Vazzoler, A. Ventura Barroso, R. Walsh, Q. Wang, Y. Wen, K. Wichmann, L. Wiens[26], C. Wissing, Y. Yang, A. Zimermmane Castro Santos

University of Hamburg, Hamburg, Germany
A. Albrecht, S. Albrecht, M. Antonello, S. Bein, L. Benato, M. Bonanomi, P. Connor, M. Eich, K. El Morabit, Y. Fischer, A. Fröhlich, C. Garbers, E. Garutti, A. Grohsjean, M. Hajheidari, J. Haller, H.R. Jabusch, G. Kasieczka, P. Keicher, R. Klanner, W. Korcari, T. Kramer, V. Kutzner, F. Labe, J. Lange, A. Lobanov, C. Matthies, A. Mehta, L. Moureaux, M. Mrowietz, A. Nigamova, Y. Nissan, A. Paasch, K.J. Pena Rodriguez, T. Quadfasel, B. Raciti, M. Rieger, D. Savoiu, J. Schindler, P. Schleper, M. Schröder, J. Schwandt, M. Sommerhalder, H. Stadie, G. Steinbrück, A. Tews, M. Wolf

Karlsruher Institut fuer Technologie, Karlsruhe, Germany
S. Brommer, M. Burkart, E. Butz, T. Chwalek, A. Dierlamm, A. Droll, N. Faltermann, M. Giffels, A. Gottmann, F. Hartmann[31], R. Hofsaess, M. Horzela, U. Husemann, J. Kieseler, M. Klute, R. Koppenhöfer, J.M. Lawhorn, M. Link, A. Lintuluoto, S. Maier, S. Mitra, M. Mormile, Th. Müller, M. Neukum, M. Oh, M. Presilla, G. Quast, K. Rabbertz, B. Regnery, N. Shadskiy, I. Shvetsov, H.J. Simonis, M. Toms, N. Trevisani, R. Ulrich, R.F. Von Cube, M. Wassmer, S. Wieland, F. Wittig, R. Wolf, X. Zuo

Institute of Nuclear and Particle Physics (INPP), NCSR Demokritos, Aghia Paraskevi, Greece
G. Anagnostou, G. Daskalakis, A. Kyriakis, A. Papadopoulos[31], A. Stakia

National and Kapodistrian University of Athens, Athens, Greece
P. Kontaxakis, G. Melachroinos, A. Panagiotou, I. Papavergou, I. Paraskevas, N. Saoulidou, K. Theofilatos, E. Tziaferi, K. Vellidis, I. Zisopoulos

National Technical University of Athens, Athens, Greece
G. Bakas, T. Chatzistavrou, G. Karapostoli, K. Kousouris, I. Papakrivopoulos, E. Siamarkou, G. Tsipolitis, A. Zacharopoulou

University of Ioánnina, Ioánnina, Greece
K. Adamidis, I. Bestintzanos, I. Evangelou, C. Foudas, P. Gianneios, C. Kamtsikis, P. Katsoulis, P. Kokkas, P.G. Kosmoglou Kioseoglou, N. Manthos, I. Papadopoulos, J. Strologas

HUN-REN Wigner Research Centre for Physics, Budapest, Hungary
M. Bartók[32], C. Hajdu, D. Horvath[33,34], F. Sikler, V. Veszpremi

MTA-ELTE Lendület CMS Particle and Nuclear Physics Group, Eötvös Loránd University, Budapest, Hungary
M. Csanád, K. Farkas, M.M.A. Gadallah[35], Á. Kadlecsik, P. Major, K. Mandal, G. Pásztor, A.J. Rádl[36], G.I. Veres

Faculty of Informatics, University of Debrecen, Debrecen, Hungary
P. Raics, B. Ujvari, G. Zilizi

Institute of Nuclear Research ATOMKI, Debrecen, Hungary
G. Bencze, S. Czellar, J. Molnar, Z. Szillasi

Karoly Robert Campus, MATE Institute of Technology, Gyongyos, Hungary
T. Csorgo[36], F. Nemes[36], T. Novak

Panjab University, Chandigarh, India
J. Babbar, S. Bansal, S.B. Beri, V. Bhatnagar, G. Chaudhary, S. Chauhan, N. Dhingra[37], A. Kaur, A. Kaur, H. Kaur, M. Kaur, S. Kumar, K. Sandeep, T. Sheokand, J.B. Singh, A. Singla

University of Delhi, Delhi, India
A. Ahmed, A. Bhardwaj, A. Chhetri, B.C. Choudhary, A. Kumar, A. Kumar, M. Naimuddin, K. Ranjan, S. Saumya

Saha Institute of Nuclear Physics, HBNI, Kolkata, India
S. Baradia, S. Barman[38], S. Bhattacharya, S. Dutta, S. Dutta, P. Palit, S. Sarkar

Indian Institute of Technology Madras, Madras, India
M.M. Ameen, P.K. Behera, S.C. Behera, S. Chatterjee, P. Jana, P. Kalbhor, J.R. Komaragiri[39], D. Kumar[39], L. Panwar[39], P.R. Pujahari, N.R. Saha, A. Sharma, A.K. Sikdar, S. Verma

Tata Institute of Fundamental Research-A, Mumbai, India
S. Dugad, M. Kumar, G.B. Mohanty, P. Suryadevara

Tata Institute of Fundamental Research-B, Mumbai, India
A. Bala, S. Banerjee, R.M. Chatterjee, R.K. Dewanjee[40], M. Guchait, Sh. Jain,

S. Karmakar, S. Kumar, G. Majumder, K. Mazumdar, S. Parolia, A. Thachayath

National Institute of Science Education and Research, An OCC of Homi Bhabha National Institute, Bhubaneswar, Odisha, India
S. Bahinipati[41], C. Kar, D. Maity[42], P. Mal, T. Mishra, V.K. Muraleedharan Nair Bindhu[42], K. Naskar[42], A. Nayak[42], P. Sadangi, P. Saha, S.K. Swain, S. Varghese[42], D. Vats[42]

Indian Institute of Science Education and Research (IISER), Pune, India
S. Acharya[43], A. Alpana, S. Dube, B. Gomber[43], B. Kansal, A. Laha, B. Sahu[43], S. Sharma

Isfahan University of Technology, Isfahan, Iran
H. Bakhshiansohi[44], E. Khazaie[45], M. Zeinali[46]

Institute for Research in Fundamental Sciences (IPM), Tehran, Iran
S. Chenarani[47], S.M. Etesami, M. Khakzad, M. Mohammadi Najafabadi

University College Dublin, Dublin, Ireland
M. Grunewald

INFN Sezione di Bari[a], Università di Bari[b], Politecnico di Bari[c], Bari, Italy
M. Abbrescia[a,b], R. Aly[a,c,48], A. Colaleo[a,b], D. Creanza[a,c], B. D'Anzi[a,b], N. De Filippis[a,c], M. De Palma[a,b], A. Di Florio[a,c], W. Elmetenawee[a,b,48], L. Fiore[a], G. Iaselli[a,c], M. Louka[a,b], G. Maggi[a,c], M. Maggi[a], I. Margjeka[a,b], V. Mastrapasqua[a,b], S. My[a,b], S. Nuzzo[a,b], A. Pellecchia[a,b], A. Pompili[a,b], G. Pugliese[a,c], R. Radogna[a], G. Ramirez-Sanchez[a,c], D. Ramos[a], A. Ranieri[a], L. Silvestris[a], F.M. Simone[a,b], Ü. Sözbilir[a], A. Stamerra[a], R. Venditti[a], P. Verwilligen[a], A. Zaza[a,b]

INFN Sezione di Bologna[a], Università di Bologna[b], Bologna, Italy
G. Abbiendi[a], C. Battilana[a,b], L. Borgonovi[a], R. Campanini[a,b], P. Capiluppi[a,b], A. Castro[a,b], F.R. Cavallo[a], M. Cuffiani[a,b], G.M. Dallavalle[a], T. Diotalevi[a,b], F. Fabbri[a], A. Fanfani[a,b], D. Fasanella[a,b], P. Giacomelli[a], L. Giommi[a,b], C. Grandi[a], L. Guiducci[a,b], S. Lo Meo[a,49], L. Lunerti[a,b], S. Marcellini[a], G. Masetti[a], F.L. Navarria[a,b], A. Perrotta[a], F. Primavera[a,b], A.M. Rossi[a,b], T. Rovelli[a,b], G.P. Siroli[a,b]

INFN Sezione di Catania[a], Università di Catania[b], Catania, Italy
S. Costa[a,b,50], A. Di Mattia[a], R. Potenza[a,b], A. Tricomi[a,b,50], C. Tuve[a,b]

INFN Sezione di Firenze[a], Università di Firenze[b], Firenze, Italy
P. Assiouras[a], G. Barbagli[a], G. Bardelli[a,b], B. Camaiani[a,b], A. Cassese[a], R. Ceccarelli[a], V. Ciulli[a,b], C. Civinini[a], R. D'Alessandro[a,b], E. Focardi[a,b], T. Kello[a], G. Latino[a,b], P. Lenzi[a,b], M. Lizzo[a], M. Meschini[a], S. Paoletti[a], A. Papanastassiou[a,b], G. Sguazzoni[a], L. Viliani[a]

INFN Laboratori Nazionali di Frascati, Frascati, Italy
L. Benussi, S. Bianco, S. Meola[51], D. Piccolo

INFN Sezione di Genova[a], Università di Genova[b], Genova, Italy
P. Chatagnon[a], F. Ferro[a], E. Robutti[a], S. Tosi[a,b]

INFN Sezione di Milano-Bicocca[a], Università di Milano-Bicocca[b], Milano, Italy
A. Benaglia[a], G. Boldrini[a,b], F. Brivio[a], F. Cetorelli[a], F. De Guio[a,b],

M.E. Dinardo[a,b], P. Dini[a], S. Gennai[a], R. Gerosa[a,b], A. Ghezzi[a,b], P. Govoni[a,b], L. Guzzi[a], M.T. Lucchini[a,b], M. Malberti[a], S. Malvezzi[a], A. Massironi[a], D. Menasce[a], L. Moroni[a], M. Paganoni[a,b], D. Pedrini[a], B.S. Pinolini[a], S. Ragazzi[a,b], T. Tabarelli de Fatis[a,b], D. Zuolo[a]

INFN Sezione di Napoli[a], Università di Napoli 'Federico II'[b], Napoli, Italy; Università della Basilicata[c], Potenza, Italy; Scuola Superiore Meridionale (SSM)[d], Napoli, Italy
S. Buontempo[a], A. Cagnotta[a,b], F. Carnevali[a,b], N. Cavallo[a,c], A. De Iorio[a,b], F. Fabozzi[a,c], A.O.M. Iorio[a,b], L. Lista[a,b,52], P. Paolucci[a,31], B. Rossi[a], C. Sciacca[a,b]

INFN Sezione di Padova[a], Università di Padova[b], Padova, Italy; Università di Trento[c], Trento, Italy
R. Ardino[a], P. Azzi[a], N. Bacchetta[a,53], M. Benettoni[a], D. Bisello[a,b], P. Bortignon[a], A. Bragagnolo[a,b], R. Carlin[a,b], P. Checchia[a], T. Dorigo[a], F. Gasparini[a,b], U. Gasparini[a,b], E. Lusiani[a], M. Margoni[a,b], F. Marini[a], A.T. Meneguzzo[a,b], M. Migliorini[a,b], J. Pazzini[a,b], P. Ronchese[a,b], R. Rossin[a,b], F. Simonetto[a,b], G. Strong[a], M. Tosi[a,b], A. Triossi[a,b], S. Ventura[a], H. Yarar[a,b], M. Zanetti[a,b], P. Zotto[a,b], A. Zucchetta[a,b]

INFN Sezione di Pavia[a], Università di Pavia[b], Pavia, Italy
S. Abu Zeid[a,54], C. Aimè[a,b], A. Braghieri[a], S. Calzaferri[a], D. Fiorina[a], P. Montagna[a,b], V. Re[a], C. Riccardi[a,b], P. Salvini[a], I. Vai[a,b], P. Vitulo[a,b]

INFN Sezione di Perugia[a], Università di Perugia[b], Perugia, Italy
S. Ajmal[a,b], P. Asenov[a,55], G.M. Bilei[a], D. Ciangottini[a,b], L. Fanò[a,b], M. Magherini[a,b], G. Mantovani[a,b], V. Mariani[a,b], M. Menichelli[a], F. Moscatelli[a,55], A. Rossi[a,b], A. Santocchia[a,b], D. Spiga[a], T. Tedeschi[a,b]

INFN Sezione di Pisa[a], Università di Pisa[b], Scuola Normale Superiore di Pisa[c], Pisa, Italy; Università di Siena[d], Siena, Italy
P. Azzurri[a], G. Bagliesi[a], R. Bhattacharya[a], L. Bianchini[a,b], T. Boccali[a], E. Bossini[a], D. Bruschini[a,c], R. Castaldi[a], M.A. Ciocci[a,b], M. Cipriani[a,b], V. D'Amante[a,d], R. Dell'Orso[a], S. Donato[a], A. Giassi[a], F. Ligabue[a,c], D. Matos Figueiredo[a], A. Messineo[a,b], M. Musich[a,b], F. Palla[a], A. Rizzi[a,b], G. Rolandi[a,c], S. Roy Chowdhury[a], T. Sarkar[a], A. Scribano[a], P. Spagnolo[a], R. Tenchini[a], G. Tonelli[a,b], N. Turini[a,d], A. Venturi[a], P.G. Verdini[a]

INFN Sezione di Roma[a], Sapienza Università di Roma[b], Roma, Italy
P. Barria[a], M. Campana[a,b], F. Cavallari[a], L. Cunqueiro Mendez[a,b], D. Del Re[a,b], E. Di Marco[a], M. Diemoz[a], F. Errico[a,b], E. Longo[a,b], P. Meridiani[a], J. Mijuskovic[a,b], G. Organtini[a,b], F. Pandolfi[a], R. Paramatti[a,b], C. Quaranta[a,b], S. Rahatlou[a,b], C. Rovelli[a], F. Santanastasio[a,b], L. Soffi[a]

INFN Sezione di Torino[a], Università di Torino[b], Torino, Italy; Università del Piemonte Orientale[c], Novara, Italy
N. Amapane[a,b], R. Arcidiacono[a,c], S. Argiro[a,b], M. Arneodo[a,c], N. Bartosik[a], R. Bellan[a,b], A. Bellora[a,b], C. Biino[a], N. Cartiglia[a], M. Costa[a,b], R. Covarelli[a,b], N. Demaria[a], L. Finco[a], M. Grippo[a,b], B. Kiani[a,b], F. Legger[a], F. Luongo[a,b], C. Mariotti[a], S. Maselli[a], A. Mecca[a,b], E. Migliore[a,b], M. Monteno[a], R. Mulargia[a], M.M. Obertino[a,b], G. Ortona[a], L. Pacher[a,b], N. Pastrone[a], M. Pelliccioni[a], M. Ruspa[a,c], F. Siviero[a,b], V. Sola[a,b], A. Solano[a,b], A. Staiano[a], C. Tarricone[a,b], D. Trocino[a], G. Umoret[a,b], E. Vlasov[a,b]

INFN Sezione di Trieste[a], Università di Trieste[b], Trieste, Italy
S. Belforte[a], V. Candelise[a,b], M. Casarsa[a], F. Cossutti[a], K. De Leo[a,b], G. Della Ricca[a,b]

Kyungpook National University, Daegu, Korea
S. Dogra, J. Hong, C. Huh, B. Kim, D.H. Kim, J. Kim, H. Lee, S.W. Lee, C.S. Moon, Y.D. Oh, M.S. Ryu, S. Sekmen, Y.C. Yang

Department of Mathematics and Physics - GWNU, Gangneung, Korea
M.S. Kim

Chonnam National University, Institute for Universe and Elementary Particles, Kwangju, Korea
G. Bak, P. Gwak, H. Kim, D.H. Moon

Hanyang University, Seoul, Korea
E. Asilar, D. Kim, T.J. Kim, J.A. Merlin

Korea University, Seoul, Korea
S. Choi, S. Han, B. Hong, K. Lee, K.S. Lee, S. Lee, J. Park, S.K. Park, J. Yoo

Kyung Hee University, Department of Physics, Seoul, Korea
J. Goh, S. Yang

Sejong University, Seoul, Korea
H. S. Kim, Y. Kim, S. Lee

Seoul National University, Seoul, Korea
J. Almond, J.H. Bhyun, J. Choi, W. Jun, J. Kim, S. Ko, H. Kwon, H. Lee, J. Lee, J. Lee, B.H. Oh, S.B. Oh, H. Seo, U.K. Yang, I. Yoon

University of Seoul, Seoul, Korea
W. Jang, D.Y. Kang, Y. Kang, S. Kim, B. Ko, J.S.H. Lee, Y. Lee, I.C. Park, Y. Roh, I.J. Watson

Yonsei University, Department of Physics, Seoul, Korea
S. Ha, H.D. Yoo

Sungkyunkwan University, Suwon, Korea
M. Choi, M.R. Kim, H. Lee, Y. Lee, I. Yu

College of Engineering and Technology, American University of the Middle East (AUM), Dasman, Kuwait
T. Beyrouthy, Y. Maghrbi

Riga Technical University, Riga, Latvia
K. Dreimanis, A. Gaile, G. Pikurs, A. Potrebko, M. Seidel, V. Veckalns[56]

University of Latvia (LU), Riga, Latvia
N.R. Strautnieks

Vilnius University, Vilnius, Lithuania
M. Ambrozas, A. Juodagalvis, A. Rinkevicius, G. Tamulaitis

National Centre for Particle Physics, Universiti Malaya, Kuala Lumpur, Malaysia
N. Bin Norjoharuddeen, I. Yusuff[57], Z. Zolkapli

Universidad de Sonora (UNISON), Hermosillo, Mexico

J.F. Benitez, A. Castaneda Hernandez, H.A. Encinas Acosta, L.G. Gallegos Maríñez, M. León Coello, J.A. Murillo Quijada, A. Sehrawat, L. Valencia Palomo

Centro de Investigacion y de Estudios Avanzados del IPN, Mexico City, Mexico
G. Ayala, H. Castilla-Valdez, E. De La Cruz-Burelo, I. Heredia-De La Cruz[58], R. Lopez-Fernandez, C.A. Mondragon Herrera, A. Sánchez Hernández

Universidad Iberoamericana, Mexico City, Mexico
C. Oropeza Barrera, M. Ramírez García

Benemerita Universidad Autonoma de Puebla, Puebla, Mexico
I. Bautista, I. Pedraza, H.A. Salazar Ibarguen, C. Uribe Estrada

University of Montenegro, Podgorica, Montenegro
I. Bubanja, N. Raicevic

University of Canterbury, Christchurch, New Zealand
P.H. Butler

National Centre for Physics, Quaid-I-Azam University, Islamabad, Pakistan
A. Ahmad, M.I. Asghar, A. Awais, M.I.M. Awan, H.R. Hoorani, W.A. Khan

AGH University of Krakow, Faculty of Computer Science, Electronics and Telecommunications, Krakow, Poland
V. Avati, L. Grzanka, M. Malawski

National Centre for Nuclear Research, Swierk, Poland
H. Bialkowska, M. Bluj, B. Boimska, M. Górski, M. Kazana, M. Szleper, P. Zalewski

Institute of Experimental Physics, Faculty of Physics, University of Warsaw, Warsaw, Poland
K. Bunkowski, K. Doroba, A. Kalinowski, M. Konecki, J. Krolikowski, A. Muhammad

Warsaw University of Technology, Warsaw, Poland
K. Pozniak, W. Zabolotny

Laboratório de Instrumentação e Física Experimental de Partículas, Lisboa, Portugal
M. Araujo, D. Bastos, C. Beirão Da Cruz E Silva, A. Boletti, M. Bozzo, T. Camporesi, G. Da Molin, P. Faccioli, M. Gallinaro, J. Hollar, N. Leonardo, T. Niknejad, A. Petrilli, M. Pisano, J. Seixas, J. Varela, J.W. Wulff

Faculty of Physics, University of Belgrade, Belgrade, Serbia
P. Adzic, P. Milenovic

VINCA Institute of Nuclear Sciences, University of Belgrade, Belgrade, Serbia
M. Dordevic, J. Milosevic, V. Rekovic

Centro de Investigaciones Energéticas Medioambientales y Tecnológicas (CIEMAT), Madrid, Spain
M. Aguilar-Benitez, J. Alcaraz Maestre, Cristina F. Bedoya, M. Cepeda, M. Cerrada, N. Colino, B. De La Cruz, A. Delgado Peris, A. Escalante Del Valle, D. Fernández Del Val, J.P. Fernández Ramos, J. Flix, M.C. Fouz, O. Gonzalez Lopez, S. Goy Lopez, J.M. Hernandez, M.I. Josa, D. Moran, C. M. Morcillo Perez, Á. Navarro Tobar, C. Perez Dengra, A. Pérez-Calero Yzquierdo, J. Puerta Pelayo, I. Redondo, D.D. Redondo Ferrero, L. Romero, S. Sánchez Navas, L. Urda Gómez,

J. Vazquez Escobar, C. Willmott

Universidad Autónoma de Madrid, Madrid, Spain
J.F. de Trocóniz

Universidad de Oviedo, Instituto Universitario de Ciencias y Tecnologías Espaciales de Asturias (ICTEA), Oviedo, Spain
B. Alvarez Gonzalez, J. Cuevas, J. Fernandez Menendez, S. Folgueras, I. Gonzalez Caballero, J.R. González Fernández, E. Palencia Cortezon, C. Ramón Álvarez, V. Rodríguez Bouza, A. Soto Rodríguez, A. Trapote, C. Vico Villalba, P. Vischia

Instituto de Física de Cantabria (IFCA), CSIC-Universidad de Cantabria, Santander, Spain
S. Bhowmik, S. Blanco Fernández, J.A. Brochero Cifuentes, I.J. Cabrillo, A. Calderon, J. Duarte Campderros, M. Fernandez, G. Gomez, C. Lasaosa García, C. Martinez Rivero, P. Martinez Ruiz del Arbol, F. Matorras, P. Matorras Cuevas, E. Navarrete Ramos, J. Piedra Gomez, L. Scodellaro, I. Vila, J.M. Vizan Garcia

University of Colombo, Colombo, Sri Lanka
M.K. Jayananda, B. Kailasapathy[59], D.U.J. Sonnadara, D.D.C. Wickramarathna

University of Ruhuna, Department of Physics, Matara, Sri Lanka
W.G.D. Dharmaratna[60], K. Liyanage, N. Perera, N. Wickramage

CERN, European Organization for Nuclear Research, Geneva, Switzerland
D. Abbaneo, C. Amendola, E. Auffray, G. Auzinger, J. Baechler, D. Barney, A. Bermúdez Martínez, M. Bianco, B. Bilin, A.A. Bin Anuar, A. Bocci, C. Botta, E. Brondolin, C. Caillol, G. Cerminara, N. Chernyavskaya, D. d'Enterria, A. Dabrowski, A. David, A. De Roeck, M.M. Defranchis, M. Deile, M. Dobson, L. Forthomme, G. Franzoni, W. Funk, S. Giani, D. Gigi, K. Gill, F. Glege, L. Gouskos, M. Haranko, J. Hegeman, B. Huber, V. Innocente, T. James, P. Janot, S. Laurila, P. Lecoq, E. Leutgeb, C. Lourenço, B. Maier, L. Malgeri, M. Mannelli, A.C. Marini, M. Matthewman, F. Meijers, S. Mersi, E. Meschi, V. Milosevic, F. Monti, F. Moortgat, M. Mulders, I. Neutelings, S. Orfanelli, F. Pantaleo, G. Petrucciani, A. Pfeiffer, M. Pierini, D. Piparo, H. Qu, D. Rabady, G. Reales Gutiérrez, M. Rovere, H. Sakulin, S. Scarfi, C. Schwick, M. Selvaggi, A. Sharma, K. Shchelina, P. Silva, P. Sphicas[61], A.G. Stahl Leiton, A. Steen, S. Summers, D. Treille, P. Tropea, A. Tsirou, D. Walter, J. Wanczyk[62], J. Wang, S. Wuchterl, P. Zehetner, P. Zejdl, W.D. Zeuner

Paul Scherrer Institut, Villigen, Switzerland
T. Bevilacqua[63], L. Caminada[63], A. Ebrahimi, W. Erdmann, R. Horisberger, Q. Ingram, H.C. Kaestli, D. Kotlinski, C. Lange, M. Missiroli[63], L. Noehte[63], T. Rohe

ETH Zurich - Institute for Particle Physics and Astrophysics (IPA), Zurich, Switzerland
T.K. Aarrestad, K. Androsov[62], M. Backhaus, A. Calandri, C. Cazzaniga, K. Datta, A. De Cosa, G. Dissertori, M. Dittmar, M. Donegà, F. Eble, M. Galli, K. Gedia, F. Glessgen, C. Grab, D. Hits, W. Lustermann, A.-M. Lyon, R.A. Manzoni, M. Marchegiani, L. Marchese, C. Martin Perez, A. Mascellani[62], F. Nessi-Tedaldi, F. Pauss, V. Perovic, S. Pigazzini, C. Reissel, T. Reitenspiess, B. Ristic, F. Riti, D. Ruini, R. Seidita, J. Steggemann[62], D. Valsecchi, R. Wallny

Universität Zürich, Zurich, Switzerland
C. Amsler[64], P. Bärtschi, D. Brzhechko, M.F. Canelli, K. Cormier, J.K. Heikkilä,

M. Huwiler, W. Jin, A. Jofrehei, B. Kilminster, S. Leontsinis, S.P. Liechti, A. Macchiolo, P. Meiring, U. Molinatti, A. Reimers, P. Robmann, S. Sanchez Cruz, M. Senger, Y. Takahashi, R. Tramontano

National Central University, Chung-Li, Taiwan
C. Adloff[65], D. Bhowmik, C.M. Kuo, W. Lin, P.K. Rout, P.C. Tiwari[39], S.S. Yu

National Taiwan University (NTU), Taipei, Taiwan
L. Ceard, Y. Chao, K.F. Chen, P.s. Chen, Z.g. Chen, W.-S. Hou, T.h. Hsu, Y.w. Kao, R. Khurana, G. Kole, Y.y. Li, R.-S. Lu, E. Paganis, X.f. Su, J. Thomas-Wilsker, L.s. Tsai, H.y. Wu, E. Yazgan

High Energy Physics Research Unit, Department of Physics, Faculty of Science, Chulalongkorn University, Bangkok, Thailand
C. Asawatangtrakuldee, N. Srimanobhas, V. Wachirapusitanand

Çukurova University, Physics Department, Science and Art Faculty, Adana, Turkey
D. Agyel, F. Boran, Z.S. Demiroglu, F. Dolek, I. Dumanoglu[66], E. Eskut, Y. Guler[67], E. Gurpinar Guler[67], C. Isik, O. Kara, A. Kayis Topaksu, U. Kiminsu, G. Onengut, K. Ozdemir[68], A. Polatoz, B. Tali[69], U.G. Tok, S. Turkcapar, E. Uslan, I.S. Zorbakir

Middle East Technical University, Physics Department, Ankara, Turkey
M. Yalvac[70]

Bogazici University, Istanbul, Turkey
B. Akgun, I.O. Atakisi, E. Gülmez, M. Kaya[71], O. Kaya[72], S. Tekten[73]

Istanbul Technical University, Istanbul, Turkey
A. Cakir, K. Cankocak[66,74], Y. Komurcu, S. Sen[75]

Istanbul University, Istanbul, Turkey
O. Aydilek, S. Cerci[69], V. Epshteyn, B. Hacisahinoglu, I. Hos[76], B. Kaynak, S. Ozkorucuklu, O. Potok, H. Sert, C. Simsek, C. Zorbilmez

Yildiz Technical University, Istanbul, Turkey
B. Isildak[77], D. Sunar Cerci[69]

Institute for Scintillation Materials of National Academy of Science of Ukraine, Kharkiv, Ukraine
A. Boyaryntsev, B. Grynyov

National Science Centre, Kharkiv Institute of Physics and Technology, Kharkiv, Ukraine
L. Levchuk

University of Bristol, Bristol, United Kingdom
D. Anthony, J.J. Brooke, A. Bundock, F. Bury, E. Clement, D. Cussans, H. Flacher, M. Glowacki, J. Goldstein, H.F. Heath, L. Kreczko, S. Paramesvaran, S. Seif El Nasr-Storey, V.J. Smith, N. Stylianou[78], K. Walkingshaw Pass, R. White

Rutherford Appleton Laboratory, Didcot, United Kingdom
A.H. Ball, K.W. Bell, A. Belyaev[79], C. Brew, R.M. Brown, D.J.A. Cockerill, C. Cooke, K.V. Ellis, K. Harder, S. Harper, M.-L. Holmberg[80], J. Linacre, K. Manolopoulos, D.M. Newbold, E. Olaiya, D. Petyt, T. Reis, G. Salvi, T. Schuh, C.H. Shepherd-Themistocleous, I.R. Tomalin, T. Williams

Imperial College, London, United Kingdom
R. Bainbridge, P. Bloch, C.E. Brown, O. Buchmuller, V. Cacchio, C.A. Carrillo Montoya, G.S. Chahal[81], D. Colling, J.S. Dancu, I. Das, P. Dauncey, G. Davies, J. Davies, M. Della Negra, S. Fayer, G. Fedi, G. Hall, M.H. Hassanshahi, A. Howard, G. Iles, M. Knight, J. Langford, J. León Holgado, L. Lyons, A.-M. Magnan, S. Malik, M. Mieskolainen, J. Nash[82], M. Pesaresi, B.C. Radburn-Smith, A. Richards, A. Rose, K. Savva, C. Seez, R. Shukla, A. Tapper, K. Uchida, G.P. Uttley, L.H. Vage, T. Virdee[31], M. Vojinovic, N. Wardle, D. Winterbottom

Brunel University, Uxbridge, United Kingdom
K. Coldham, J.E. Cole, A. Khan, P. Kyberd, I.D. Reid

Baylor University, Waco, Texas, USA
S. Abdullin, A. Brinkerhoff, B. Caraway, J. Dittmann, K. Hatakeyama, J. Hiltbrand, B. McMaster, M. Saunders, S. Sawant, C. Sutantawibul, J. Wilson

Catholic University of America, Washington, DC, USA
R. Bartek, A. Dominguez, C. Huerta Escamilla, A.E. Simsek, R. Uniyal, A.M. Vargas Hernandez

The University of Alabama, Tuscaloosa, Alabama, USA
B. Bam, R. Chudasama, S.I. Cooper, S.V. Gleyzer, C.U. Perez, P. Rumerio[83], E. Usai, R. Yi

Boston University, Boston, Massachusetts, USA
A. Akpinar, D. Arcaro, C. Cosby, Z. Demiragli, C. Erice, C. Fangmeier, C. Fernandez Madrazo, E. Fontanesi, D. Gastler, F. Golf, S. Jeon, I. Reed, J. Rohlf, K. Salyer, D. Sperka, D. Spitzbart, I. Suarez, A. Tsatsos, S. Yuan, A.G. Zecchinelli

Brown University, Providence, Rhode Island, USA
G. Benelli, X. Coubez[26], D. Cutts, M. Hadley, U. Heintz, J.M. Hogan[84], T. Kwon, G. Landsberg, K.T. Lau, D. Li, J. Luo, S. Mondal, M. Narain[†], N. Pervan, S. Sagir[85], F. Simpson, M. Stamenkovic, W.Y. Wong, X. Yan, W. Zhang

University of California, Davis, Davis, California, USA
S. Abbott, J. Bonilla, C. Brainerd, R. Breedon, M. Calderon De La Barca Sanchez, M. Chertok, M. Citron, J. Conway, P.T. Cox, R. Erbacher, F. Jensen, O. Kukral, G. Mocellin, M. Mulhearn, D. Pellett, W. Wei, Y. Yao, F. Zhang

University of California, Los Angeles, California, USA
M. Bachtis, R. Cousins, A. Datta, G. Flores Avila, J. Hauser, M. Ignatenko, M.A. Iqbal, T. Lam, E. Manca, A. Nunez Del Prado, D. Saltzberg, V. Valuev

University of California, Riverside, Riverside, California, USA
R. Clare, J.W. Gary, M. Gordon, G. Hanson, W. Si, S. Wimpenny[†]

University of California, San Diego, La Jolla, California, USA
J.G. Branson, S. Cittolin, S. Cooperstein, D. Diaz, J. Duarte, L. Giannini, J. Guiang, R. Kansal, V. Krutelyov, R. Lee, J. Letts, M. Masciovecchio, F. Mokhtar, S. Mukherjee, M. Pieri, M. Quinnan, B.V. Sathia Narayanan, V. Sharma, M. Tadel, E. Vourliotis, F. Würthwein, Y. Xiang, A. Yagil

University of California, Santa Barbara - Department of Physics, Santa Barbara, California, USA

A. Barzdukas, L. Brennan, C. Campagnari, A. Dorsett, J. Incandela, J. Kim, A.J. Li, P. Masterson, H. Mei, J. Richman, U. Sarica, R. Schmitz, F. Setti, J. Sheplock, D. Stuart, T.Á. Vámi, S. Wang

California Institute of Technology, Pasadena, California, USA
A. Bornheim, O. Cerri, A. Latorre, J. Mao, H.B. Newman, M. Spiropulu, J.R. Vlimant, C. Wang, S. Xie, R.Y. Zhu

Carnegie Mellon University, Pittsburgh, Pennsylvania, USA
J. Alison, S. An, M.B. Andrews, P. Bryant, M. Cremonesi, V. Dutta, T. Ferguson, A. Harilal, C. Liu, T. Mudholkar, S. Murthy, M. Paulini, A. Roberts, A. Sanchez, W. Terrill

University of Colorado Boulder, Boulder, Colorado, USA
J.P. Cumalat, W.T. Ford, A. Hassani, G. Karathanasis, E. MacDonald, N. Manganelli, A. Perloff, C. Savard, N. Schonbeck, K. Stenson, K.A. Ulmer, S.R. Wagner, N. Zipper

Cornell University, Ithaca, New York, USA
J. Alexander, S. Bright-Thonney, X. Chen, D.J. Cranshaw, J. Fan, X. Fan, D. Gadkari, S. Hogan, P. Kotamnives, J. Monroy, M. Oshiro, J.R. Patterson, J. Reichert, M. Reid, A. Ryd, J. Thom, P. Wittich, R. Zou

Fermi National Accelerator Laboratory, Batavia, Illinois, USA
M. Albrow, M. Alyari, O. Amram, G. Apollinari, A. Apresyan, L.A.T. Bauerdick, D. Berry, J. Berryhill, P.C. Bhat, K. Burkett, J.N. Butler, A. Canepa, G.B. Cerati, H.W.K. Cheung, F. Chlebana, G. Cummings, J. Dickinson, I. Dutta, V.D. Elvira, Y. Feng, J. Freeman, A. Gandrakota, Z. Gecse, L. Gray, D. Green, A. Grummer, S. Grünendahl, D. Guerrero, O. Gutsche, R.M. Harris, R. Heller, T.C. Herwig, J. Hirschauer, L. Horyn, B. Jayatilaka, S. Jindariani, M. Johnson, U. Joshi, T. Klijnsma, B. Klima, K.H.M. Kwok, S. Lammel, D. Lincoln, R. Lipton, T. Liu, C. Madrid, K. Maeshima, C. Mantilla, D. Mason, P. McBride, P. Merkel, S. Mrenna, S. Nahn, J. Ngadiuba, D. Noonan, V. Papadimitriou, N. Pastika, K. Pedro, C. Pena[86], F. Ravera, A. Reinsvold Hall[87], L. Ristori, E. Sexton-Kennedy, N. Smith, A. Soha, L. Spiegel, S. Stoynev, J. Strait, L. Taylor, S. Tkaczyk, N.V. Tran, L. Uplegger, E.W. Vaandering, I. Zoi

University of Florida, Gainesville, Florida, USA
C. Aruta, P. Avery, D. Bourilkov, L. Cadamuro, P. Chang, V. Cherepanov, R.D. Field, E. Koenig, M. Kolosova, J. Konigsberg, A. Korytov, K.H. Lo, K. Matchev, N. Menendez, G. Mitselmakher, K. Mohrman, A. Muthirakalayil Madhu, N. Rawal, D. Rosenzweig, S. Rosenzweig, K. Shi, J. Wang

Florida State University, Tallahassee, Florida, USA
T. Adams, A. Al Kadhim, A. Askew, N. Bower, R. Habibullah, V. Hagopian, R. Hashmi, R.S. Kim, S. Kim, T. Kolberg, G. Martinez, H. Prosper, P.R. Prova, M. Wulansatiti, R. Yohay, J. Zhang

Florida Institute of Technology, Melbourne, Florida, USA
B. Alsufyani, M.M. Baarmand, S. Butalla, T. Elkafrawy[54], M. Hohlmann, R. Kumar Verma, M. Rahmani, E. Yanes

University of Illinois Chicago, Chicago, USA, Chicago, USA

M.R. Adams, A. Baty, C. Bennett, R. Cavanaugh, R. Escobar Franco, O. Evdokimov, C.E. Gerber, D.J. Hofman, J.h. Lee, D. S. Lemos, A.H. Merrit, C. Mills, S. Nanda, G. Oh, B. Ozek, D. Pilipovic, R. Pradhan, T. Roy, S. Rudrabhatla, M.B. Tonjes, N. Varelas, Z. Ye, J. Yoo

The University of Iowa, Iowa City, Iowa, USA
M. Alhusseini, D. Blend, K. Dilsiz[88], L. Emediato, G. Karaman, O.K. Köseyan, J.-P. Merlo, A. Mestvirishvili[89], J. Nachtman, O. Neogi, H. Ogul[90], Y. Onel, A. Penzo, C. Snyder, E. Tiras[91]

Johns Hopkins University, Baltimore, Maryland, USA
B. Blumenfeld, L. Corcodilos, J. Davis, A.V. Gritsan, L. Kang, S. Kyriacou, P. Maksimovic, M. Roguljic, J. Roskes, S. Sekhar, M. Swartz

The University of Kansas, Lawrence, Kansas, USA
A. Abreu, L.F. Alcerro Alcerro, J. Anguiano, P. Baringer, A. Bean, Z. Flowers, D. Grove, J. King, G. Krintiras, M. Lazarovits, C. Le Mahieu, C. Lindsey, J. Marquez, N. Minafra, M. Murray, M. Nickel, M. Pitt, S. Popescu[92], C. Rogan, C. Royon, R. Salvatico, S. Sanders, C. Smith, Q. Wang, G. Wilson

Kansas State University, Manhattan, Kansas, USA
B. Allmond, A. Ivanov, K. Kaadze, A. Kalogeropoulos, D. Kim, Y. Maravin, K. Nam, J. Natoli, D. Roy, G. Sorrentino

Lawrence Livermore National Laboratory, Livermore, California, USA
F. Rebassoo, D. Wright

University of Maryland, College Park, Maryland, USA
A. Baden, A. Belloni, Y.M. Chen, S.C. Eno, N.J. Hadley, S. Jabeen, R.G. Kellogg, T. Koeth, Y. Lai, S. Lascio, A.C. Mignerey, S. Nabili, C. Palmer, C. Papageorgakis, M.M. Paranjpe, L. Wang

Massachusetts Institute of Technology, Cambridge, Massachusetts, USA
J. Bendavid, W. Busza, I.A. Cali, M. D'Alfonso, J. Eysermans, C. Freer, G. Gomez-Ceballos, M. Goncharov, G. Grosso, P. Harris, D. Hoang, D. Kovalskyi, J. Krupa, L. Lavezzo, Y.-J. Lee, K. Long, C. Mironov, N. Paladino, C. Paus, D. Rankin, C. Roland, G. Roland, S. Rothman, G.S.F. Stephans, Z. Wang, B. Wyslouch, T. J. Yang

University of Minnesota, Minneapolis, Minnesota, USA
B. Crossman, B.M. Joshi, C. Kapsiak, M. Krohn, D. Mahon, J. Mans, B. Marzocchi, S. Pandey, M. Revering, R. Rusack, R. Saradhy, N. Schroeder, N. Strobbe, M.A. Wadud

University of Mississippi, Oxford, Mississippi, USA
L.M. Cremaldi

University of Nebraska-Lincoln, Lincoln, Nebraska, USA
K. Bloom, D.R. Claes, G. Haza, J. Hossain, C. Joo, I. Kravchenko, J.E. Siado, W. Tabb, A. Vagnerini, A. Wightman, F. Yan, D. Yu

State University of New York at Buffalo, Buffalo, New York, USA
H. Bandyopadhyay, L. Hay, I. Iashvili, A. Kharchilava, M. Morris, D. Nguyen, S. Rappoccio, H. Rejeb Sfar, A. Williams

Northeastern University, Boston, Massachusetts, USA
G. Alverson, E. Barberis, J. Dervan, Y. Haddad, Y. Han, A. Krishna, J. Li, M. Lu, G. Madigan, R. Mccarthy, D.M. Morse, V. Nguyen, T. Orimoto, A. Parker, L. Skinnari, A. Tishelman-Charny, B. Wang, D. Wood

Northwestern University, Evanston, Illinois, USA
S. Bhattacharya, J. Bueghly, Z. Chen, S. Dittmer, K.A. Hahn, Y. Liu, Y. Miao, D.G. Monk, M.H. Schmitt, A. Taliercio, M. Velasco

University of Notre Dame, Notre Dame, Indiana, USA
G. Agarwal, R. Band, R. Bucci, S. Castells, A. Das, R. Goldouzian, M. Hildreth, K.W. Ho, K. Hurtado Anampa, T. Ivanov, C. Jessop, K. Lannon, J. Lawrence, N. Loukas, L. Lutton, J. Mariano, N. Marinelli, I. Mcalister, T. McCauley, C. Mcgrady, C. Moore, Y. Musienko[17], H. Nelson, M. Osherson, A. Piccinelli, R. Ruchti, A. Townsend, Y. Wan, M. Wayne, H. Yockey, M. Zarucki, L. Zygala

The Ohio State University, Columbus, Ohio, USA
A. Basnet, B. Bylsma, M. Carrigan, L.S. Durkin, C. Hill, M. Joyce, M. Nunez Ornelas, K. Wei, B.L. Winer, B. R. Yates

Princeton University, Princeton, New Jersey, USA
F.M. Addesa, H. Bouchamaoui, P. Das, G. Dezoort, P. Elmer, A. Frankenthal, B. Greenberg, N. Haubrich, G. Kopp, S. Kwan, D. Lange, A. Loeliger, D. Marlow, I. Ojalvo, J. Olsen, A. Shevelev, D. Stickland, C. Tully

University of Puerto Rico, Mayaguez, Puerto Rico, USA
S. Malik

Purdue University, West Lafayette, Indiana, USA
A.S. Bakshi, V.E. Barnes, S. Chandra, R. Chawla, S. Das, A. Gu, L. Gutay, M. Jones, A.W. Jung, D. Kondratyev, A.M. Koshy, M. Liu, G. Negro, N. Neumeister, G. Paspalaki, S. Piperov, V. Scheurer, J.F. Schulte, M. Stojanovic, J. Thieman, A. K. Virdi, F. Wang, W. Xie

Purdue University Northwest, Hammond, Indiana, USA
J. Dolen, N. Parashar, A. Pathak

Rice University, Houston, Texas, USA
D. Acosta, T. Carnahan, K.M. Ecklund, P.J. Fernández Manteca, S. Freed, P. Gardner, F.J.M. Geurts, W. Li, O. Miguel Colin, B.P. Padley, R. Redjimi, J. Rotter, E. Yigitbasi, Y. Zhang

University of Rochester, Rochester, New York, USA
A. Bodek, P. de Barbaro, R. Demina, J.L. Dulemba, A. Garcia-Bellido, O. Hindrichs, A. Khukhunaishvili, N. Parmar, P. Parygin[93], E. Popova[93], R. Taus

The Rockefeller University, New York, New York, USA
K. Goulianos

Rutgers, The State University of New Jersey, Piscataway, New Jersey, USA
B. Chiarito, J.P. Chou, Y. Gershtein, E. Halkiadakis, A. Hart, M. Heindl, D. Jaroslawski, O. Karacheban[29], I. Laflotte, A. Lath, R. Montalvo, K. Nash, P. Pajarillo, H. Routray, S. Salur, S. Schnetzer, S. Somalwar, R. Stone, S.A. Thayil, S. Thomas, J. Vora, H. Wang

University of Tennessee, Knoxville, Tennessee, USA
H. Acharya, D. Ally, A.G. Delannoy, S. Fiorendi, S. Higginbotham, T. Holmes, A.R. Kanuganti, N. Karunarathna, L. Lee, E. Nibigira, S. Spanier

Texas A&M University, College Station, Texas, USA
D. Aebi, M. Ahmad, O. Bouhali[94], R. Eusebi, J. Gilmore, T. Huang, T. Kamon[95], H. Kim, S. Luo, R. Mueller, D. Overton, D. Rathjens, A. Safonov

Texas Tech University, Lubbock, Texas, USA
N. Akchurin, J. Damgov, V. Hegde, A. Hussain, Y. Kazhykarim, K. Lamichhane, S.W. Lee, A. Mankel, T. Peltola, I. Volobouev, A. Whitbeck

Vanderbilt University, Nashville, Tennessee, USA
E. Appelt, Y. Chen, S. Greene, A. Gurrola, W. Johns, R. Kunnawalkam Elayavalli, A. Melo, F. Romeo, P. Sheldon, S. Tuo, J. Velkovska, J. Viinikainen

University of Virginia, Charlottesville, Virginia, USA
B. Cardwell, B. Cox, J. Hakala, R. Hirosky, A. Ledovskoy, C. Neu, C.E. Perez Lara

Wayne State University, Detroit, Michigan, USA
P.E. Karchin

University of Wisconsin - Madison, Madison, Wisconsin, USA
A. Aravind, S. Banerjee, K. Black, T. Bose, S. Dasu, I. De Bruyn, P. Everaerts, C. Galloni, H. He, M. Herndon, A. Herve, C.K. Koraka, A. Lanaro, R. Loveless, J. Madhusudanan Sreekala, A. Mallampalli, A. Mohammadi, S. Mondal, G. Parida, D. Pinna, A. Savin, V. Shang, V. Sharma, W.H. Smith, D. Teague, H.F. Tsoi, W. Vetens, A. Warden

Authors affiliated with an institute or an international laboratory covered by a cooperation agreement with CERN
S. Afanasiev, V. Andreev, Yu. Andreev, T. Aushev, M. Azarkin, A. Babaev, A. Belyaev, V. Blinov[96], E. Boos, V. Borshch, D. Budkouski, V. Bunichev, V. Chekhovsky, R. Chistov[96], M. Danilov[96], A. Dermenev, T. Dimova[96], D. Druzhkin[97], M. Dubinin[86], L. Dudko, A. Ershov, G. Gavrilov, V. Gavrilov, S. Gninenko, V. Golovtcov, N. Golubev, I. Golutvin, I. Gorbunov, A. Gribushin, Y. Ivanov, V. Kachanov, V. Karjavine, A. Karneyeu, V. Kim[96], M. Kirakosyan, D. Kirpichnikov, M. Kirsanov, V. Klyukhin, O. Kodolova[98], V. Korenkov, A. Kozyrev[96], N. Krasnikov, A. Lanev, P. Levchenko[99], N. Lychkovskaya, V. Makarenko, A. Malakhov, V. Matveev[96], V. Murzin, A. Nikitenko[100,98], S. Obraztsov, V. Oreshkin, V. Palichik, V. Perelygin, S. Petrushanko, S. Polikarpov[96], V. Popov, O. Radchenko[96], M. Savina, V. Savrin, V. Shalaev, S. Shmatov, S. Shulha, Y. Skovpen[96], S. Slabospitskii, V. Smirnov, A. Snigirev, D. Sosnov, V. Sulimov, E. Tcherniaev, A. Terkulov, O. Teryaev, I. Tlisova, A. Toropin, L. Uvarov, A. Uzunian, A. Vorobyev†, N. Voytishin, B.S. Yuldashev[101], A. Zarubin, I. Zhizhin, A. Zhokin

†: Deceased
[1]Also at Yerevan State University, Yerevan, Armenia
[2]Also at TU Wien, Vienna, Austria
[3]Also at Institute of Basic and Applied Sciences, Faculty of Engineering, Arab Academy for Science, Technology and Maritime Transport, Alexandria, Egypt

[4]Also at Ghent University, Ghent, Belgium
[5]Also at Universidade Estadual de Campinas, Campinas, Brazil
[6]Also at Federal University of Rio Grande do Sul, Porto Alegre, Brazil
[7]Also at UFMS, Nova Andradina, Brazil
[8]Also at Nanjing Normal University, Nanjing, China
[9]Now at The University of Iowa, Iowa City, Iowa, USA
[10]Also at University of Chinese Academy of Sciences, Beijing, China
[11]Also at China Center of Advanced Science and Technology, Beijing, China
[12]Also at University of Chinese Academy of Sciences, Beijing, China
[13]Also at China Spallation Neutron Source, Guangdong, China
[14]Now at Henan Normal University, Xinxiang, China
[15]Also at Université Libre de Bruxelles, Bruxelles, Belgium
[16]Also at University of Latvia (LU), Riga, Latvia
[17]Also at an institute or an international laboratory covered by a cooperation agreement with CERN
[18]Also at Suez University, Suez, Egypt
[19]Now at British University in Egypt, Cairo, Egypt
[20]Also at Purdue University, West Lafayette, Indiana, USA
[21]Also at Université de Haute Alsace, Mulhouse, France
[22]Also at Department of Physics, Tsinghua University, Beijing, China
[23]Also at The University of the State of Amazonas, Manaus, Brazil
[24]Also at Erzincan Binali Yildirim University, Erzincan, Turkey
[25]Also at University of Hamburg, Hamburg, Germany
[26]Also at RWTH Aachen University, III. Physikalisches Institut A, Aachen, Germany
[27]Also at Isfahan University of Technology, Isfahan, Iran
[28]Also at Bergische University Wuppertal (BUW), Wuppertal, Germany
[29]Also at Brandenburg University of Technology, Cottbus, Germany
[30]Also at Forschungszentrum Jülich, Juelich, Germany
[31]Also at CERN, European Organization for Nuclear Research, Geneva, Switzerland
[32]Also at Institute of Physics, University of Debrecen, Debrecen, Hungary
[33]Also at Institute of Nuclear Research ATOMKI, Debrecen, Hungary
[34]Now at Universitatea Babes-Bolyai - Facultatea de Fizica, Cluj-Napoca, Romania
[35]Also at Physics Department, Faculty of Science, Assiut University, Assiut, Egypt
[36]Also at HUN-REN Wigner Research Centre for Physics, Budapest, Hungary
[37]Also at Punjab Agricultural University, Ludhiana, India
[38]Also at University of Visva-Bharati, Santiniketan, India
[39]Also at Indian Institute of Science (IISc), Bangalore, India
[40]Also at Birla Institute of Technology, Mesra, Mesra, India
[41]Also at IIT Bhubaneswar, Bhubaneswar, India
[42]Also at Institute of Physics, Bhubaneswar, India
[43]Also at University of Hyderabad, Hyderabad, India
[44]Also at Deutsches Elektronen-Synchrotron, Hamburg, Germany
[45]Also at Department of Physics, Isfahan University of Technology, Isfahan, Iran
[46]Also at Sharif University of Technology, Tehran, Iran
[47]Also at Department of Physics, University of Science and Technology of Mazandaran, Behshahr, Iran
[48]Also at Helwan University, Cairo, Egypt
[49]Also at Italian National Agency for New Technologies, Energy and Sustainable Economic Development, Bologna, Italy

[50]Also at Centro Siciliano di Fisica Nucleare e di Struttura Della Materia, Catania, Italy
[51]Also at Università degli Studi Guglielmo Marconi, Roma, Italy
[52]Also at Scuola Superiore Meridionale, Università di Napoli 'Federico II', Napoli, Italy
[53]Also at Fermi National Accelerator Laboratory, Batavia, Illinois, USA
[54]Also at Ain Shams University, Cairo, Egypt
[55]Also at Consiglio Nazionale delle Ricerche - Istituto Officina dei Materiali, Perugia, Italy
[56]Also at Riga Technical University, Riga, Latvia
[57]Also at Department of Applied Physics, Faculty of Science and Technology, Universiti Kebangsaan Malaysia, Bangi, Malaysia
[58]Also at Consejo Nacional de Ciencia y Tecnología, Mexico City, Mexico
[59]Also at Trincomalee Campus, Eastern University, Sri Lanka, Nilaveli, Sri Lanka
[60]Also at Saegis Campus, Nugegoda, Sri Lanka
[61]Also at National and Kapodistrian University of Athens, Athens, Greece
[62]Also at Ecole Polytechnique Fédérale Lausanne, Lausanne, Switzerland
[63]Also at Universität Zürich, Zurich, Switzerland
[64]Also at Stefan Meyer Institute for Subatomic Physics, Vienna, Austria
[65]Also at Laboratoire d'Annecy-le-Vieux de Physique des Particules, IN2P3-CNRS, Annecy-le-Vieux, France
[66]Also at Near East University, Research Center of Experimental Health Science, Mersin, Turkey
[67]Also at Konya Technical University, Konya, Turkey
[68]Also at Izmir Bakircay University, Izmir, Turkey
[69]Also at Adiyaman University, Adiyaman, Turkey
[70]Also at Bozok Universitetesi Rektörlügü, Yozgat, Turkey
[71]Also at Marmara University, Istanbul, Turkey
[72]Also at Milli Savunma University, Istanbul, Turkey
[73]Also at Kafkas University, Kars, Turkey
[74]Now at stanbul Okan University, Istanbul, Turkey
[75]Also at Hacettepe University, Ankara, Turkey
[76]Also at Istanbul University - Cerrahpasa, Faculty of Engineering, Istanbul, Turkey
[77]Also at Yildiz Technical University, Istanbul, Turkey
[78]Also at Vrije Universiteit Brussel, Brussel, Belgium
[79]Also at School of Physics and Astronomy, University of Southampton, Southampton, United Kingdom
[80]Also at University of Bristol, Bristol, United Kingdom
[81]Also at IPPP Durham University, Durham, United Kingdom
[82]Also at Monash University, Faculty of Science, Clayton, Australia
[83]Also at Università di Torino, Torino, Italy
[84]Also at Bethel University, St. Paul, Minnesota, USA
[85]Also at Karamanoğlu Mehmetbey University, Karaman, Turkey
[86]Also at California Institute of Technology, Pasadena, California, USA
[87]Also at United States Naval Academy, Annapolis, Maryland, USA
[88]Also at Bingol University, Bingol, Turkey
[89]Also at Georgian Technical University, Tbilisi, Georgia
[90]Also at Sinop University, Sinop, Turkey
[91]Also at Erciyes University, Kayseri, Turkey
[92]Also at Horia Hulubei National Institute of Physics and Nuclear Engineering (IFIN-HH), Bucharest, Romania
[93]Now at an institute or an international laboratory covered by a cooperation agreement with

CERN
[94]Also at Texas A&M University at Qatar, Doha, Qatar
[95]Also at Kyungpook National University, Daegu, Korea
[96]Also at another institute or international laboratory covered by a cooperation agreement with CERN
[97]Also at Universiteit Antwerpen, Antwerpen, Belgium
[98]Also at Yerevan Physics Institute, Yerevan, Armenia
[99]Also at Northeastern University, Boston, Massachusetts, USA
[100]Also at Imperial College, London, United Kingdom
[101]Also at Institute of Nuclear Physics of the Uzbekistan Academy of Sciences, Tashkent, Uzbekistan